COO-3246-19

NUCLEAR RESEARCH WITH HEAVY IONS

Annual Progress Report
For the Period January 1, 1979-December 31, 1979

Morton Kaplan
Principal Investigator

Department of Chemistry
Carnegie-Mellon University
Pittsburgh, Pennsylvania 15213

October 1979

PREPARED FOR THE
U. S. DEPARTMENT OF ENERGY
UNDER CONTRACT NO. EY-76-S-02-3246

DISCLAIMER

NOTICE

This report was prepared as an account of work sponsored by the United States Government. Neither the United States nor the United States Department of Energy, nor any of their employees, nor any of their contractors, subcontractors, or their employees, makes any warranty, express or implied, or assumes any legal liability or responsibility for the accuracy, completeness, or usefulness of any information, apparatus, product or process disclosed or represents that its use would not infringe privately owned rights.

TABLE OF CONTENTS

NUCLEAR RESEARCH WITH HEAVY IONS

CONTRACT EY-76-S-02-3246

ABSTRACT

The experimental research emphasizes the detection and measurement of light charged particles emitted in reactions between heavy ions and complex nuclei. The program involves a collaboration between Carnegie-Mellon University and SUNY at Stony Brook and utilizes the SuperHILAC and 88" Cyclotron accelerator facilities of the Lawrence Berkeley Laboratory. Correlations between light charged particles and heavy fragments provide detailed insights into the dynamics of the reaction mechanism. The light charged particles evaporated from fully accelerated fragments yield information on the excitation energies and spins of the equilibrated reaction products, whereas those particles which are emitted prior to thermal equilibration give us a view of the early stages of the reaction. Experimental results of fusion and charged particle emission cross sections are discussed for a variety of heavy ion reactions, particularly those induced by ^{40}Ar ions. The theoretical development of the statistical model as applied to particle evaporation is reviewed and semiempirical methods for facilitating comparisons with experimental data are presented. Current results from singles and coincidence experiments are given in detail for reactions of 340-MeV ^{40}Ar with Au, and analyses of average spins and energy sharing among particles are discussed.

Morton Kaplan
Principal Investigator

CONTRACT EY-76-S-02-3246

(U. S. Department of Energy--Carnegie-Mellon University)

Annual Report: October 1979

I. INTRODUCTION

The experimental research program supported by Contract EY-76-S-02-3246 is concerned primarily with nuclear reactions between complex nuclei and heavy ion projectiles. Such systems are currently of considerable interest because of the diversity of reaction mechanisms which participate in heavy ion collisions and because they provide an opportunity for probing the behavior of nuclear matter at extremes of temperature, pressure, and angular momentum. We have concentrated on studies of charged particle emission from heavy ion induced reactions as sensitive indicators of nuclear dynamics, and have been carrying out a multipronged approach involving (1) deeply inelastic reactions of very heavy ions; (2) model compound nuclei synthesized with appropriate excitation energies and spins; and (3) theoretical calculations via the statistical model using experimental data to help improve parameterization within the model. The basic ideas underlying this philosophy and its detailed application in our research program have been described in previous Annual Reports, particularly COO-3246-18 dated October 1978. We continue the successful and productive collaboration with Professor J. M. Alexander's group from the State University of New York at Stony Brook. Over the past few years, a very close interaction has developed between our two groups and the combined programs have been able to carry the commitments and responsibilities of the planning, execution, and analysis phases associated with research in the User Group mode.

During the past contract year, we have continued with our planned programs

at the SuperHILAC and 88" Cyclotron accelerator facilities of the Lawrence Berkeley Laboratory. The Program Advisory Committees of the two accelerators have favorably reviewed our research proposals, and accelerator time has been allocated for carrying out the proposed experiments. This year we have also made considerable progress in the analysis and assembling of a large backlog of experimental data, and we are optimistic that most of our results are in (or close to) the publication draft stage. The remainder of this report describes in some detail several of the projects which have recently been completed.

The excellent performance of the LBL accelerators has been an important factor in the success of our program, and we gratefully acknowledge the LBL staff for their dedicated efforts and their hospitality. The power and versatility of the ModComp data acquisition systems at both the SuperHILAC and the Cyclotron Laboratories have been invaluable for our experiments, and full credit as well as our appreciation goes to Dr. Creve Maples and his staff for persistence, insight, and commitment to a noble cause. The principal investigator on this research project, Professor Morton Kaplan, devoted one-half time to the program during the academic year and full time for two summer months. Dr. Douglas Logan was a full time research associate in the experimental program this year, and Dr. Ludwik Kowalski from Montclair State College worked with us for the summer. Our collaborators in the research program were Professor J. M. Alexander, Dr. M. Rajagopalan, Dr. H. Delagrange, Dr. M-F Rivet, and Mr. E. Duek from Stony Brook, and Dr. M. S. Zisman from LBL. Dr. G. L. Catchen of Columbia University has completed his Ph.D. dissertation under the joint supervision of the Stony Brook/Carnegie-Mellon collaboration and has now moved on to a new position.

FUSION AND EMISSION OF ^{1}H and ^{4}He IN REACTIONS BETWEEN COMPLEX NUCLEI AT HIGH ENERGIES

H. Delagrange[a]
Department of Chemistry, State University of New York at Stony Brook
Stony Brook New York 11794

D. Logan
Department of Chemistry, Carnegie-Mellon University
Pittsburgh, Pennsylvania 15213

M. F. Rivet[b], M. Rajagopalan, and John M. Alexander
Department of Chemistry, State University of New York at Stony Brook
Stony Brook, New York 11794

M. S. Zisman
Lawrence Berkeley Laboratory, Berkeley, California 94720

Morton Kaplan and Jane W. Ball[c]
Department of Chemistry, Carnegie-Mellon University
Pittsburgh, Pennsylvania 15213

ABSTRACT

We have measured cross sections for evaporation residues, fission, direct and evaporative ^{1}H and ^{4}He in reactions of 222-340 MeV ^{40}Ar with ^{116}Sn, ^{154}Sm, ^{164}Dy and ^{197}Au. Fusion cross sections are also presented for 77-167 MeV ^{12}C + ^{182}W and 187 MeV ^{40}Ar + ^{116}Sn. The Z dependence of the evaporative H/He indicates a breakdown of phase-space models for fission-evaporation competition. The large cross sections observed for direct H/He emission force serious consideration of energy dissipation by H/He ejection during the initial impact.

Since 1960, ^{1}H and ^{4}He have been found to be emitted with large cross sections in many reactions between complex nuclei.[1] Forward-peaked (direct) emission[2] seems to dominate for projectiles of ^{12}C, ^{14}N and ^{16}O and evaporative emission[3] (symmetric about $\theta_{c.m.} = 90^{o}$) for $^{40}Ar + ^{77}Se$. First interpretations were that the direct H/He came from projectile breakup,[2] but more recent evidence[4] is for massive transfer or incomplete fusion (capture of the projectile residue). Currently there is great interest in gaining an understanding of complete fusion at high energies, and it is natural to ask about the possible role of the incomplete-fusion events. Experimentally, can one adequately distinguish complete from incomplete fusion in the measurements, and correspondingly, do the reaction models take adequate account of the fast ejection of H/He during the impact processes? Models currently in use assume that complete fusion occurs prior to significant loss of energy or angular momentum from the composite system. Our new results along with other data strongly suggest that this assumption is not valid. We discuss the trends of a body of new data on fusion cross sections for several reactions induced by ^{12}C and ^{40}Ar. Also, we show a pattern of new results on the emission of H/He in ^{40}Ar reactions. Extensive direct and evaporative emission are observed. We discuss the possible relationships between direct emission and fusion cross sections and between evaporative emission and fission.

The experimental arrangement is described elsewhere[5,6] so we shall give only a sketch here. Beams of ^{12}C and ^{40}Ar were obtained from the Lawrence Berkeley Laboratory 88" Cyclotron and SuperHILAC, respectively. Self supporting targets of ^{116}Sn, ^{154}Sm, ^{164}Dy, ^{182}W and ^{197}Au were used. Three member solid state telescopes (Si of 45 μm, 500 μm, 5 mm at solid angles $\approx$ 8 msr) identified and measured H/He; gas ionization telescopes (methane at $\approx$ 20 torr with stopping detector of 500 μm Si at 0.2 or 1 msr)[7] determined evaporation residues (ER) and fission. Data were recorded event-by-event on magnetic tape,

and we now report some of the results taken in the singles mode.

In Fig. 1 we show angular distributions at two incident energies for $^{1}H/^{4}He$ and fission-like events for a ^{164}Dy target. Also, we show the angular dependence of the effective temperatures obtained by fitting the spectra to the equation $P(\epsilon) \propto (\epsilon-B) \exp(-\epsilon/T)$, with barrier parameters B from Ref. 8. Results for the ^{154}Sm and ^{116}Sn targets are similar. In contrast with the data[3] for $^{40}Ar + ^{77}Se$, there is a clear forward-peaked component with a high effective temperature. We have attempted to resolve the direct and evaporative components by fitting to the function, $W(\theta) = A \exp(-\gamma\theta) + B + C \cos^2\theta$. We assign to evaporative processes the integral of the symmetric part $(B + C \cos^2\theta)$ and the rest to direct processes. The symmetric emission could be the result of evaporation from the composite nuclear system or perhaps from fission fragments with symmetric distributions. As can be seen from Fig. 1, the direct processes at 222 MeV so dominate the integrated cross sections that the evaporation cross sections can be assigned only with large uncertainties.

The angular distributions for fission-like events (as taken from ΔE-E contour maps[9]) are not quite symmetric about $\theta_{c.m.} = 90°$. This is probably due to the difficulties of separating the so called "fission" and "deeply inelastic" reactions[9]. Near $\theta_{c.m.} = 90°$ one finds that the heavy fragment energy spectra resolve into three well-defined groups that one is tempted to call projectile-like, target-like and fission-like fragments. Therefore we assign to the fission cross section the value $\sigma_f = 2\pi^2 (d\sigma/d\Omega)_{c.m.}$ (at $\theta_{c.m.} = 90°$). These values provide upper limits to the symmetric part of the fission cross sections.

In Fig. 2 we present the cross sections for ^{40}Ar reactions at two excitation energies as functions of Z of the composite system. As the

incident energies are well over the barrier, the fusion cross sections (fission plus ER) are relatively constant ($\approx$ 0.6 to $\approx$ 1.0 b). However, with increasing Z_{CN}, the fraction of ER drops dramatically (lower curve). The direct component of $^{1}H/^{4}He$ emission is relatively constant (with Z_{CN}) at $\approx$ 120 mb and $\approx$ 200 mb for excitations of 100 and 140 MeV, respectively. Presumably, direct H/He ejection occurs much faster than the subsequent fission or evaporative decays and is unaffected by them. By contrast the evaporative component of H/He must compete with fission and its cross section decreases drastically from Z_{CN} = 52 to 84. However, from Z = 84 to 97 there are actually increases in the evaporative H/He while the ER cross sections have been reduced tremendously by fission. These increases are contrary to statistical model expectations for evaporation prior to fission. In Ref. 6 we show that even for the very fissile system with Z_{CN} = 97 the bulk of this evaporative H/He component must be emitted prior to scission and cannot be attributed to emission from the fission fragments. One must conclude that it comes from the composite system with intrinsic rate comparable to fission regardless of the rapid dependence of the number of open fission channels on Z. It would thus appear that the fission-evaporation competition is determined primarily by the reaction dynamics rather than the available phase space. Hence the energy spectra of H/He should reflect the temperatures and barriers of the composite system prior to fission and largely unmindful of it. The experimental spectra are consistent with this argument. Thus, it would appear that these emissions of H/He are very powerful, if not unique, reflectors of the early life of the composite system. They may allow testing of many interesting questions such as the possible persistance of shell effects to very high excitations.[10]

In Fig. 3 our new data for ER and fission cross sections are compared to other similar data[5,6,9,11] and to calculated curves from the semiempirical

systematics of Ref. 12. These curves simply provide a common reference and are not intended as sophisticated models for the fusion process at high energies. Let us summarize the pattern in Fig. 3. (1) All the data approach the reference curves at low energies simply because the calculations were taken from empirical fusion barriers. (2) With increasing energy, the data seem to flatten out compared to the reference curves. This tendency is especially clear for ^{12}C and ^{14}N projectiles and for ^{40}Ar + Sn, Sm, Dy and Au. (3) For ^{40}Ar + Pd, Ag and Sb, there are only small deviations from the reference curves, while our new measurements for ^{116}Sn fall below the curve at 222 and 274 MeV, but agree with the curve at 187 MeV. In the model of Ref. 12, and others presented so far, the fusion decision is presumed to precede significant particle emission. However, particle ejection during impact and from a band of ℓ-waves near ℓ_{crit} would present an element so far unaddressed in the models for complete fusion.

Our purpose here is to emphasize the possible importance of energy dissipation by H/He ejection during the impact stage. First consider reactions with the lighter projectiles ^{12}C and ^{14}N. For energies well over the barrier we know that forward-peaked H/He emission is very large.[2,4] Also, we now believe that the projectile residue often fuses with the target.[4] For ER measurements near the detection threshold of a gas telescope (e.g. recoils of a few MeV from reactions such as ~ 100 MeV ^{12}C + ^{182}W), the heavy residuals after forward-peaked direct ^{4}He emission may not be detected.[5] As the projectile energy is increased, however, such residual nuclei will often be detected and possibly included in the integrated cross section assigned to ER. One possible experimental complication of the trends in Fig. 3 for the ^{12}C and ^{14}N reactions (and for most published data) is as follows. For energies near the calculated cross-section maximum, the observed ER cross sections could suffer from

competition with incomplete fusion reactions that are largely undetected. For higher energies the observed ER cross sections could increase due to an increased detection efficiency for the incomplete fusion residues. In the case of ^{40}Ar induced reactions, the experiments probably include most incomplete fusion reactions along with the complete fusion; at high energies there may also be some confusion of fission with deeply inelastic reactions.[9]

What do we actually want to include in the experimental fusion cross section? This clearly depends on the reaction model that we want to test.[13] Refs. 4 and 6 give evidence that the probability for direct ^{4}He emission is greatest for ℓ-waves near to or greater than the high ℓ cutoff for fusion (ℓ_{crit}). Therefore a model calculation of ℓ_{crit} must consider in detail both the nucleon transfers and the particle emissions for ℓ near ℓ_{crit}. Energy dissipation by nucleon transfer alters both the energy and angular momentum of the relative motion and therefore the calculated values of ℓ_{crit}.[14] Experiments show that the cross sections for direct H/He emission are often quite large ($\sim$ 1000 mb for 126 MeV ^{12}C + Bi; $\sim$ 200 mb each for H/He for 274 MeV ^{40}Ar), and could thus perturb collision trajectories for many ℓ values. Therefore, the role of the incomplete fusion residues vis-a-vis a "fusion" cross section of ~1000 mb has obvious importance. To our knowledge no current reaction model for fusion includes this aspect; i.e. energy dissipation and perturbation of the assumed potential barrier due to direct particle ejection during the impact.

This work was supported by the U. S. Department of Energy.

References

[a]Permanent address: Centre d'Etudes Nucléaires de Bordeaux-Gradignan, Laboratoire de Chimie Nucléaire ERA No. 144, Le Haut Vigneau, 33170 Gradignan, France.

[b]Permanent address: Laboratoire de Chimie Nucléaire, Institut de Physique Nucléaire, B.P. No. 1, 91406 Orsay, France.

[c]Present address: Laboratory for Nuclear Science, Massachusetts Institute of Technology, Cambridge, Mass. 02139

1. W. U. Schröder and J. R. Huizenga, Ann. Rev. Nucl. Sci. 27, 465 (1977); A. Fleury and J. M. Alexander, Ann. Rev. Nucl. Sci. 24, 279 (1974); and references therein.
2. See particularly H. C. Britt and A. R. Quinton, Phys. Rev. 124, 877 (1961).
3. J. Galin et al., Phys. Rev. C9, 1113 (1974); ibid C9, 1126 (1974).
4. R. Bimbot et al., Nucl. Phys. A189, 193 (1972); T. Inamura et al., Phys. Letts. 68B, 51 (1977); T. Nomura et al., Phys. Rev. Letts. 40, 694 (1978); D. R. Zolnowski et al., Phys. Rev. Letts. 41, 92 (1978); K. Siwek-Wilczyńska et al., Phys. Rev. Letts. 42, 1599 (1979); D. G. Sarantites et al., Phys. Rev. C18, 774 (1978).
5. J. M. Miller et al., Phys. Rev. Letts 40, 1074 (1978).
6. D. Logan et al., submitted to Phys. Rev. C.
7. M. M. Fowler and R. C. Jared, Nucl. Instr. Meth. 124, 341 (1975).
8. M. A. McMahan and J. M. Alexander, Phys. Rev. C (in press).
9. See for example, H. C. Britt et al., Phys. Rev. C13, 1483 (1976).
10. N. Cârjan et al., Phys. Rev. C19, 2267 (1979).
11. J. B. Natowitz et al., Phys. Rev. C6, 2133 (1972); M. N. Namboodiri et al., Phys. Rev. C11, 401 (1975); S. Della Negra et al., Z. Physik A282, 65 (1977); N. H. Lu et al., Phys. Rev. C13, 1496 (1976); W. Scobel et al., Phys. Rev. C14, 1808 (1976); H. Gauvin et al., Phys. Letts. 58B, 163 (1975);

B. Tamain et al., Nucl. Phys. A252, 187 (1975); B. Largarde and Y. Le Beyec, Z. Physik A288, 415 (1978); C. Ngô et al., Z. Physik A283, 161 (1977).

12. L. C. Vaz and J. M. Alexander, Phys. Rev. C18, 2152 (1978).

13. See for example, M. Lefort, J. Physique C5, 57 (1976).

14. J. R. Birkelund et al., Phys. Rev. Letts. 40, 1123 (1978).

Figure Captions

Figure 1. Measured angular dependence of $(d\sigma/d\Omega)$ and T for ^{1}H, ^{4}He and $(d\sigma/d\theta)$ for fission-like events from $^{40}Ar + ^{164}Dy$. The open points are for 274-MeV and the filled points are for 222-MeV. Results for ^{116}Sn and ^{154}Sm targets are similar; for Au see Ref. 6.

Figure 2. Integrated cross sections at two excitation energies for fusion, fission, ^{1}H, ^{4}He and ER vs. charge of the composite nucleus, Z_{CN}. Data for a target of ^{77}Se are from Ref. 3.

Figure 3. Excitation functions for fusion (●), fission (F) and ER (open symbols as indicated) from this work ⊙ and other studies △ ▽ □ (Refs. 5, 9, 11).

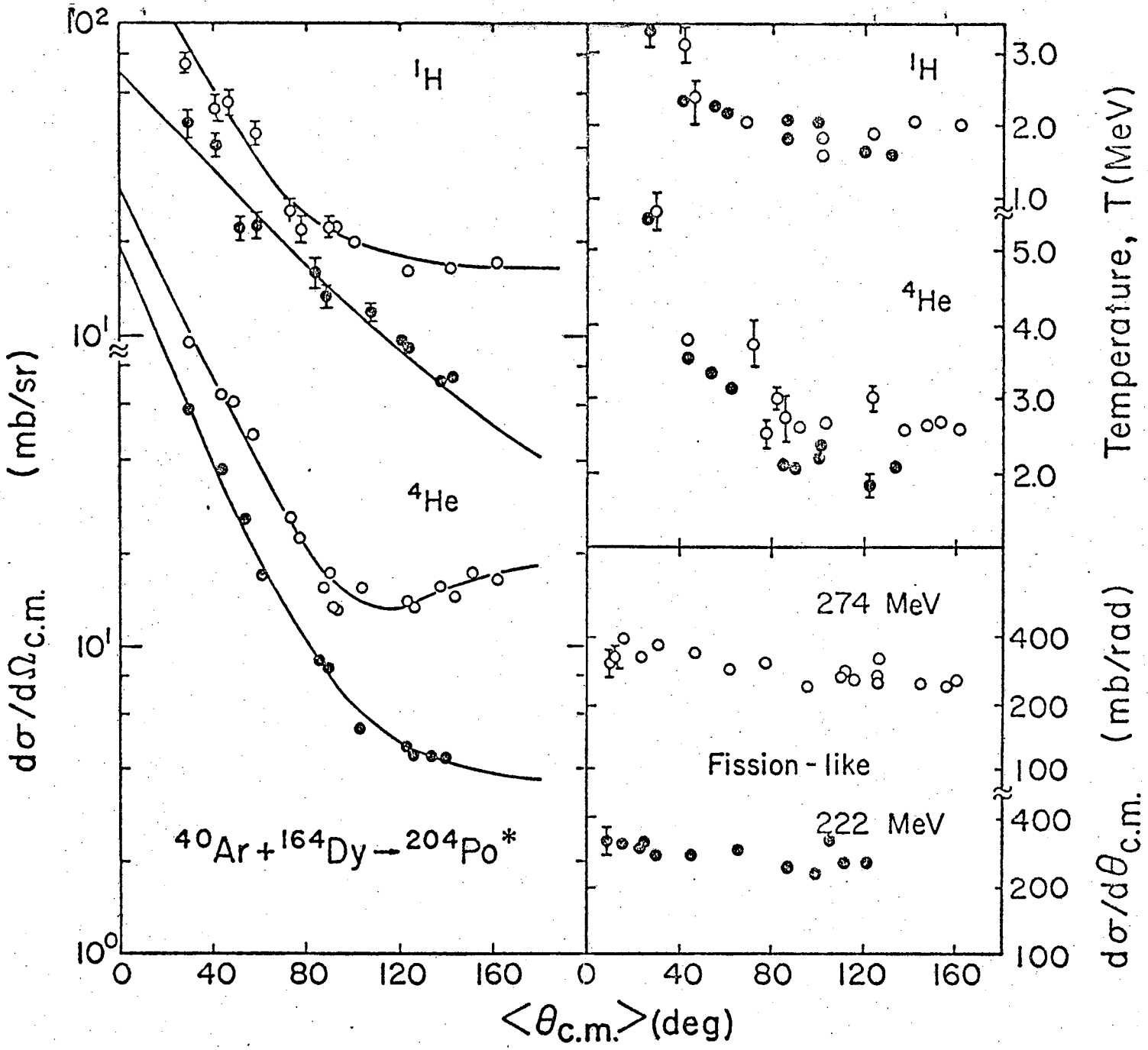
10^2
10^1
10^1
10^0
$d\sigma/d\Omega_{c.m.}$ (mb/sr)
^{1}H
^{4}He
^{40}Ar + ^{164}Dy → ^{204}Po*
0
40
80
120
160
$\langle\theta_{c.m.}\rangle$ (deg)
^{1}H
^{4}He
Temperature, T (MeV)
3.0
2.0
1.0
5.0
4.0
3.0
2.0
274 MeV
Fission - like
222 MeV
400
200
100
400
200
100
$d\sigma/d\theta_{c.m.}$ (mb/rad)

Fig 1

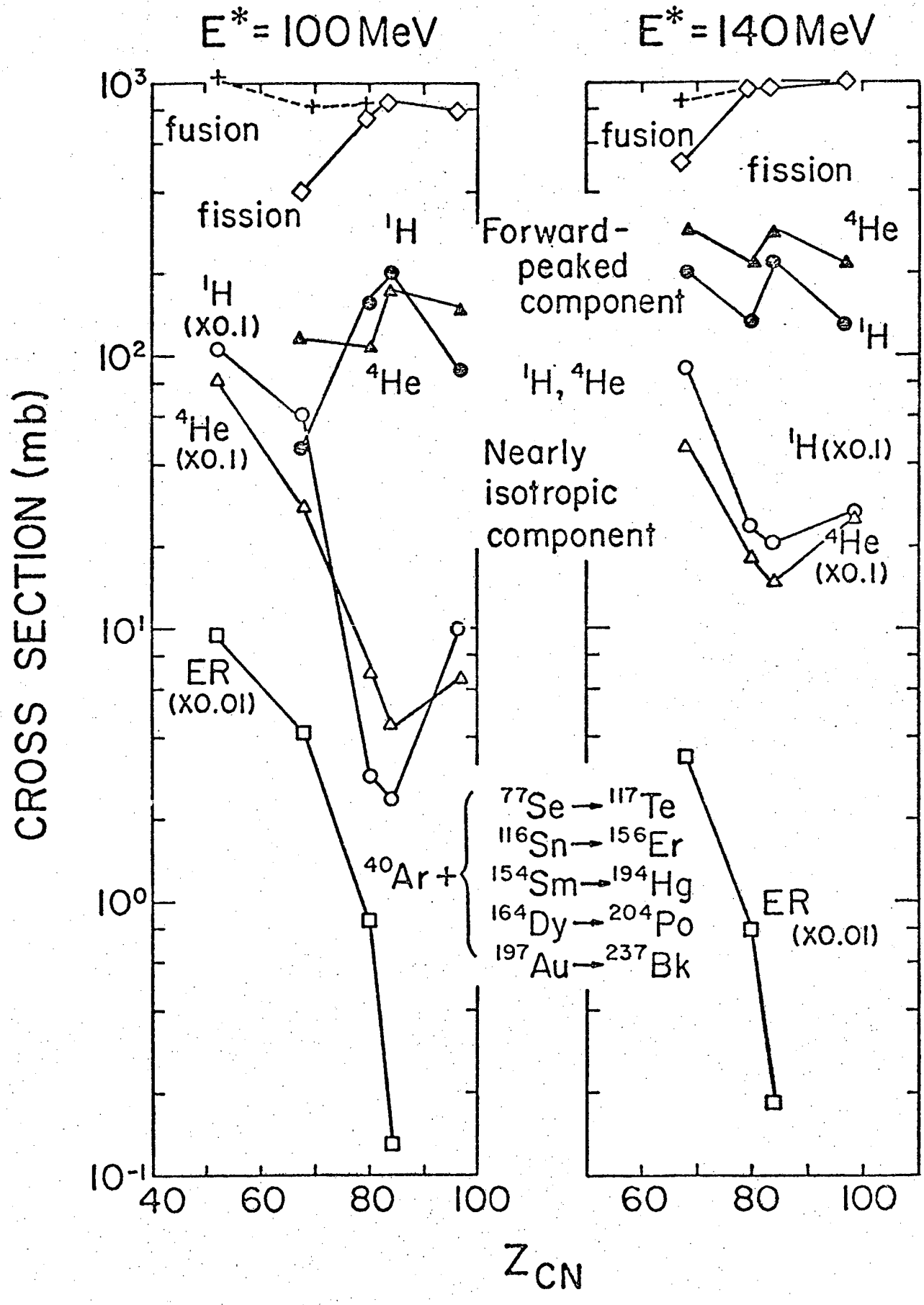
E* = 100 MeV
E* = 140 MeV
fusion
fission
¹H
⁴He
¹H (x0.1)
⁴He (x0.1)
ER (x0.01)
Forward-peaked component
¹H, ⁴He
Nearly isotropic component
⁴⁰Ar +
⁷⁷Se → ¹¹⁷Te
¹¹⁶Sn → ¹⁵⁶Er
¹⁵⁴Sm → ¹⁹⁴Hg
¹⁶⁴Dy → ²⁰⁴Po
¹⁹⁷Au → ²³⁷Bk
CROSS SECTION (mb)
Z_CN

Fig 2

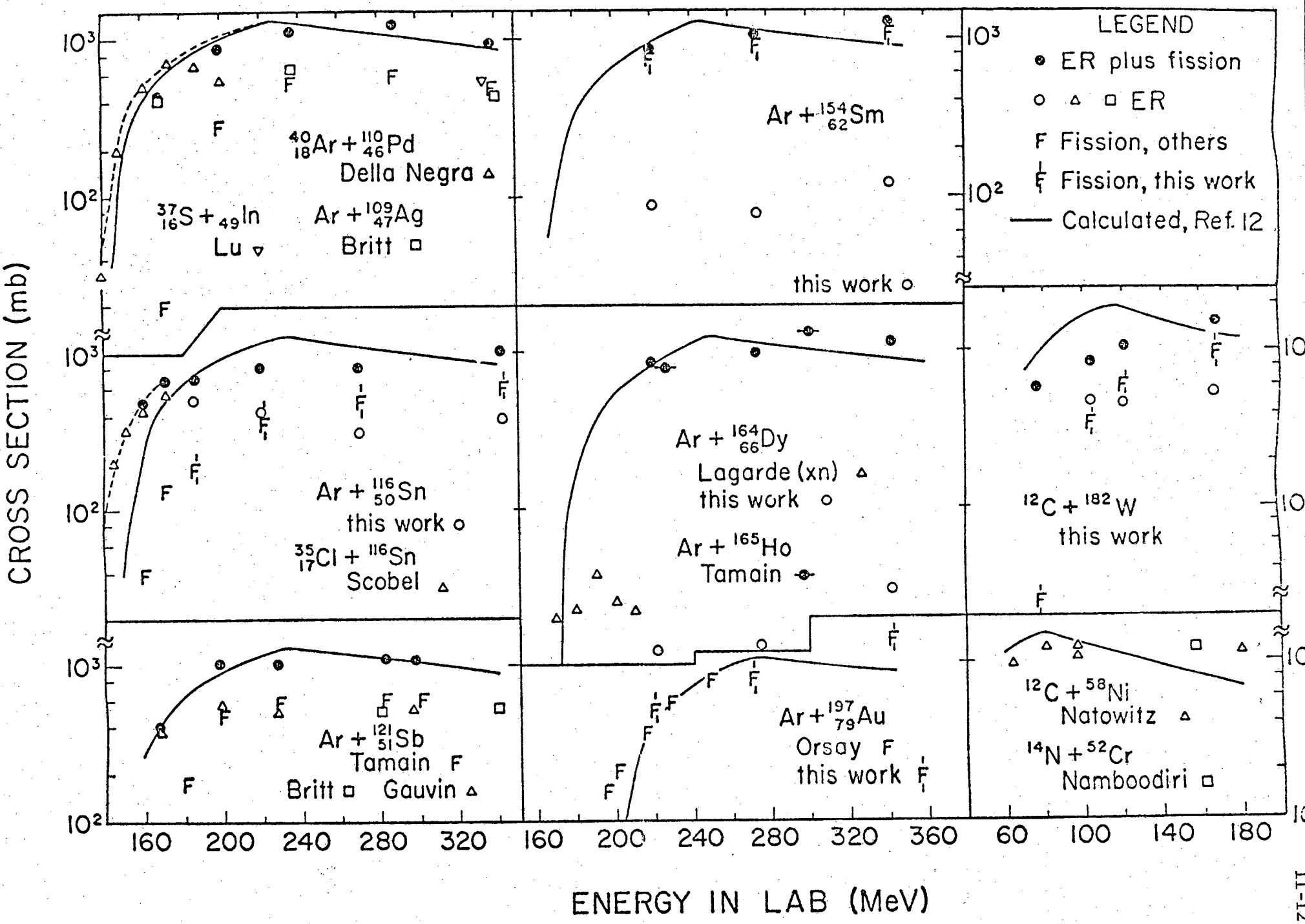
CROSS SECTION (mb)
ENERGY IN LAB (MeV)
LEGEND
ER plus fission
ER
F Fission, others
F1 Fission, this work
Calculated, Ref. 12
40 18Ar + 110 46Pd
Della Negra
37 16S + 49In
Lu
Ar + 109 47Ag
Britt
Ar + 154 62Sm
this work
Ar + 116 50Sn
this work
35 17Cl + 116Sn
Scobel
Ar + 164 66Dy
Lagarde (xn)
this work
Ar + 165Ho
Tamain
12C + 182W
this work
Ar + 121 51Sb
Tamain
Britt
Gauvin
Ar + 197 79Au
Orsay
this work
12C + 58Ni
Natowitz
14N + 52Cr
Namboodiri

Fig 3

SEMIEMPIRICAL METHODS FOR ESTIMATING FRAGMENT SPINS FROM STUDIES OF ^{4}He AND ^{1}H EMISSION

Gary L. Catchen
Department of Chemistry
Columbia University, New York, NY 10027

Morton Kaplan
Department of Chemistry
Carnegie-Mellon University, Pittsburgh, PA 15213

John M. Alexander and M. F. Rivet[(a)]
Department of Chemistry
State University of New York at Stony Brook
Stony Brook, New York 11794

Abstract

The statistical model provides equations that relate the angular correlations of evaporated particles to the angular momenta of the emitters. We discuss the relationships between several theoretical approaches and their application to experimental measurements. Available calibration data are collected from studies of the compound nuclei $^{75}Br^{*}$ and $^{117}Te^{*}$. Semiempirical use of the theory and these calibrations provides a very interesting possibility for determining fragment spins in deeply inelastic reactions. A further possibility is provided by empirical use of the emission multiplicity ratios for ^{4}He to ^{1}H. These methods are used to estimate the root-mean-square spin of the projectile-like fragments produced in deeply inelastic reactions of 724 MeV ^{86}Kr + Au.

NUCLEAR REACTIONS: Synthesis of theoretical equations that relate anisotropies in particle evaporation to spin of the emitter. Semiempirical correlations presented with data from the literature on both anisotropies and multiplicities of ^{1}H and ^{4}He.

I. Introduction

It is currently of great interest to extract experimental information on the spins of heavy fragments formed in nuclear reactions.[1,2] In particular, for deeply inelastic reactions between complex nuclei there are a number of lines of investigation in progress and their initial results have provided some very interesting tests of the reaction models. Lefort and Ngô have recently reviewed both the reaction models and the experimental methods that are being used.[2]

Several groups have made measurements of angular distributions of fission products with respect to the reaction plane and the direction of recoil of the fissile nucleus.[3-6] The utilization of these angular correlations as a reflection of the spins of the fissile nucleus depends on independent measures or estimates of the effective moments of inertia and nuclear temperatures. As our knowledge of nuclear properties is not yet well enough developed to make absolute calculations of these quantities, one must use experimental studies of fission after compound-nucleus formation to build up a systematic pattern of the relevant parameters.[7]

The probability of sequential fission following deeply inelastic collisions provides another probe of the spins of the fissile product.[8-11] Similarly, the interpretation of these fission probabilities depends on a systematic knowledge of fissionability as a function of atomic and mass number (Z,A), excitation energy (E^*), and spin (J). Very few of the fission probability measurements that have so far been made are for systems that have all important variables (Z,A,E^* and J) very near to those of fissile nuclei produced in deeply inelastic reactions.[8,9]

The measurement of γ-ray multiplicities and angular correlations are also potentially powerful probes of the spins of fragment nuclei. A number of

experiments are in progress to obtain the basic calibration information needed for this approach (see for example Refs. 12-15).

Our concern in this paper is the utilization of measurements of angular distributions of ^{1}H and ^{4}He as probes of the spin distribution of the emitting fragments. The situation here is parallel to that for fission studies. Namely, a basic theoretical treatment has been worked out in the context of the statistical model.[16-18] Also, a number of experiments have been reported on emission probabilities and angular distributions after compound-nucleus formation.[19-25] The theory depends on a knowledge of the transmission coefficients T_{ℓ}, the effective moments of inertia $\mathcal{J}$, and the temperatures T. Unfortunately, the experimental papers rarely come to clear conclusions on how well the separate roles of these parameters can be established. Several experimental studies of ^{4}He emission in deeply inelastic reactions have already been interpreted in terms of the spins of the emitters.[26,27] These interpretations depend on absolute estimates of the values of $\mathcal{J}$ and T.

In this paper we have several objectives. Firstly, we discuss the relationships between the various theoretical equations needed to describe angular distributions of evaporated particles. Some graphs and tables are also presented that can simplify their utilization. Secondly, we organize in this context the experimental data on angular distributions of H/He from several compound nuclei. Then we show, for one example, how the estimate of emitter spin can be made on the one hand from empirical correlations and on the other from absolute estimation of $\mathcal{J}$ and T. Finally, we show some calculated trends for the ratio of ^{4}He to ^{1}H in evaporation reactions. An associated empirical correlation of measured $^{4}He/^{1}H$ ratios suggests that these ratios also may provide information concerning the spins of the emitting nuclei.

II. Theoretical background and some numerical generalizations.

Some years ago Ericson and Strutinski (ES) derived equations for the angular distributions of evaporated particles with respect to the angular momenta of the emitting nuclei.[16] Similar, but not identical relations, were also worked out by Halpern.[28] Recently, Dφssing has elaborated on these early works and has discussed the relationships between them.[18] In this section we give some of the important equations in Dφssing's format, and we give some tables and figures that might be useful for numerical evaluations. All the equations begin with a simple approximation to the nuclear level density ρ of the residual nucleus in the region of (E,J) space near (E',J'):

$$\rho(E,J)= \frac{(2J+1)}{(2J'+1)}\ \rho(E',J')\ \exp\{\frac{1}{T}\ (E-E') - \frac{\hbar^2}{2\mathcal{J}T}\ [J(J+1) - J'(J'+1)]\}, \qquad (1)$$

where $\mathcal{J}$ and T are the moment of inertia and the temperature of the residual nucleus. The derivations are classical;[29] that is, they assume that particle emission is strictly confined to a plane perpendicular to the orbital angular momentum of the emitted particle, $(\ell + \frac{1}{2})\hbar$.

Following ES, for the evaporation of a particle of energy ϵ there is a correlation of emission probability $W(\theta)$ with the angle θ between the emitted particle and the angular momentum of the emitter, $(J_o + \frac{1}{2})\hbar$:

$$W_{J_o,\ell,\mathcal{J}T}(\theta) \propto I_o \left\{\frac{\hbar^2(J_o+\frac{1}{2})\ (\ell+\frac{1}{2})}{\mathcal{J}T}\ \sin\theta\right\}, \qquad (2)$$

where I_o is the modified Bessel function of zero order. (The specification of $\mathcal{J}$ T requires selection of particular emissions (e.g. E^*, ϵ, etc.) and a knowledge of the level density.) For an ensemble of compound nuclei with angular momenta

uniformly distributed perpendicular to the beam axis, particles are expected to be emitted at angles Θ with respect to the beam

$$W_{J_o,\ell,\mathcal{J}T}(\Theta) \propto \sum_{k=0}^{\infty} (-)^k (4k+1)\, j_{2k} \left\{(i\hbar^2)\frac{(J_o+\frac{1}{2})(\ell+\frac{1}{2})}{\mathcal{J}T}\right\} [P_{2k}(0)]^2 P_{2k}(\cos\Theta), \quad (3)$$

where j_{2k} is a spherical Bessel function of order 2k. These two relations depend only on the parameter $\beta_1 = \hbar^2 (J_o+\frac{1}{2})(\ell+\frac{1}{2})/2\mathcal{J}T$. On expansion of Eqs. (2) and (3) the first term is of order β_1^2:

$$\beta_1^2 = \hbar^4 \frac{(J_o+\frac{1}{2})^2(\ell+\frac{1}{2})^2}{4\mathcal{J}^2T^2}, \quad (4)$$

and therefore the root-mean-square values of $(J_o+\frac{1}{2})$ and $(\ell+\frac{1}{2})$ are of primary importance. For small values of J_o one has

$$\hbar^2(\ell+\tfrac{1}{2})^2 \approx (E-B)\mu R^2 \approx 2T\mu R^2, \quad (5)$$

where B is the emission barrier, μ is the reduced mass of the emitted particle and R and T the radius and temperature of the residual nucleus. For J_o values of any practical interest Eq. (5) is not adequate and Døssing has given the following relation for the distribution of ℓ values[18]

$$P_{J_o,\mathcal{J}T}(\ell) \propto \left[\exp\left\{\frac{\hbar^2(J_o+\frac{1}{2})(\ell+\frac{1}{2})}{\mathcal{J}T} - \frac{\hbar^2(\ell+\frac{1}{2})^2}{2T\mu R^2}\left(\frac{\mathcal{J}_\perp}{\mathcal{J}}\right)\right\}\right]$$

$$\times \left[1-\exp\left(-\frac{2\hbar^2(J_o+\frac{1}{2})(\ell+\frac{1}{2})}{\mathcal{J}T}\right)\right] \quad (6)$$

where $\mathcal{J}_\perp = \mathcal{J} + \mu R^2$. He has used the sharp cutoff approximation for the transmission coefficients, T_ℓ

$$T_\ell(\varepsilon) = \begin{cases} 0 \text{ for } \varepsilon < B + \dfrac{\hbar^2 (\ell+\frac{1}{2})^2}{2\mu R^2} \\ \\ 1 \text{ for } \varepsilon \geq B + \dfrac{\hbar^2 (\ell+\frac{1}{2})^2}{2\mu R^2} \end{cases} \tag{7}$$

Note that B and μR^2 refer to the coulomb-nuclear and centrifugal barriers respectively for evaporation. From the principle of detailed balance the evaporation barrier is identified with that for the inverse reaction.[17] Refs. 30 and 31 discuss complete fusion as our best approximation to the inverse reaction and the related choice of parameters for B and μR^2. We have found that the Gaussian approximation to Eq. (6) (result of the neglect of the exponential in the last bracket) is not adequate for the purposes of this paper. It is, however, useful for getting a rough idea of the qualitative features of the ℓ distribution so we include it here

$$P_{J_o, \mathcal{J}T}(\ell) \propto \exp\left(- \frac{\hbar^2 (\ell-\ell_{10})^2}{2T\mu R^2} \frac{\mathcal{J}_\perp}{\mathcal{J}}\right), \tag{8}$$

where ℓ_{10} is an approximation to the mean value of ℓ for the first emitted particle,

$$(\ell_{10} + \tfrac{1}{2}) = \frac{\mu R^2}{\mathcal{J}_\perp} (J_o + \tfrac{1}{2}). \tag{9}$$

Eq. (9) expresses the oft-used classical approximation of exit channel spinoff of a particle of reduced mass μ from the equator of the rotating system. This approximation to Eq. (6) is only valid at very high spins beyond the range of most practical applications.

The utilization of Eqs. (2), (3) and (6) is somewhat tedious so we have developed some computational aids. The first terms in the expansion of Eqs. (2) and (3) are of order β_1^2 so the most important average related to $P_{J_o,\mathcal{J}T}(\ell)$ is $\langle(\ell+\frac{1}{2})^2\rangle$. From Eq. (6) one can obtain an exact expression for this average:

$$\langle(\ell+\tfrac{1}{2})^2\rangle = \frac{[1+(\gamma^2/2)]\ \mathrm{erf}\ (\gamma/2) + (\gamma/\sqrt{\pi})\ \exp\ (-\gamma^2/4)}{2b\ \mathrm{erf}\ (\gamma/2)}\ , \tag{10}$$

where

$$\gamma = (J_o+\tfrac{1}{2})\ /b^{1/2}\ \sigma^2 = \eta\ (J_o+\tfrac{1}{2})\ , \tag{11}$$

$$\sigma^2 = \mathcal{J}T/\hbar^2\ , \tag{12}$$

$$b = \hbar^2\ \mathcal{J}_\perp/\ 2\mu R^2\ \mathcal{J}T\ , \tag{13}$$

and

$$\eta = (2\mu R^2\ \hbar^2/\mathcal{J}\mathcal{J}_\perp T)^{1/2}\ . \tag{14}$$

Hence the quantity $b[\langle(\ell+\frac{1}{2})^2\rangle]$ is a function of J_o for each value of η. In Fig. 1 we give a family of curves calculated from Eq. (10) from which one can obtain $\langle(\ell+\frac{1}{2})^2\rangle$; if greater precision is needed one can use Eq. (10) directly. Then in Table I we give numerical values of the functions from Eqs. (2) and (3) that depend on β_1 and hence $\langle(\ell+\frac{1}{2})^2\rangle^{1/2}$.

Equations (2) and (3) are strictly applicable for one value of $\beta_1 \equiv \hbar^2\ (J_o+\frac{1}{2})\ (\ell+\frac{1}{2})/2\mathcal{J}T$ and therefore for distributions of J_o, ℓ and/or $\mathcal{J}T$ one should take the most appropriate average or specifically perform the summations of interest. The approach given above is to estimate

$$\beta_1^2 = \frac{\hbar^4\langle(J_o+\frac{1}{2})^2\rangle\ \langle(\ell+\frac{1}{2})^2\rangle}{4\mathcal{J}^2T^2} \tag{4'}$$

and use it in Eqs. (2) and (3). A second and more attractive approach is to weight Eqs. (2) and (3) appropriately and sum over the spectrum of ℓ and ϵ for

the evaporated particles. Dössing has used the approximations of Eqs. (1) and (7) to perform these integrals over ϵ and ℓ of the emitted particle.[18] Analogous to Eq. (2) he obtains

$$W_{J_o, \mathcal{J}T}(\theta) \propto \exp(\beta_2 \sin^2\theta) , \tag{15}$$

and analogous to Eq. (3) he obtains

$$W_{J_o, \mathcal{J}T}(\Theta) \propto [\exp(-\beta_2 \sin^2\Theta/2)] I_o(\beta_2 \sin^2\Theta/2) , \tag{16}$$

where

$$\beta_2 = \frac{\hbar^2 (J_o + \frac{1}{2})^2}{2\mathcal{J}T} \left(\frac{\mu R^2}{\mathcal{J}_\perp}\right) . \tag{17}$$

A result very similar to Eq. (15) was obtained earlier by Halpern by a different method.[28] As the utilization of Eqs. (15) and (16) is also somewhat tedious we have included numerical values in Table I, along with those from Eqs. (2) and (3).

For experimental planning or rough evaluations it is helpful to estimate anisotropy values. In Fig. 2(a) we show anisotropies from Eqs. (2) and (15) for angular correlations with respect to a spin vector. These functions are useful for interpreting angular correlation measurements in which an evaporated particle (n, ^{1}H, ^{4}He, etc.) is detected in coincidence with a heavy reaction product (from fission, deeply inelastic reaction, etc.). The direction of the spin vector will be close to the normal to the reaction plane (defined by the direction of the beam and the heavy reaction product). In Fig. 2(b) we show anisotropies from Eqs. (3) and (16) for angular distributions with respect to the beam in compound-nucleus experiments. In these experiments no unique reaction plane is defined and the spin vectors of the compound nuclei are uniformly distributed in (or close to) a plane perpendicular to the beam direction.

Either Eq. (2) or Eq. (15) can be used to interpret angular correlation

measurements in deeply inelastic reactions (with attention to the appropriate choice of β_1 and β_2). If one assumes that the spin of the emitter is perpendicular to the reaction plane then the out-of-plane correlation (in a coincidence experiment) is given by these equations. In Fig. 3 we show β_1 and β_2 as a function of $J + \frac{1}{2}$ for one specific case $Z = 42$, $A = 101$, $E^* = 86$ MeV. The construction of such curves requires absolute estimates of μR^2, $\mathcal{J}$ and T which we have made as follows: For μR^2 we use $\mu (r_o A^{1/3} + R_p \text{ or } R_\alpha)^2$ for complete fusion following Refs. 30 and 31. For $\mathcal{J}$ we use

$$\mathcal{J} = \frac{2}{5} Mr^2 , \tag{18}$$

with M the mass of the nucleus and $r = 1.2A^{1/3}$ fm (for the matter radius). The temperature is related to the average energy available for thermal excitation:

$$U = aT^2 , \tag{19}$$

with "a" = (A/10) MeV^{-1} and

$$U = E^* - \langle \epsilon \rangle - S - E_{rot} . \tag{20}$$

The separation energy of the emitted particle is S and its average kinetic energy is $\langle \epsilon \rangle$,

$$\langle \epsilon \rangle \approx B + 2T \tag{21}$$

where E_{rot} and $\mathcal{J}$ refer to the rotational energy and moment of inertia of the emitting nucleus and B to the exit channel barrier,[31]

$$E_{rot} = \hbar^2 (J_o + \tfrac{1}{2})^2 / 2\mathcal{J} . \tag{22}$$

These estimates of $\mathcal{J}$ and T assume first chance emission from a spherical nucleus of known radius.[31] Confidence in the results can be greatly improved if one can calibrate these parameters from compound-nucleus studies. This is the task of the next section.

III. Semiempirical use of the angular correlations.

Of the many experimental studies that have been published for H/He emission in compound-nucleus reactions, we have selected two that report extensive data on angular distributions as functions of energy and spin. Reedy et al.[24] give results for the reactions

$$^{11}B + {}^{64}Zn \rightarrow {}^{75}Br^* \quad (23a)$$

$$^{12}C + {}^{63}Cu \rightarrow {}^{75}Br^* \quad (23b)$$

$$^{16}O + {}^{59}Co \rightarrow {}^{75}Br^* \quad (23c)$$

leading to $^{75}Br^*$ at excitation energies of 49 and 88 MeV. Similarly Galin et al.[25] give results for the reactions

$$^{14}N + {}^{103}Rh \rightarrow {}^{117}Te^* \quad (24a)$$

$$^{40}Ar + {}^{77}Se \rightarrow {}^{117}Te^* \quad (24b)$$

that give $^{117}Te^*$ at 71 and 107 MeV. In this section we will use their data on angular distributions and in the next section their relative cross sections.

In Fig. 4 we show some samples of the data for ^{4}He emission from Refs. 24 and 25 with fits to Eq. (3). The measured parameter β_{1m} can be determined with good precision from such fits, as can β_{2m} from similar fits of Eq. (16). With Eqs. (6), (10) and (17)-(22) we can calculate theoretical values of β_1 and β_2 if we assume that all H/He emission occurs at the first step of the evaporation chain. We give some calculated values of β_1 and β_2 in Table II along with E_{rot}, $\langle(\ell+\frac{1}{2})^2\rangle^{1/2}$ and the kinetic energy (above the barrier) from spinoff ξ plus thermal motions,[17] where:

$$\xi = 4E_{rot}\mu R^2/3\,\mathcal{J}. \quad (25)$$

In Fig. 5 we reproduce the anisotropy values vs exit-channel energy as measured by Reedy et al.[24] The qualitative features of these data follow the trends of the calculated values of β_1 and β_2 from Table II and Fig. 2: (1) Anisotropies for ^{4}He are about twice those for ^{1}H. (2) Anisotropy for H/He increases with mass of projectile (and presumably with the spin of the emitting compound nucleus). (3) Anisotropy increases with energy of the detected ^{4}He following the calculated trend of $\xi+2T$. (4) Anisotropy for ^{1}H varies less strongly with energy than for ^{4}He. (The opposite sense of this variation is not accounted for by the calculations given in Table II, and presumably indicates that ^{1}H emission is not confined to the first step.)

It would be desirable to use these data to fix the individual parameters in the statistical model and then adopt the calibrated model in its entirety. This would require an evaporation code to follow the emission probabilities in ε and Θ for each step in the deexcitation chain. An extensive data base of the partial reaction cross sections and possibly additional data would also be required to unravel the separate effects of $\mathcal{J}$, "a" and the transmission coefficients. We will follow the more limited objective of developing an empirical correlation between the data and the theoretical parameters calculated for first step emission only. Table III lists the experimental values of β_{1m} and β_{2m} for each reaction along with estimates of some other quantities that appear in Eqs. (14)-(18). Our objectives with these data are two fold: (1) to test the simple theoretical estimates in an absolute way and (2) to achieve a semiempirical correlation that can avoid the necessity of the determination of $\mathcal{J}$ or T or their correct averages over the whole evaporation chain. For this end we must treat the spins of the emitters as known quantities. We therefore assume the validity of the sharp cutoff approximation for P(J)

$$P(J)\begin{cases}\alpha\ (J+\frac{1}{2}) & \text{for } J \leq \ell_{cr} \\ = 0 & \text{for } J > \ell_{cr}\end{cases} \tag{26}$$

and therefore

$$\langle (J+\tfrac{1}{2})^2 \rangle = (\ell_{cr}+\tfrac{1}{2})^2/2 \ . \tag{27}$$

(We use the symbol J when a distribution of angular momenta is involved, as opposed to J_o which refers to a unique value.) Then to evaluate $\langle (J+\frac{1}{2})^2 \rangle$ we take ℓ_{cr} values from the equations and empirical systematics of Vaz and Alexander.[30] These values of ℓ_{cr} are given in column 3 of Table III. As we want to reduce the mass and temperature dependence of our correlation we divide the measured parameter β_{1m} by β_1'

$$\beta_1' = \frac{\hbar^2 \langle (\ell+\frac{1}{2})^2 \rangle^{1/2}}{2\,\mathcal{J}\,T} \tag{28}$$

and the measured parameter β_{2m} by β_2'

$$\beta_2' = \frac{\hbar^2 \mu R^2}{2\,\mathcal{J}\,\mathcal{J}_\perp T} \ . \tag{29}$$

Now in Table III and Fig. 6 we give (β_{1m}/β_1') and $(\beta_{2m}/\beta_2')^{1/2}$ vs $\langle (J+\frac{1}{2})^2 \rangle^{1/2}$. If we have calculated β_1' and β_2' correctly (i.e. as nature selects them) then we expect from Eqs. (4) and (17)

$$(\beta_{1m}/\beta_1') = \langle (J+\tfrac{1}{2})^2 \rangle^{1/2} \tag{30}$$

and

$$(\beta_{2m}/\beta_2')^{1/2} = \langle (J+\tfrac{1}{2})^2 \rangle^{1/2} . \tag{31}$$

If all particles are evaporated in the first step and if our parametrizations of Eqs. (18)-(22) are correct then all the points should lie on a 45 degree line

as in Eqs. (30) and (31) above. Nature is not quite this accommodating, however, and the actual results require two separate lines, one for $^{75}Br^{*}$ and one for $^{117}Te^{*}$. (The latter indicates a distinct saturation for the highest spin, but this is beyond our range of interest). These lines can be used as references for estimating the spins of emitters from measured values of β_{1m} or β_{2m}.

To illustrate this procedure we take an example from the work of Catchen et al.[27] for the reaction 724 MeV $^{86}Kr + ^{197}Au$. They have measured the out-of-plane correlation of ^{4}He from a collection of deeply inelastic products with estimated values of $\langle Z\rangle = 42$, $\langle A\rangle = 101$ and $\langle E^{*}\rangle = 86$ MeV. From fits of Eqs. (2) and (15) to their data, β_{1m} is reported to be 1.3 and β_{2m} to be 1.25. We wish to estimate the root-mean-square spin of the emitters from the data in Fig. 6. As T and $\langle(\ell+\frac{1}{2})^{2}\rangle$ in β_1' and T in β_2' depend on $\langle(J+\frac{1}{2})^{2}\rangle^{1/2}$ we must use an iterative (or trial and error) approach.

The quantities relevant to this trial and error technique are given in Table IV. Suppose we wish to obtain $J+\frac{1}{2}$ from a measured value of β_{1m} and an absolute estimate of β_1' from Eqs. (10), (18-22), and (28). First we assume a value of $J_o+\frac{1}{2}$ (e.g. 10); then we calculate β_1' and we obtain $\beta_{1m}/\beta_1' = 33$. From Eq. (30), β_{1m}/β_1' should give back our initially assumed value of 10 for $J+\frac{1}{2}$, but as $10 \neq 33$ we must try again. Next we assume $J_o+\frac{1}{2} = 20$ and recalculate $\beta_{1m}/\beta_1' = 28$; better but not yet the same. Then successively for initially assumed values of $J_o+\frac{1}{2}$ of 30, 40 and 50 we calculate $\beta_{1m}/\beta_1' = 22$, 17 and 11. From the trends of columns 1 and 2 in Table IV we see that an initially assumed $J_o+\frac{1}{2} \approx 25$ will give back a value of $J+\frac{1}{2} \approx 25$ for β_{1m}/β_1'. Therefore $J+\frac{1}{2} \approx 25$ is our estimate of the spin of the emitter by this path. From the path of β_2' from Eqs. (18-22) and (29) we would estimate $J+\frac{1}{2} \approx 28$ (columns 1 and 3 of Table IV).

For the above estimates we have not invoked any of the empirical information from the data for $^{75}Br^{*}$ and $^{117}Te^{*}$ in Fig. 6. For this purpose we can refer to columns 1, 2 and 4 in Table IV. First we assume a value of $J_o+\frac{1}{2} = 10$, then

calculate $\beta_{1m}/\beta_1' = 33$ and then from Fig. 6 for $^{75}Br^*$, we read $J+\frac{1}{2} \approx 47$. As $47 \neq 10$, we try again and for an initially assumed $J_o+\frac{1}{2} = 20$ we obtain (from Fig. 6 for $^{75}Br^*$) $J+\frac{1}{2} = 40$. Now from the trends of columns 1 and 4 in Table IV we estimate $J+\frac{1}{2} \approx 31$ from $^{75}Br^*$ and 21 from $^{117}Te^*$. Similar use of β_{2m}/β_2' leads to $\langle(J+\frac{1}{2})^2\rangle^{1/2}$ of 32 from $^{75}Br^*$ and 22 from $^{117}Te^*$. Thus it seems that one obtains consistent results from either the Ericson-Strutinski Eqs. (2) and (3), or the Halpern-Døssing Eqs. (15) and (16). For Z = 42, A = 101, one would probably take the mean or $\langle(J+\frac{1}{2})^2\rangle^{1/2} \approx 26$.

It is interesting to compare the results from this semiempirical analysis to that from Fig. 3 and absolute estimates of $\mathcal{J}$, μR^2 and T from Eqs. (18-22). As shown in Fig. 3 and Table IV the measured value β_{1m} yields a spin of 25 and that for β_{2m} gives 28. These estimates of the spin from absolute calculations are very close to those from empirical analysis. To some extent this is probably fortuitous for the following reasons:[17] (a) The absolute values of $\mathcal{J}$, μR^2 or "a" may be in error. (b) The ^4He emission may occur for several steps in the evaporation cascade and thus T may be in error. (c) For small T values the approximations of Eq. (1) and/or (7) may become inadequate. (d) Our estimates of ℓ_{cr} from Ref. 30 may be in error. (e) Spin fractionation may occur in the reference compound nuclei such that $\langle(J+\frac{1}{2})^2\rangle$ differs from $(\ell_{cr}+\frac{1}{2})^2/2$. Effects from (a, b, c and e) could alter the results obtained by use of the theory in an a priori way. However, all these are cancelled out to a large extent by the semiempirical use of the theory via Fig. 6. The mistakes made in calculating β_1' and β_2' for the construction of Fig. 6 are largely repeated for our system of unknown spin and therefore are cancelled out. In fact, if $(\ell_{cr}+\frac{1}{2})^2/2 = \langle(J+\frac{1}{2})^2\rangle$ for our reference systems $^{75}Br^*$ and $^{117}Te^*$ and if they are representative of the unknown group then all these errors are cancelled. The most important assumption in this procedure is that the distribution of evaporation probability in (E',J') space is comparable for unknown and

reference systems. For example, the neutron deficient reference nucleus $^{75}Br^*$ could possibly give a different weighting to evaporation of H or He near the end of its deexcitation chain compared to neutron rich products from $^{86}Kr + ^{197}Au$. Studies similar to those of Refs. 24 and 25 for more neutron rich compound nuclei can provide a way to evaluate this assumption. Also important are the values of ℓ_{cr} for the compound nuclei used for reference. Fusion cross sections have not been measured for $^{75}Br^*$ and $^{117}Te^*$ and thus we have had to resort to systematics. These systematics are far from secure at present for the higher energies of interest here.[30]

Exactly parallel problems exist for the calibration of J and T for sequential fission studies. For the H/He emission discussed in this paper the calibration studies of $^{75}Br^*$ and $^{117}Te^*$ have been made for compound nuclei with E^* and J very similar to those of the deeply inelastic fragments. For the fission studies most angular distribution calibrations have been made with incident ^4He projectiles that form fissile nuclei with much smaller excitations and spins.[6,7] Thus, at present, the calibrations must be more severely extrapolated for the fission studies. Also, only a few fission probability calibrations have been made for nuclei with Z, E and J very near to those studied in deeply inelastic reactions.[8,9]

IV. Empirical use of the $^4He/^1H$ ratio.

Thomas[32] and Gilat and Grover[33] have given very nice discussions of the expected spin dependence for the emission probabilities of $n/^1H/^4He$. The evaporation theory predicts that the ratio of ^4He to ^1H (or n) emission will increase with the spin of the emitter. Some quantitative calculations have been made by Galin et al.[25] for $^{117}Te^*$ and by Lu[34] for $^{78}Kr^*$, $^{84}Kr^*$ and $^{86}Kr^*$. Some of their results are shown on the right side of Fig. 7. The very steep

dependence of the $^4He/^1H$ ratio on J_{CN} suggests that this ratio can possibly be developed as another tool for reflecting spins of the fragments. The calculations of Lu for several isotopes of Kr^* indicate strong variations with mass number for the expected multiplicities of both ^1H and ^4He. As an accident of the binding energies, however, Lu finds that the ratio of ^4He to ^1H emission depends only slightly on mass for Kr^*. Calculations have not been made for the expected dependence on excitation energy so we must use the measurements as a guide.

On the left side of Fig. 7 we show the measured[35] multiplicity (or cross section) ratios for ^4He to ^1H evaporated from $^{75}Br^*$ and $^{117}Te^*$. The data are plotted against $\langle(J+\frac{1}{2})^2\rangle^{1/2}$ and ℓ_{cr}, obtained as discussed above and given in Table III. The calculations (right) were made for individual spin values (J_{CN}), but the measurements arise from a distribution of spins (as for example in Eqs. (26) and (27)). Therefore the increase of the measured multiplicity ratio with $\langle(J+\frac{1}{2})^2\rangle^{1/2}$ is less rapid than that calculated for J_{CN}. Nevertheless, there is a marked correlation with $\langle(J+\frac{1}{2})^2\rangle^{1/2}$ and no clear dependence on E^*. This result suggests that measurments of the $^4He/^1H$ ratio in deeply inelastic collisions can provide a probe of the fragment spins. Such measurements have been made in Refs. 27 and 36, and will be discussed there. For the example $^{101}_{42}Mo$ with $E^* = 86$ MeV, Ref. 27 reports $M_{He}/M_H = 0.5$; from Fig. 7 we would deduce $\langle(J_o+\frac{1}{2})^2\rangle^{1/2} \approx 33$ or $\ell_{cr} \approx 47$. It is clear that we can bolster our confidence in this tool by more extensive evaporation calculations and by more calibration measurements of ℓ_{cr} for other compound nuclei.

It should be emphasized that the multiplicity ratio (or indeed each value of M_{He} and M_H) will depend on the magnitudes of the spins only and not on their directions. The angular correlations as discussed in Sections II and III will

depend on their alignment also. Thus, in principle, the combination of these two types of measurement can provide evidence on both the spins and their degree of alignment. To exploit these possibilities, good precision is needed both for the calibration measurements of compound nuclei and for the angular correlation measurements in deeply inelastic reactions.

V. Conclusions

(1) The equations of Ericson and Strutinski,[16] Halpern,[28] and Døssing[18] give a consistent set for discussing angular correlations in compound-nucleus reactions and in deeply inelastic reactions, provided care is taken to use the appropriate averages of $(\ell+\frac{1}{2})$ and $(J+\frac{1}{2})$.

(2) A priori use of these equations to estimate fragment spins requires absolute calculation of appropriate averages of $\mathcal{J}$, μR^2 and T or the calculation of sums over an evaporation chain.

(3) Semiempirical estimates of fragment spins can be made by use of experimental data on angular distributions of H/He in compound nucleus reactions. This approach circumvents the absolute determination of $\mathcal{J}$ or T.

(4) Semiempirical use of multiplicity ratios for $^4He/^1H$ can also provide information concerning spins of the fragments.

(5) The combination of (3) and (4) above can, in principle, also give a probe of the alignment of the angular momenta.

Appendix

In experiments where one measures light particles (e.g. ^4He) in coincidence with a heavy reaction fragment, it is frequently important to carry out an integration of the data over the "light-particle space" to obtain a multiplicity or cross section. The theoretical angular correlations of such light particle emission with respect to the spin axis of the emitter are given by Eqs. (2) and

(15), above. In the course of our work, we have performed the required integrations of these theoretical relationships, and it may be useful to present the results here.

The coincidence experiment measures the double differential cross section $(d^2\sigma_L/d\Omega_H d\Omega_L)$, where the subscripts denote the light and heavy detected particles, respectively, and we want to integrate over the light-particle space to yield the cross section $(d\sigma_L/d\Omega_H)$. The angle θ is measured with respect to the spin axis (generally $\theta = 90°$ is in the reaction plane), and we assume that the angular correlation $W(\theta)$ is independent of the angle Θ in the reaction plane. Then we have

$$\left(\frac{d\sigma_L}{d\Omega_H}\right) = \int_{4\pi} \left(\frac{d^2\sigma_L}{d\Omega_H d\Omega_L}\right) d\Omega_L = \int_0^{2\pi} d\Theta \int_0^{\pi} W(\theta) \sin\theta d\theta$$

$$= 4\pi \int_0^{\pi/2} W(\theta) \sin\theta d\theta . \qquad \text{(A1)}$$

Using the Ericson-Strutinski expression, Eq. (2):

$$W_{J_o, \ell, \mathcal{J}^T}(\theta) \propto I_o\ (2\beta_1 \sin\theta) \qquad (2)$$

we have

$$\left(\frac{d\sigma_L}{d\Omega_H}\right)_{ES} = 4\pi C \int_0^{\pi/2} I_o\ (2\beta_1 \sin\theta) \sin\theta d\theta, \qquad \text{(A2)}$$

where C is a normalization constant. Eq. (A2) cannot be integrated in closed form; however, a standard power series expansion and integration term-by-term leads to the result:

$$\left(\frac{d\sigma_L}{d\Omega_H}\right)_{ES} = 4\pi C \sum_{n=0}^{\infty} \frac{\beta_1^{2n}(2n)!!}{(n!)^2(2n+1)!!} . \qquad \text{(A3)}$$

The constant C corresponds to the magnitude of the double differential cross section in the spin direction ($\theta = 0$). While somewhat laborious to use,

Eq. (A3) can be programmed for a computer without much difficulty.

It turns out that the Døssing-Halpern expression, Eq. (15)

$$W_{J_o, \mathcal{J}T}(\theta) \propto \exp(\beta_2 \sin^2 \theta), \tag{15}$$

has a practical advantage in the present context, namely that the required integration can be carried out in closed form. Analogous to Eq. (A2) we write

$$\left(\frac{d\sigma_L}{d\Omega_H}\right)_{DH} = 4\pi C \int_0^{\pi/2} \exp(\beta_2 \sin^2 \theta) \sin \theta d\theta, \tag{A4}$$

which integrates (by change of variable and several substitutions) to:

$$\left(\frac{d\sigma_L}{d\Omega_H}\right)_{DH} = 4\pi C \left\{\frac{1}{2} \left(\frac{\pi}{\beta_2}\right)^{1/2} \exp(\beta_2) \operatorname{erf}(\beta_2^{1/2})\right\}. \tag{A5}$$

The normalization constant C has the same significance as in Eq. (A3). It is interesting to note that a relation completely equivalent to Eq. (A5) (but less convenient) can be derived from Eq. (A4) by series expansion and integration as was done in deriving Eq. (A3). The result is

$$\left(\frac{d\sigma_L}{d\Omega_H}\right)_{DH} = 4\pi C \sum_{n=0}^{\infty} \frac{\beta_2^n (2n)!!}{(n!)(2n+1)!!}, \tag{A6}$$

which demonstrates once again the similarity of the E-S and D-H approaches.

In terms of Eq. (A5), the analysis of out-of-plane coincidence data is straightforward and simple:

1) Fit the out-of-plane correlation data to the function $W(\theta) = C \exp(\beta_2 \sin^2 \theta)$ to evaluate the parameters C and β_2. (This is very easy to do graphically.) C is the intensity at $\theta = 0$ (the spin axis) and is easily obtained as $C = W(90°)/\exp(\beta_2)$, where $W(90°)$ is the in-plane measurement.

2) Look up erf $(\beta_2^{1/2})$ in standard tables.

3) Substitute C, β_2, and erf $(\beta_2^{1/2})$ into Eq. (A5) to obtain the cross section integrated over the "light particle space".

Acknowledgements

We would like to thank Dr. H. Ho for calling our attention to Ref. 18 and Dr. T. Døssing for providing us with a preprint of his unpublished work. Dr. N. H. Lu kindly made available the results of his unpublished calculations. We appreciate helpful discussions with each of the above, as well as with Dr. P. J. Karol. This work was supported in part by the Division of Nuclear Physics of the U. S. Department of Energy.

References

(a) Permanent address: Laboratoire de Chimie Nucléaire, Institut de Physique Nucléaire, B.P. No. 1, 91406, Orsay, France.

1. W. U. Schröder and J. R. Huizenga, Ann. Rev. Nucl. Sci. 27, 465 (1977).
2. M. Lefort and C. Ngô, La Rivista del Nuovo Cimento (to be published 1979); M. Lefort and C. Ngô, Ann. Phys. (Paris) 3, 5 (1978).
3. P. Dyer, R. J. Puigh, R. Vandenbosch, T. D. Thomas, and M. S. Zisman, Phys. Rev. Lett. 39, 392 (1977).
4. G. J. Wozniak, R. P. Schmitt, P. Glässel, R. C. Jared, G. Bizard, and L. G. Moretto, Phys. Rev. Lett. 40, 1436 (1978).
5. H. J. Specht, Max Planck Institut, Report MPI H V 26 (1978); D. v. Harrach, P. Glässel, Y. Civelekoglu, R. Männer, and H. J. Specht, Phys. Rev. Lett. 42, 1728 (1979).
6. P. Dyer, R. J. Puigh, R. Vandenbosch, T. D. Thomas, M. S. Zisman, and L. Nunnelley, Nucl. Phys. (in press).
7. J. R. Huizenga, R. Vandenbosch, Nuclear Fission, Academic Press, New York (1973).
8. M. Rajagopalan, L. Kowalski, D. Logan, M. Kaplan, J. M. Alexander, M. S. Zisman, and J. M. Miller, Phys. Rev. C19, 54 (1979).
9. J. M. Miller, D. Logan, G. L. Catchen, M. Rajagopalan, J. M. Alexander, M. Kaplan, J. W. Ball, M. S. Zisman, and L. Kowalski, Phys. Rev. Lett. 40, 1074 (1978).
10. P. Russo, R. P. Schmitt, G. J. Wozniak, B. Cauvin, P. Glässel, R. C. Jared, and L. G. Moretto, Phys. Lett. 67B, 155 (1977).
11. L. G. Moretto, LBL-6587, 1977 (unpublished).
12. R. S. Simon, M. V. Banaschik, J. O. Newton, R. M. Diamond, and F. S. Stephens, Phys. Rev. Lett. 36, 359 (1976); J. O. Newton, S. H. Sie, and G. D. Dracoulis, Phys. Rev. Lett. 40, 625 (1978).

13. R. A. Dayras, R. G. Stokstad, C. B. Fulmer, D. C. Hensley, M. L. Halbert, R. L. Robinson, A. H. Snell, D. G. Sarantites, L. Westerberg, and J. H. Barker, Phys. Rev. Lett. 42, 697 (1979).

14. R. J. Liotta and R. A. Sorenson, Nucl. Phys. A297, 136 (1978).

15. J. B. Natowitz, M. N. Namboodiri, P. Kasiraj, R. Eggers, L. Ader, P. Gonthier, C. Cerruti, and T. Alleman, Phys. Rev. Lett. 40, 751 (1978).

16. T. Ericson and V. Strutinski, Nucl. Phys. 8, 284 (1958); ibid 9, 689 (1959).

17. T. Ericson, Adv. in Phys. 9, 423 (1960).

18. T. Døssing, preprint, 1978.

19. W. J. Knox, A. R. Quinton, and C. E. Anderson, Phys. Rev. 120, 2120 (1960).

20. C. E. Hunting, Phys. Rev. 123, 606 (1961).

21. H. C. Britt and A. R. Quinton, Phys. Rev. 124, 877 (1961).

22. F. E. Durham and M. L. Halbert, Phys. Rev. 137, B850 (1965).

23. C. Brun, B. Gatty, M. Lefort and X. Tarrago, Nucl. Phys. A116, 177 (1968).

24. R. C. Reedy, M. J. Fluss, G. F. Herzog, L. Kowalski, and J. M. Miller, Phys. Rev. 188, 1771 (1969); R. C. Reedy, Ph.D. Thesis, Columbia University, 1969 (unpuslished).

25. J. Galin, B. Gatty, D. Guerreau, C. Rousset, U. C. Schlotthauer-Voos, and X. Tarrago, Phys. Rev. C9, 1113 (1974); ibid C9, 1126 (1974); ibid C10, 638 (1974).

26. R. Albrecht, W. Dünnweber, G. Graw, H. Ho, S. G. Steadman, and J. P. Wurm, Phys. Rev. Lett. 34, 1400 (1975); H. Ho, R. Albrecht, W. Dünwebber, G. Graw, S. G. Steadman, J. P. Wurm, D. Disdier, V. Rauch, and F. Scheibling, Z. Physik A283, 235 (1977).

27. G. L. Catchen, D. Logan, J. M. Miller, D. Benson, N. H. Lu, T. W. Debiak, M. Rajagopalan, J. M. Alexander, M. Kaplan, and M. S. Zisman, preprint, 1979; G. L. Catchen, Ph.D. Thesis, Columbia University, 1979 (unpublished).

28. C. R. Gruhn, Ph.D. Thesis, University of Washington, 1961 (unpublished).

29. Following Ref. 18, however, we use semiclassical approximations for the magnitudes of the various angular momenta; i.e. $J(J+1) \rightarrow (J+\frac{1}{2})^2$ and $\ell(\ell+1) \rightarrow (\ell+\frac{1}{2})^2$.

30. L. C. Vaz and J. M. Alexander, Phys. Rev. C18, 2152 (1978); H. Delagrange, D. Logan, M. F. Rivet, M. Rajagopalan, J. M. Alexander, M. S. Zisman, M. Kaplan, and J. W. Ball, preprint (1979). Fig. 3 in the latter paper shows a number of comparisons between recent data and the systematics for ℓ_{cr} given in the former paper.

31. M. A. McMahan and J. M. Alexander, Phys. Rev. C (in press). Values of r_o, R_p and R_α for fusion are discussed in this paper. We have used r_o = 1.42 fm, R_p = 1.44 fm and R_α = 2.53 fm. (These values are from empirical correlations. Potential models generally give larger values of r_o, especially for ^{1}H, and this can be important for absolute estimates of β_1' or β_2'.).

32. T. D. Thomas, Nucl. Phys. 53, 538 (1964); Ann. Rev. Nucl. Sci. 18, 343 (1968).

33. J. Gilat and J. R. Grover, Phys. Rev. C3, 734 (1971).

34. N. H. Lu, private communication, 1978.

35. In Ref. 24 the spectra for ^{1}H and ^{4}He did not cover the complete energy span of the evaporated particles. We have estimated corrections due to these unobserved parts of the energy spectra. For ^{75}Br*, E^* = 49 MeV, we estimate the total emission multiplicity for ^{1}H (M_H) to be 1.08, 1.09 and 1.23 for reactions induced by ^{11}B, ^{12}C and ^{16}O respectively. For ^{4}He the corresponding total emission multiplicities M_{He} are 0.29, 0.37 and 0.41. For ^{75}Br*, E^* = 88 MeV, M_H = 1.73, 1.87 and 1.70 while M_{He} = 0.70, 0.87 and 1.0 for ^{11}B, ^{12}C and ^{16}O reactions respectively. In each case we have divided the estimated evaporative cross section for ^{1}H or ^{4}He by the fusion cross section σ_{cf} from Ref. 30; i.e., $\sigma_{cf} = \pi\lambda^2 (\ell_{cr}+1)^2$ (values of ℓ_{cr} listed in Table III.)

36. D. Logan, M. Rajagopalan, M. S. Zisman, J. M. Alexander, M. Kaplan, and L. Kowalski, preprint, 1979.

TABLE I

Theoretical angular dependence of evaporation probabilities.

	Correlation with respect to a unique spin vector (coincidence experiment) $W(\theta)/W(90^\circ)$							Distribution with respect to beam axis, spin vectors perpendicular to the beam (singles experiment) $W(\Theta)/W(90^\circ)$					
β_1	20°	30°	40°	50°	60°	70°	80°	120°	140°	150°	160°	170°	180°
				Eq. (2)							Eq. (3)		
0.5	0.813	0.840	0.874	0.910	0.945	0.974	0.993	1.03	1.07	1.09	1.11	1.12	1.12
1.0	0.491	0.555	0.640	0.736	0.835	0.920	0.979	1.09	1.23	1.30	1.37	1.41	1.42
1.5	0.262	0.337	0.444	0.579	0.727	0.865	0.964	1.15	1.40	1.55	1.68	1.77	1.80
2.0	0.135	0.202	0.307	0.455	0.633	0.813	0.949	1.19	1.54	1.76	1.97	2.12	2.18
2.5	0.069	0.121	0.213	0.359	0.553	0.765	0.934	1.21	1.63	1.92	2.21	2.43	2.52
3.0	0.035	0.073	0.149	0.283	0.482	0.720	0.920	1.21	1.68	2.04	2.41	2.71	2.82
3.5	0.018	0.044	0.104	0.224	0.422	0.677	0.906	1.21	1.71	2.12	2.58	2.95	3.10
5.0	0.003	0.010	0.034	0.111	0.282	0.565	0.865	1.19	1.72	2.24	2.92	3.53	3.78
β_2				Eq. (15)							Eq. (16)		
0.5	0.643	0.687	0.746	0.813	0.883	0.943	0.985	1.06	1.14	1.19	1.23	1.26	1.26
1.0	0.414	0.472	0.556	0.662	0.779	0.890	0.970	1.10	1.27	1.37	1.46	1.53	1.55
1.5	0.266	0.325	0.415	0.538	0.687	0.839	0.956	1.14	1.39	1.55	1.70	1.81	1.85
2.0	0.171	0.223	0.309	0.438	0.607	0.791	0.941	1.16	1.48	1.70	1.92	2.08	2.15
2.5	0.110	0.153	0.231	0.356	0.535	0.746	0.927	1.18	1.55	1.83	2.12	2.35	2.44
3.0	0.071	0.105	0.172	0.290	0.472	0.704	0.913	1.19	1.61	1.94	2.30	2.60	2.72
3.5	0.045	0.072	0.128	0.235	0.417	0.664	0.900	1.19	1.65	2.02	2.46	2.84	2.99
5.0	0.012	0.023	0.053	0.127	0.287	0.557	0.860	1.19	1.69	2.18	2.82	3.44	3.70

TABLE II

Absolute calculations for ^{1}H and ^{4}He evaporated from ^{75}Br excited to 88 MeV.

		^{4}He				^{1}H			
$J_0+\frac{1}{2}$	E_{rot} (MeV)	$\langle(\ell+\frac{1}{2})^2\rangle^{1/2}$	β_1	β_2	ξ +2T	$\langle(\ell+\frac{1}{2})^2\rangle^{1/2}$	β_1	β_2	ξ +2T
0	0	5.4	0	0	6.2	2.8	0	0	6.4
10	2.7	5.8	0.56	0.27	7.1	2.8	0.25	0.059	6.5
20	10.9	7.1	1.47	1.15	9.8	2.9	0.55	0.25	6.9
33	28.8	9.6	3.90	3.65	15.4	3.1	1.12	0.79	7.6
40	43.6	11.5	7.18	6.93	19.9	3.2	1.75	1.45	8.0
50	68.0	13.9	48.1	47.9	25.9	3.5	5.01	4.76	8.0

TABLE III

Measured and calculated quantities related to evaporation of ^{4}He and ^{1}H.

Reaction	E^{*} [a] (MeV)	ℓ_{cr} [b]	J_{rms} [c]	$W(180^{\circ})/W(90^{\circ})$ [d]		T [e] (MeV)		$\langle(\ell+\frac{1}{2})^2\rangle^{1/2}$ [f]		β_{1m} [g]		β_{1m}/β'_1 [h]		β_{2m} [g]		$(\beta_{2m}/\beta'_2)^{1/2}$ [h]	
				^{4}He	^{1}H	^{4}He	^{1}H	^{4}He	^{1}H	^{4}He	^{1}H	^{4}He	^{1}H	^{4}He	^{1}H	^{4}He	^{1}H
$^{11}B + ^{64}Zn$	49	24	17	1.49	1.23	1.9	2.0	5.8	2.4	1.09	0.71	12	21	0.90	0.45	14	22
$^{12}C + ^{63}Cu$	49	29	21	1.78	1.36	1.7	1.9	6.5	2.4	1.47	0.93	13	26	1.38	0.69	17	26
$^{16}O + ^{59}Co$	49	27	19	1.86	1.32	1.8	1.9	6.2	2.4	1.58	0.85	15	24	1.51	0.60	18	25
$^{11}B + ^{64}Zn$	88	38	27	1.89	1.28	2.6	2.7	8.4	3.0	1.62	0.79	17	26	1.56	0.53	22	28
$^{12}C + ^{63}Cu$	88	40	28	2.21	1.46	2.6	2.7	8.7	3.0	2.05	1.06	21	34	2.10	0.85	26	35
$^{16}O + ^{59}Co$	88	46	33	2.58	1.47	2.4	2.5	9.6	3.1	2.56	1.07	21	31	2.74	0.86	28	34
$^{14}N + ^{103}Rh$	71	41	29	1.87	1.32	2.2	2.0	7.0	2.7	1.60	0.85	36	48	1.53	0.60	36	47
$^{40}Ar + ^{77}Te$	71	49	35	2.53	1.43	2.1	1.9	7.7	2.8	2.51	1.02	49	54	2.66	0.80	47	53
$^{14}N + ^{103}Rh$	107	53	37	1.94	1.34	2.7	2.6	8.5	3.1	1.69	0.89	39	55	1.65	0.63	42	54
$^{40}Ar + ^{77}Se$	107	83	59	3.16	1.53	2.2	2.1	11.4	3.3	3.62	1.15	50	54	3.84	0.97	58	60

a Cross excitation energy without subtraction of E_{rot}.
b Estimated according to Ref. 30.
c $J_{rms} = \langle(J+\frac{1}{2})^2\rangle^{1/2} = [(\ell_{cr}+\frac{1}{2})^2/2]^{1/2}$
d From Refs. 24 and 25; we estimate uncertainties to be $\approx \pm$ 10%. The data were fit to Eq.(3); for $^{75}Br^{*}$ in Ref. 24 the fitting curve included only $P_2(\cos\theta)$.
e Eqs. (18-20) and (22) with $\langle\epsilon\rangle$ taken from experimental data.
f Eqs. (10-14)
g From fits to measurements as in Fig. 4.
h If the equations are all absolutely correct $(\beta_{1m}/\beta'_1) = (\beta_{2m}/\beta_2')^{1/2} = J_{rms}$; see Eqs. (28-31).

TABLE IV

Estimation of $\langle (J+\frac{1}{2})^2 \rangle^{1/2}$ by trial and error for one case $^{101}_{42}Mo$, $E^* = 86$ MeV, $\beta_{1m} = 1.30$, $\beta_{2m} = 1.25$.

Initially assumed $J_o+\frac{1}{2}$	Calculated $\frac{\beta_{1m}}{\beta_1}\left(\frac{\beta_{2m}}{\beta_2}\right)^{1/2}$		$\langle (J+\frac{1}{2})^2 \rangle^{1/2}$ Reestimated from Fig. 6 from (β_{1m}/β_1')		$(\beta_{2m}/\beta_2')^{1/2}$	
			$^{75}Br^*$	$^{117}Te^*$	$^{75}Br^*$	$^{117}Te^*$
10	33	30	47	26	36	25
20	28	29	40	22	35	24
30	22	28	32	18	33	23
40	17	26	25		30	
50	11	24	15		28	

Figure Captions

Fig. 1. $\langle(\ell+\frac{1}{2})^2\rangle^{1/2}\ b^{1/2}$ vs. $(J_o+\frac{1}{2})$ for various values of η. From Eq. (10) $\langle(\ell+\frac{1}{2})^2\rangle^{1/2}\ b^{1/2}$ is a universal function of J and η for all emitters, where $b = (\hbar^2 \mathcal{J}_\perp / 2\mu R^2 \mathcal{J} T)$ and $\eta = (2\hbar^2 \mu R^2 / \mathcal{J} \mathcal{J}_\perp T)^{1/2}$.

Fig. 2. (a) Anisotropy with respect to the angular momentum vector vs. β_1 from Eq. (2) and vs. β_2 from Eq. (15). A coincidence requirement is needed to specify the direction of the spin vector.

(b) Anisotropy with respect to the beam axis in compound nucleus reactions vs. β_1 from Eq. (3) and vs. β_2 from Eq. (16). This representation corresponds to angular distributions measured in the singles mode.

Fig. 3. β_1 and β_2 vs. $J_o+\frac{1}{2}$ for one nuclide (Z = 42, A = 101, E^* = 86 MeV). Eqs. (4, 17-22). The crosses (+) indicate measured values of β_{1m} and β_{2m} (Ref. 27).

Fig. 4. Sample fits of Eq. (3) to some of the ^{4}He data from Refs. 24 and 25. Values of β_{1m} from the fits are as indicated.

Fig. 5. W(180°)/W(90°)-1 vs. exit channel energy for ^{4}He and ^{1}H from the three reactions forming ^{75}Br* compound nuclei at gross excitation energy 88 MeV (after Ref. 24). See Table II and Fig. 2 for comparisons to theory.

Fig. 6. (β_{1m}/β_1') and $(\beta_{2m}/\beta_2')^{1/2}$ vs. $\langle(J+\frac{1}{2})^2\rangle^{1/2}$ for ^{75}Br* and ^{117}Te*. Symbols are for the reactions indicated; filled for ^{4}He (left scale), open for ^{1}H (right scale). The lines — . — . (^{117}Te*) and — — — (^{75}Br*) were drawn from the origin to the experimental data points.

Fig. 7. Right: Multiplicity ratio M_{He}/M_H for $^4He/^1H$ calculated from evaporation theory (Refs. 25 and 34) for individual initial spin values J_{CN}. For ^{117}Te only first step emission is considered; for ^{75}Br the complete deexcitation was followed.

Left: Measured ratios of $^4He/^1H$ evaporated from $^{75}Br^*$ and $^{117}Te^*$, Refs. 24 and 25. A correction was made for the unobserved part of the spectra for Ref. 24.

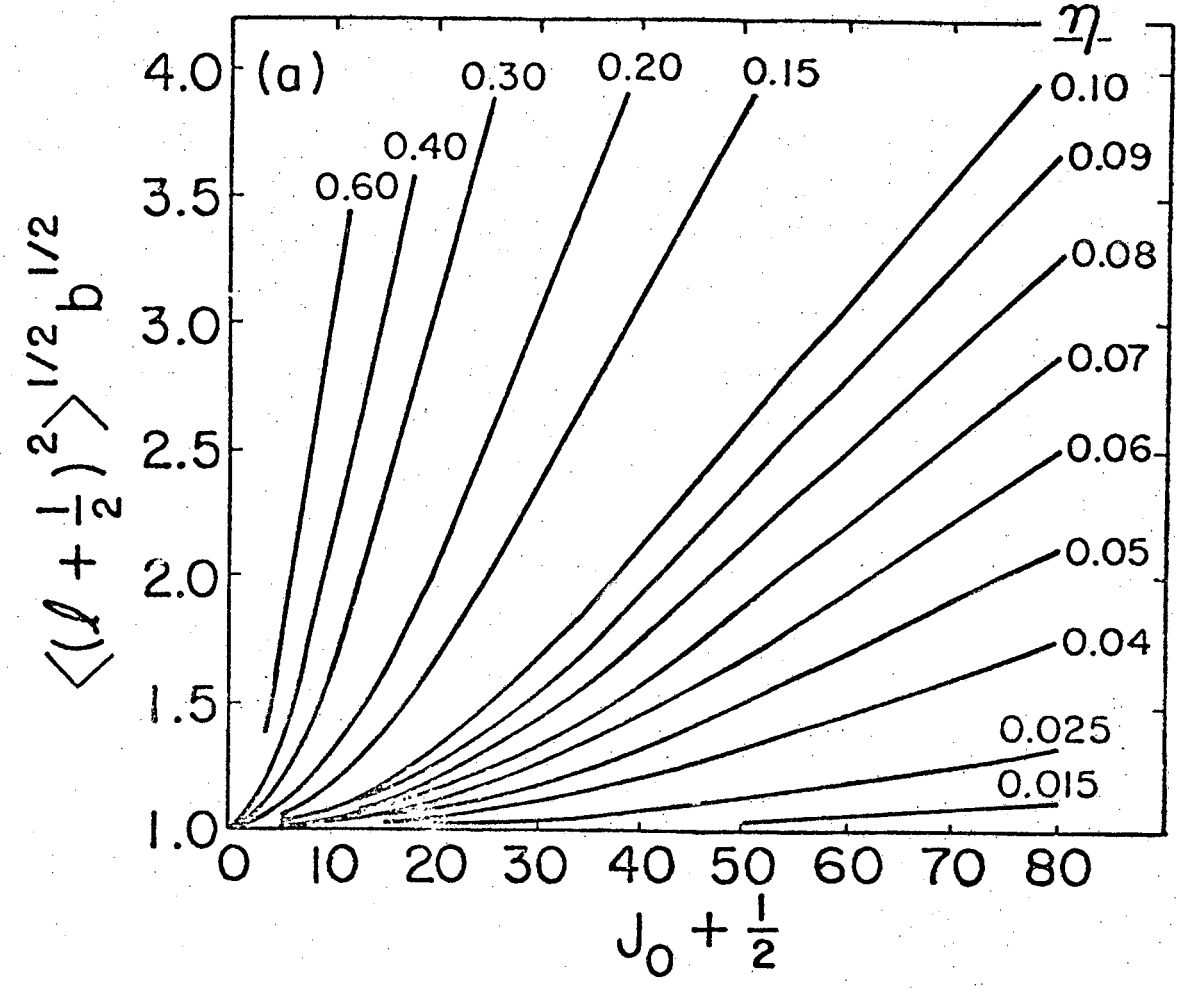
(a)
η_-
0.60
0.40
0.30
0.20
0.15
0.10
0.09
0.08
0.07
0.06
0.05
0.04
0.025
0.015
4.0
3.5
3.0
2.5
2.0
1.5
1.0
0
10
20
30
40
50
60
70
80
$\langle(\ell+\frac{1}{2})^2\rangle^{1/2} b^{1/2}$
$J_0+\frac{1}{2}$

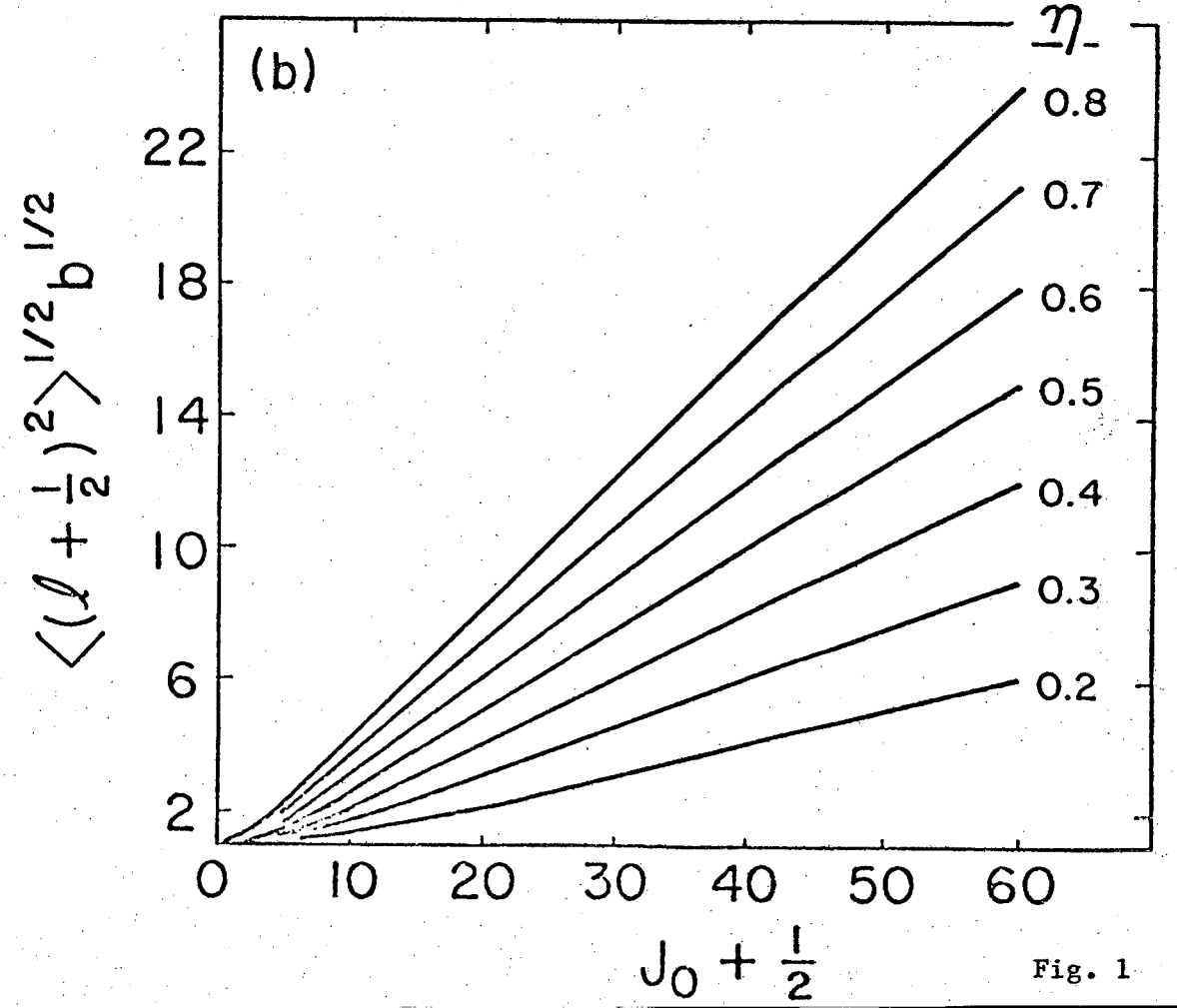
(b)
η_-
0.8
0.7
0.6
0.5
0.4
0.3
0.2
22
18
14
10
6
2
0
10
20
30
40
50
60
$\langle(\ell+\frac{1}{2})^2\rangle^{1/2} b^{1/2}$
$J_0+\frac{1}{2}$

Fig. 1

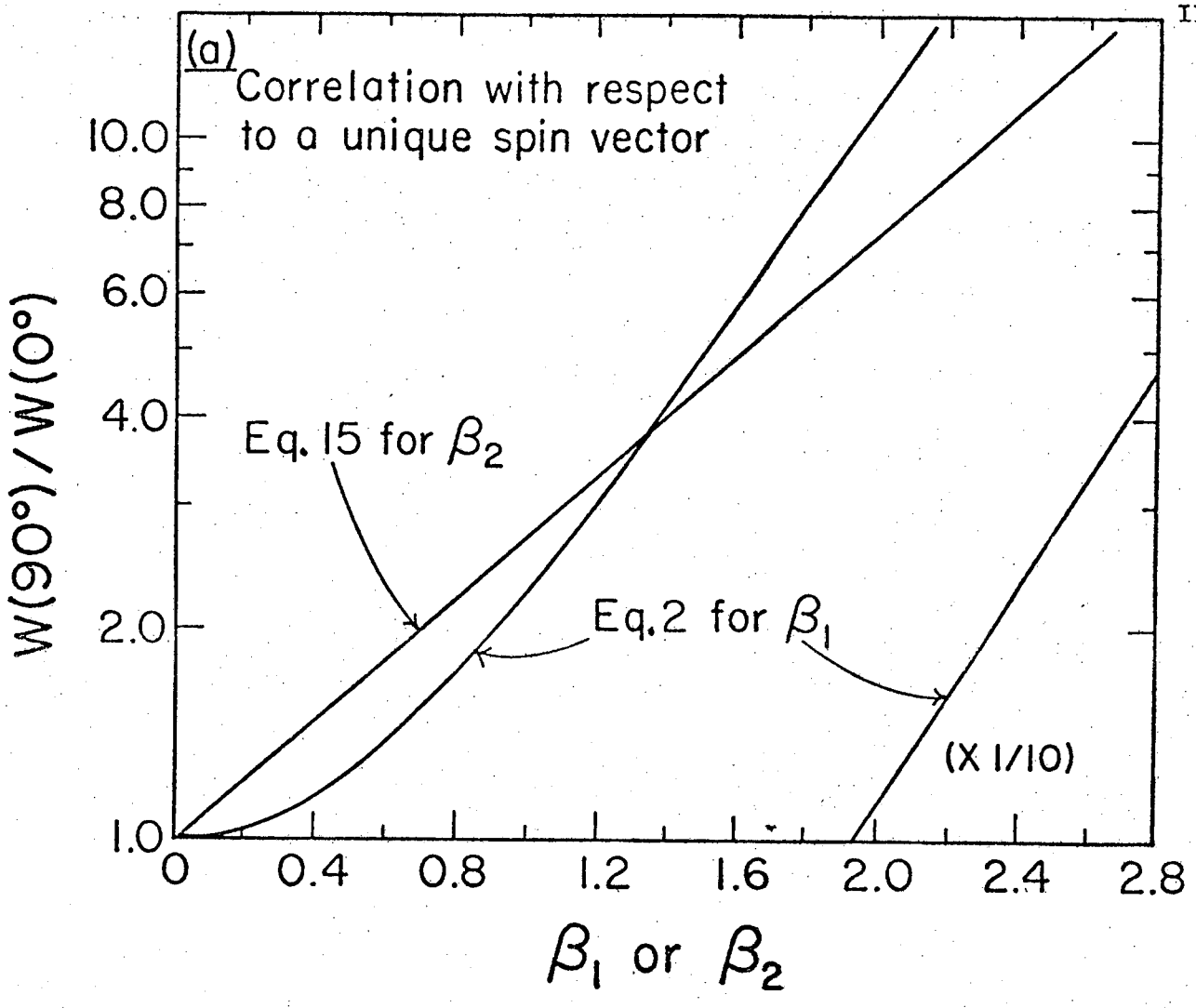
(a) Correlation with respect to a unique spin vector
W(90°)/W(0°)
10.0
8.0
6.0
4.0
2.0
1.0
Eq. 15 for β_2
Eq. 2 for β_1
(X 1/10)
0
0.4
0.8
1.2
1.6
2.0
2.4
2.8
β_1 or β_2

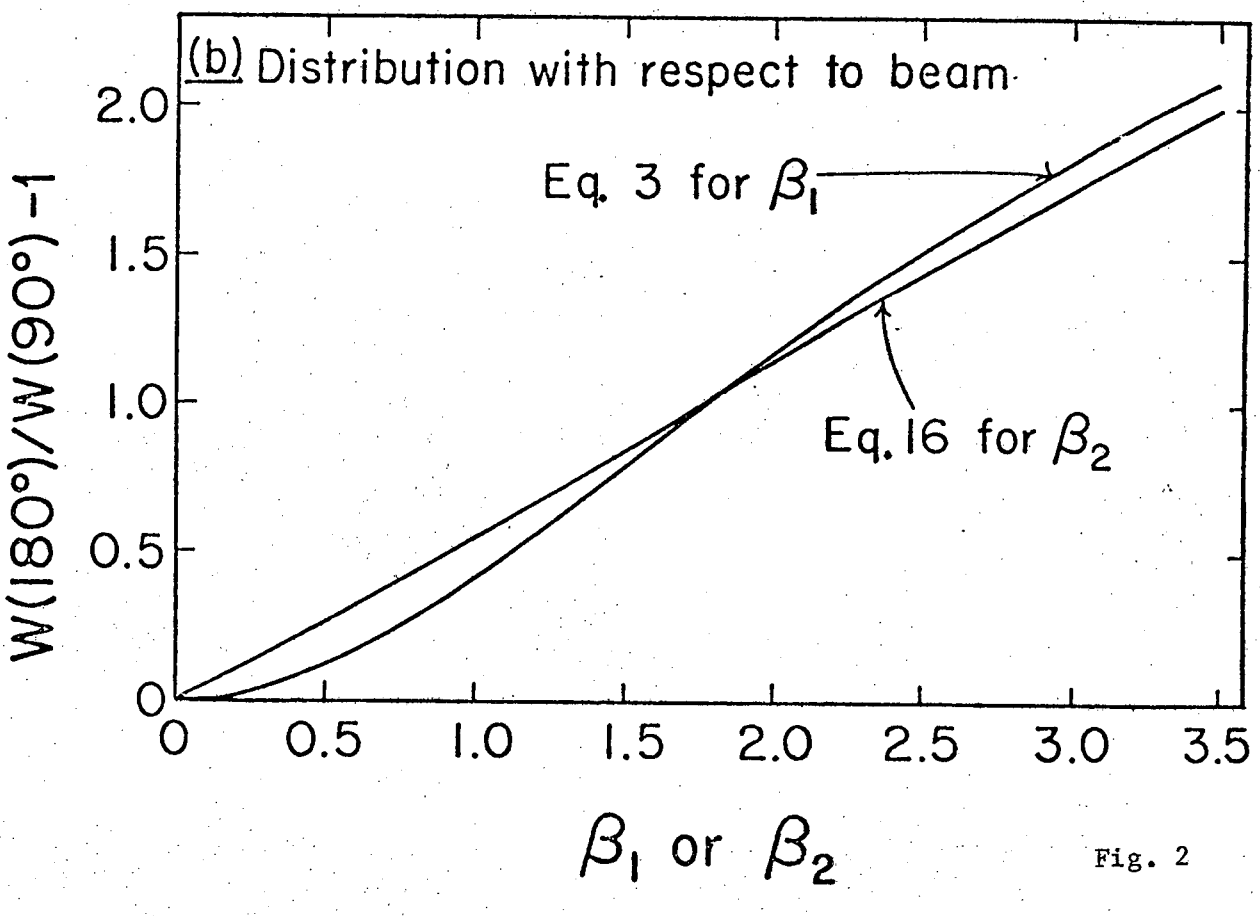
(b) Distribution with respect to beam
W(180°)/W(90°)-1
2.0
1.5
1.0
0.5
0
Eq. 3 for β_1
Eq. 16 for β_2
0
0.5
1.0
1.5
2.0
2.5
3.0
3.5
β_1 or β_2

Fig. 2

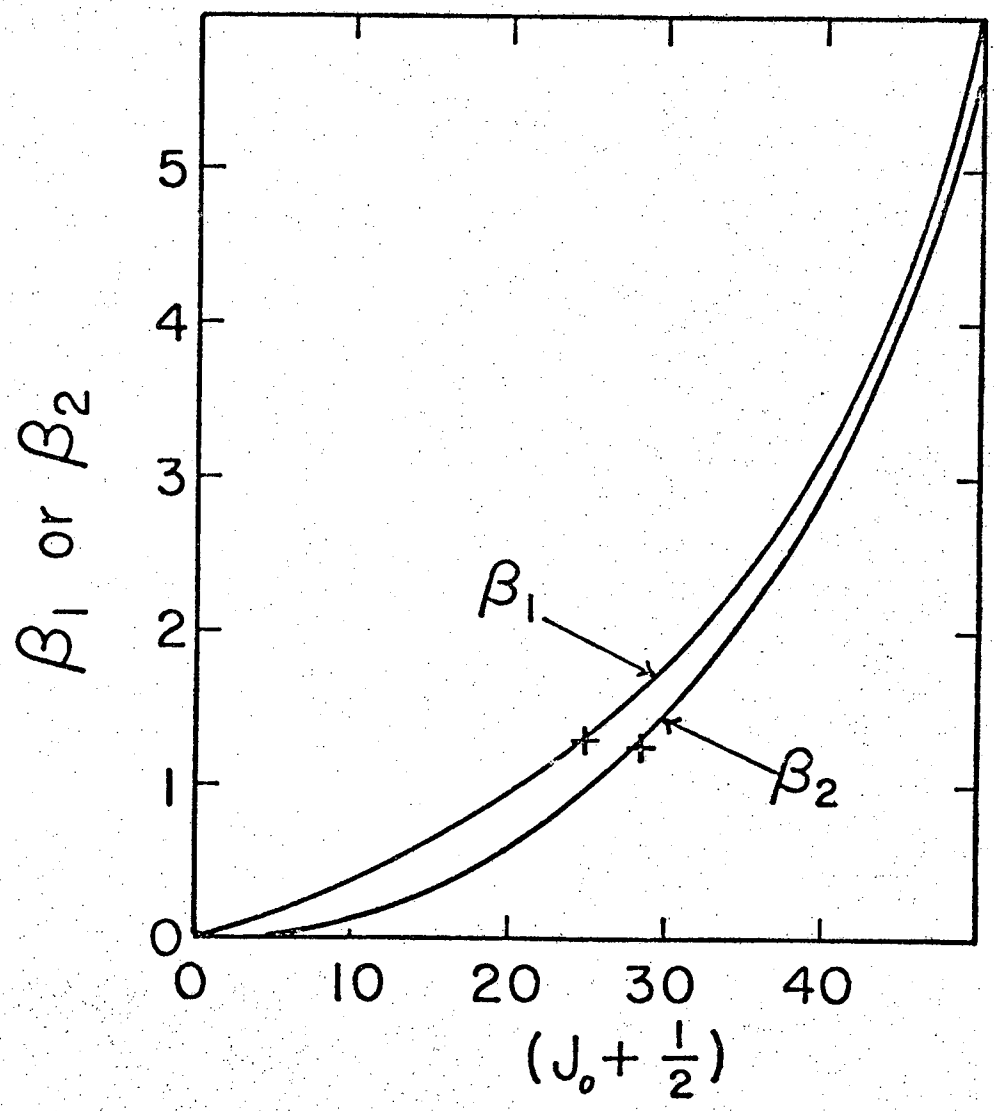

Fig. 3

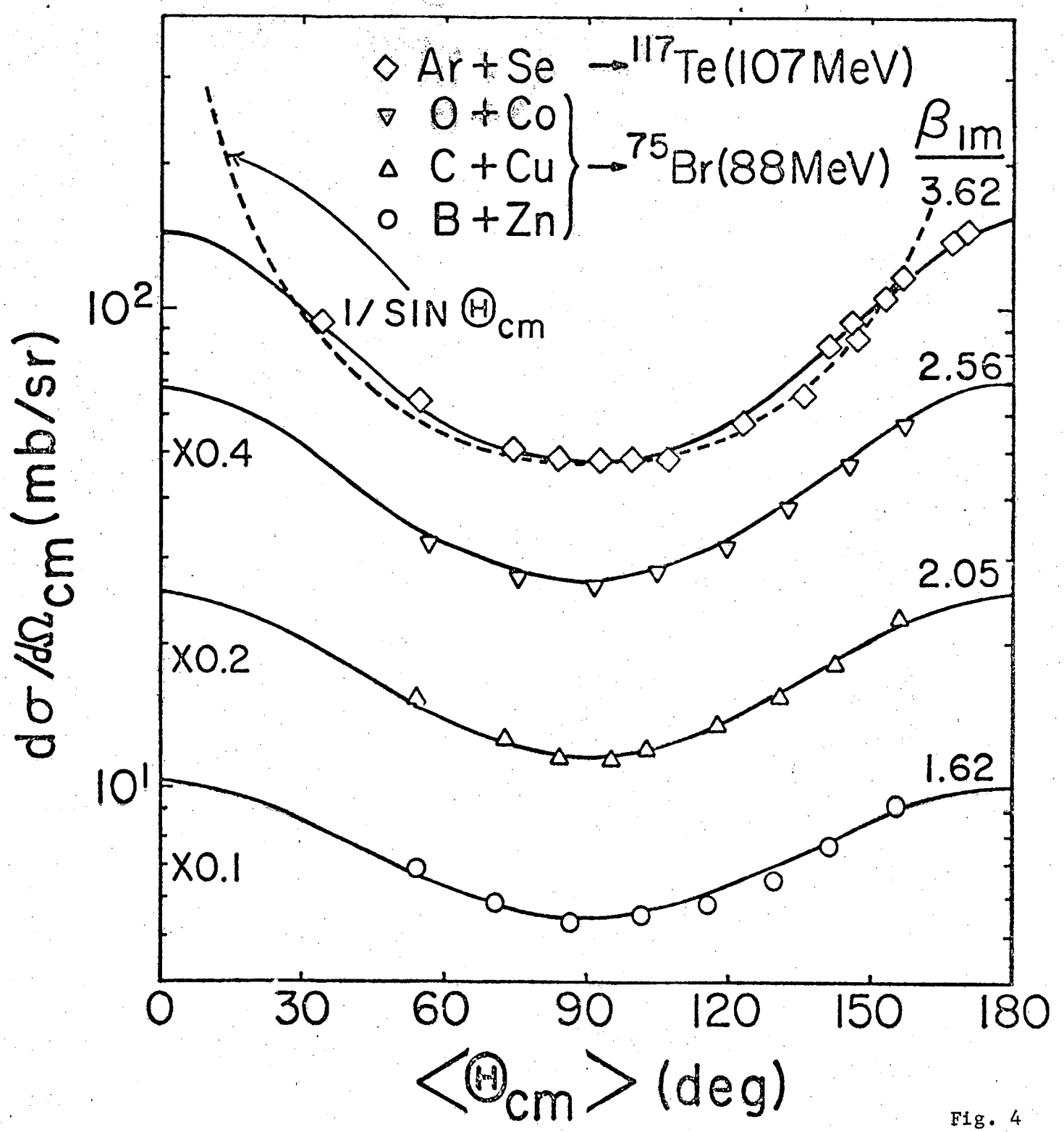
◇ Ar + Se → 117Te(107 MeV)
▽ O + Co
△ C + Cu → 75Br(88 MeV)
○ B + Zn
βim
3.62
2.56
2.05
1.62
1/SIN Θcm
X0.4
X0.2
X0.1
10²
10¹
dσ/dΩcm (mb/sr)
0
30
60
90
120
150
180
<Θcm> (deg)

Fig. 4

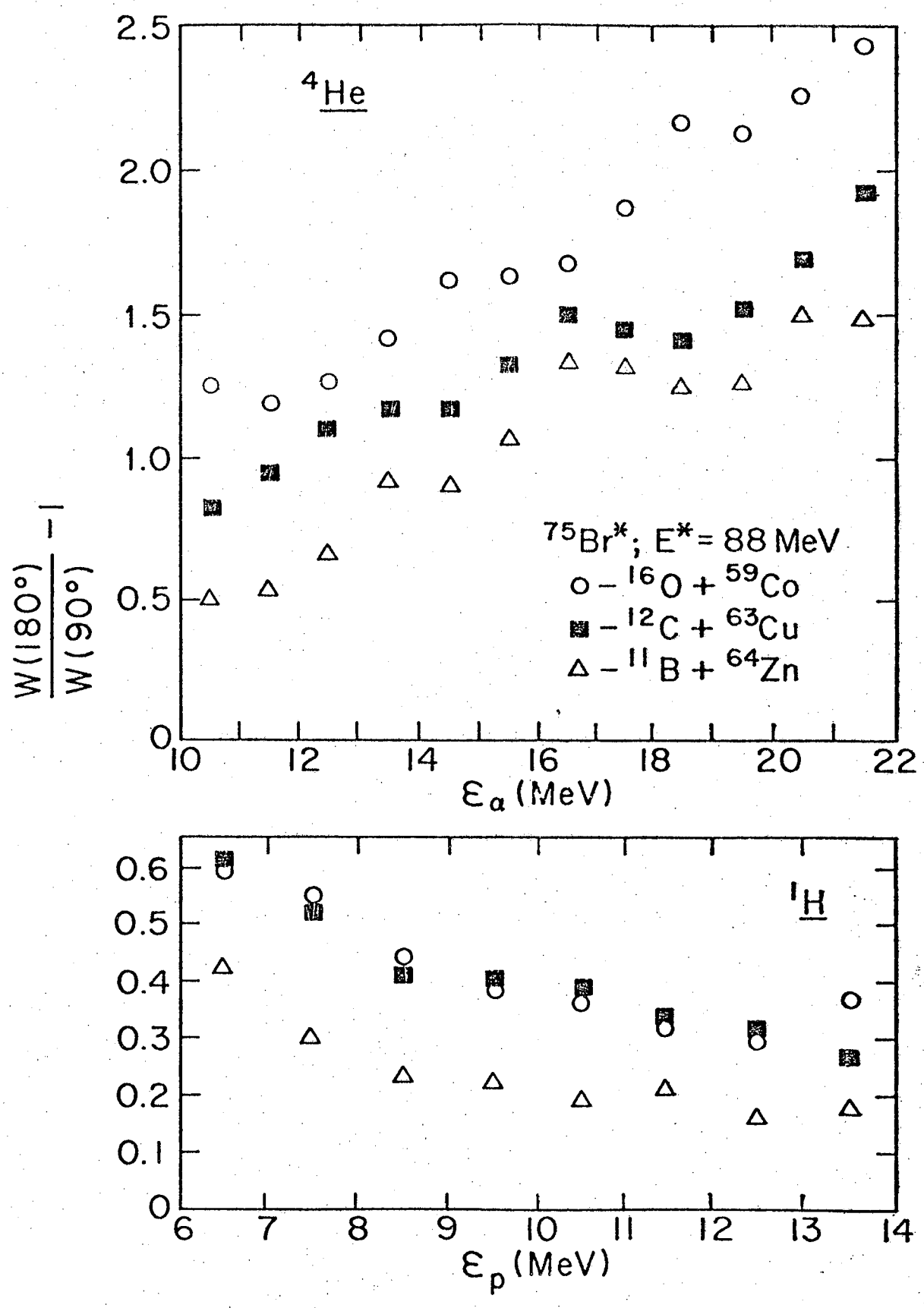
^{4}He
^{75}Br*; E* = 88 MeV
o – ^{16}O + ^{59}Co
■ – ^{12}C + ^{63}Cu
Δ – ^{11}B + ^{64}Zn
$\frac{W(180°)}{W(90°)}$
ε_α (MeV)
^{1}H
ε_p (MeV)

Fig. 5

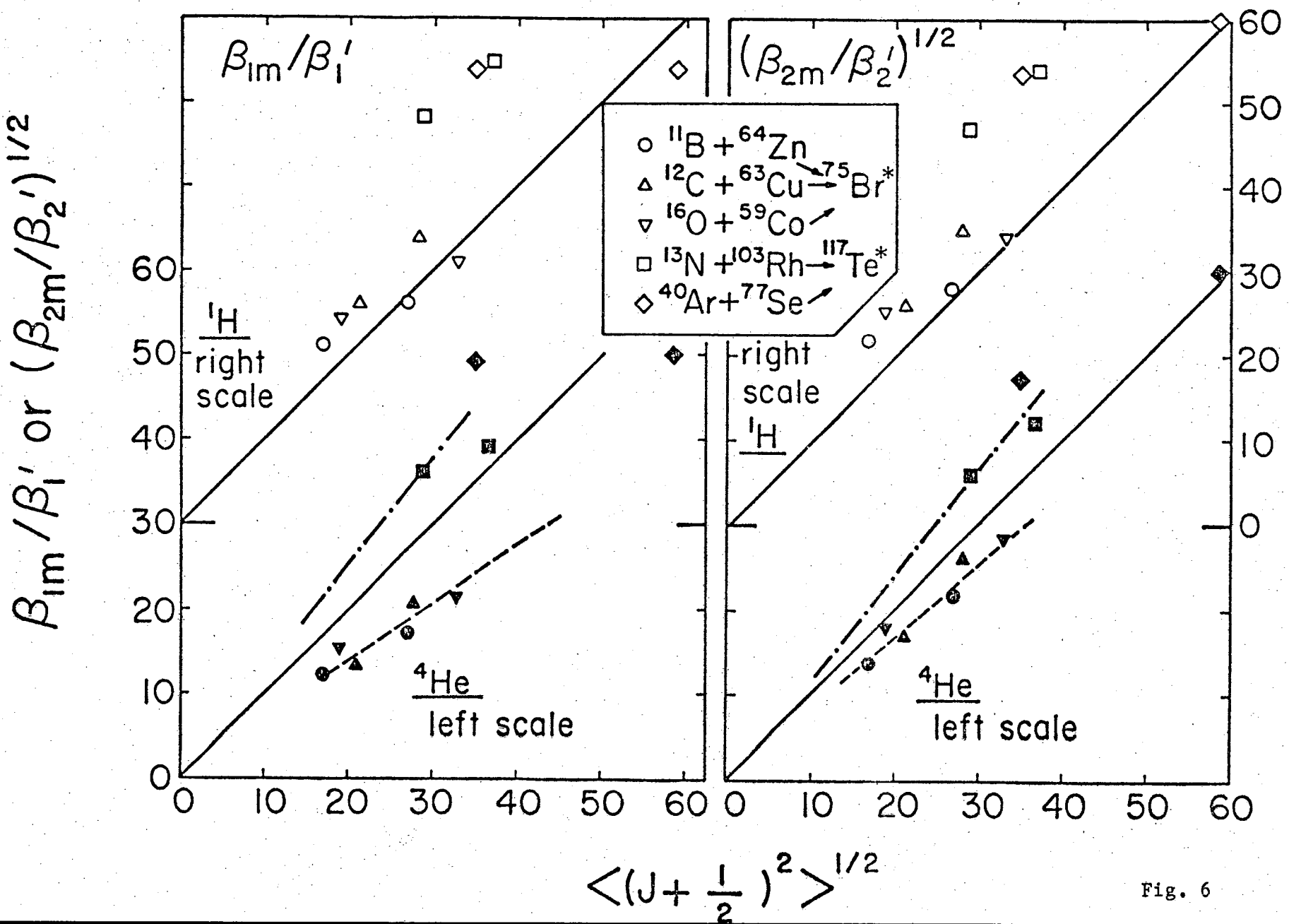
β_{1m}/β_1'
$(\beta_{2m}/\beta_2')^{1/2}$
β_{1m}/β_1' or $(\beta_{2m}/\beta_2')^{1/2}$
$^{11}B + ^{64}Zn \rightarrow ^{75}Br^*$
$^{12}C + ^{63}Cu \rightarrow$
$^{16}O + ^{59}Co \rightarrow$
$^{13}N + ^{103}Rh \rightarrow ^{117}Te^*$
$^{40}Ar + ^{77}Se \rightarrow$
^1H right scale
^4He left scale
^1H right scale
^4He left scale
$\langle (J+\frac{1}{2})^2 \rangle^{1/2}$
0 10 20 30 40 50 60
0 10 20 30 40 50 60

Fig. 6

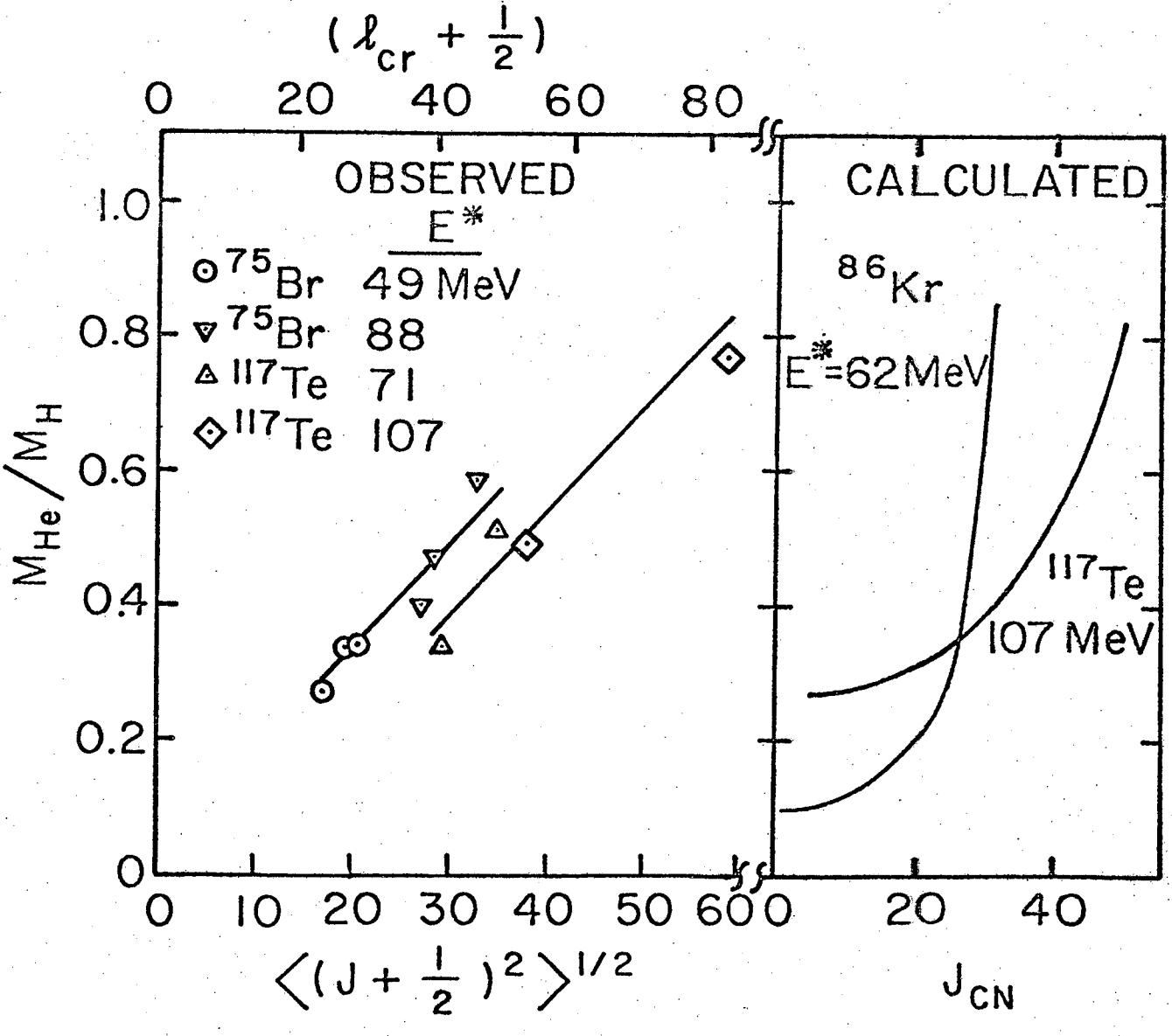
$(\ell_{cr} + \frac{1}{2})$
0 20 40 60 80
OBSERVED
CALCULATED
$\frac{E^*}{}$
^{75}Br 49 MeV
^{75}Br 88
^{117}Te 71
^{117}Te 107
^{86}Kr
E^*=62MeV
^{117}Te
107 MeV
M_{He}/M_H
1.0
0.8
0.6
0.4
0.2
0
0 10 20 30 40 50 60
$\langle (J + \frac{1}{2})^2 \rangle^{1/2}$
0 20 40
J_{CN}

Fig. 7

RAPID ENERGY EQUILIBRATION AND EMISSION OF H AND He IN THE REACTION OF 340 MeV ^{40}Ar WITH ^{197}Au

D. Logan
Department of Chemistry, Carnegie-Mellon University, Pittsburgh, PA 15213

M. Rajagopalan
Department of Chemistry
State University of New York at Stony Brook, Stony Brook, NY 11794

M. S. Zisman
Lawrence Berkeley Laboratory, Berkeley, CA 94720

John M. Alexander
Department of Chemistry
State University of New York at Stony Brook, Stony Brook, NY 11794

Morton Kaplan
Department of Chemistry, Carnegie-Mellon University, Pittsburgh, PA 15213

Ludwik Kowalski
Montclair State College, Upper Montclair, NJ 07043

ABSTRACT

Energy and angular distributions have been measured for H and He both in singles and in coincidence with a heavy fragment. Large cross sections have been observed for both a low-temperature component at backward angles and a high-temperature component at forward angles. Both the preequilibrium and evaporation-like components are apparently emitted prior to scission, predominantly in coincidence with fragments of $Z > 27$. The angular anisotropy and out-of-plane correlation for ^{4}He are not consistent with emission from the composite systems of highest spin ($\approx 190\ \hbar$) but are consistent with emission from the ^{237}Bk composite with average spin $\approx 70\ \hbar$. Extensive energy sharing and H/He emission occur in many reactions so rapidly as to precede fission which is heavily favored by energetic and phase space considerations.

[NUCLEAR REACTIONS: $^{197}Au(^{40}Ar$, fission and H/He), E = 340 MeV, measured energy and angular distributions for $^{1,2,3}H$ and ^{4}He in singles mode and coincidences between H/He and one fission-like fragment.]

I. INTRODUCTION

Studies of light charged particle emission have provided many very interesting views of reactions between complex nuclei. In most cases, both an evaporative component and a direct component have been identified by their characteristic angular and energy distributions.[1-15] The energy distributions of the evaporative component give information on nuclear temperatures[1-15] and effective barriers to emission.[1,3,7-9,16-19] Their angular distributions give information on the angular momenta involved.[1,5,7-9,18,20-22]

The direct emission can involve a significant fraction of the reaction cross section. For light projectiles of Z up to 10 this contribution has been observed to increase rapidly with incident energy.[3,9,12-15] In reactions such as $^{16}O + {}^{209}Bi$, Britt and Quinton found direct ^{4}He emission to be favored near the grazing angle and with velocities close to that of the projectile.[3] On this basis they argued that projectile break-up may be responsible for such reactions. By contrast, for $^{159}Tb(^{14}N,\alpha xn)$ reactions, Inamura et al.[10] observed similar forward peaked ^{4}He angular distributions and cross sections but found that the resulting projectile residue fused with the target. Both studies however have indicated that such reactions are associated with the higher angular momenta. Recently, coincidence measurements have been made between γ-rays and high energy ^{4}He at forward angles.[11,13,14] These studies also confirmed that large cross sections for $(HI,\alpha xn\gamma)$ reactions via direct mechanisms are associated with the larger partial waves in the entrance channel.

The high-energy H and ^{4}He emission at forward angles was found by Galin et al.[9] to be strong for ^{14}N + Rh but totally absent for $^{40}Ar + {}^{77}Se$. This result is suggestive of the idea that only the lighter projectiles give rise to the direct ejection of H and He. By contrast however, recent coincidence studies have indicated such direct processes in high-energy quasi-elastic

and deeply-inelastic reactions (^{32}S + Au and ^{86}Kr + Au).[15,23] In both of these reactions direct ^{4}He ejection was identified at forward angles possibly focused by the Coulomb fields of the separating fragments. In the ^{86}Kr induced reaction, prescission H and He emission were found in addition at backward angles and with rather low temperatures ($\approx$ 3 MeV).[24]

Very interesting angular correlations both in and out of the reaction plane have also been reported for the reactions (^{16}O, $^{12}C\,\alpha$) with Al, Ni and Pb.[25-27] For both Al and Ni, direct ^{4}He emission is strongly favored in the reaction plane. Apparently the spin vector of the composite system is dictating this correlation even for the very rapidly ejected ^{4}He. An unexpected preference for out-of-plane emission has been observed for H in deeply inelastic reactions of ^{86}Kr with Au.[24]

These coincidence studies for deeply inelastic reactions are very interesting indeed. In order to understand them, however, we need to improve our background understanding for angular correlations in more simple reactions. At present, our knowledge is limited to anisotropies in compound nucleus reactions[1-9,21,22] and to the angular correlations of long-range particle emission in fission.[28,29] For the compound nucleus studies, clear separation of the roles of temperature and spin has rarely been achieved,[1-9,21] and for fission we only have data at excitations up to $\approx$ 40 MeV.[30]

We have chosen to study H and He emission in the reaction ^{40}Ar + ^{197}Au at 340 MeV; here sizable cross sections have been observed for fragments of $Z < 30$ (forward-peaked) and also for heavier products that are emitted with $(1/\sin\theta)$ angular distributions.[31-34] The latter reactions seem to have all the characteristics of fission although the liquid-drop fission barrier is calculated to vanish even for rather low spins.[35] Some workers have chosen to identify the cross section for $30 \lesssim Z \lesssim 67$ with a "slow" fission process

and to use this cross section to define a value of the critical ℓ for fusion ($\sigma = \pi\lambda\!\!\!^{-2}(\ell_{cr} + 1)^2$).[36] Others have argued that the distinction between fission and deeply inelastic reactions is not clear[31] and thus the meaning of such a value of ℓ_{cr} is obscure. Therefore this reaction system is of special interest as an intermediate between those for very heavy reactants (e.g. $^{86}Kr + ^{209}Bi$) where no complete fusion is clearly identifiable and those for lighter reactants (e.g. $^{12}C + ^{182}W$) where the fusion cross section (and ℓ_{cr}) is identified by fission plus evaporation-residue formation. Our hope is that the characteristics of emission of direct and/or evaporative H/He for the $^{40}Ar + ^{197}Au$ system will help to provide a link between the information from fission and evaporation studies at medium energies and the deeply inelastic reactions between heavier nuclei.

The specific questions we ask are as follows:

(1) What is the nature of the H/He emission and with what reaction products is it associated?

(2) Does emission of H/He precede or follow the scission of the composite nuclear system?

(3) To what extent has the translational energy of the entrance channel been damped in these processes?

(4) What information do the H/He energy spectra give regarding the energy sharing among particles in the composite system?

(5) What can be inferred about the angular momenta involved from the angular distributions of H/He?

(6) Can one account for the cross sections for fission and H/He emission (at back angles) by an equilibrium statistical model?

(7) What are the characteristics of H/He emission at forward angles and how do they compare with those in other reaction systems?

II. EXPERIMENTAL ARRANGEMENT

The 340 MeV ^{40}Ar beam from the Lawrence Berkeley Laboratory SuperHILAC was defined by two four-jaw collimators (2 mm x 2 mm) and an antiscattering shield. Beam intensity was measured by a Faraday cup and two fixed monitor detectors after traversal of the Au target of thickness 1.25 mg/cm^2. Fission-like and projectile-like fragments were detected with a gas ionization telescope (GT)[37] operated with methane gas at 15 torr and a polypropylene window of 35 μg/cm^2. The angle of this telescope with respect to the beam is denoted θ_G. The direction from target to GT and the beam line define the reaction plane for light particles detected in coincidence with heavy fragments. The 500 μm Si stopping detector in the GT was calibrated for energy and pulse-height defect with fission fragments from ^{252}Cf and the elastically scattered beam.[38] Atomic numbers (Z) for the fragments were determined relative to the elastically scattered ^{40}Ar by reference to the Northcliffe-Schilling tables.[39] For the main emphasis of this study we divide the fragments into two groups (a) $Z \leq 27$ and (b) $Z > 27$. Earlier work has shown that the former group has a distinctly forward-peaked angular distribution, while for 248 MeV ^{40}Ar, the latter group seems to be symmetric about 90 deg c.m.[31-34]

The H and He particles were detected by two three-member solid-state telescopes (SST) (45 μm, 500 μm, 5 mm Si detectors) mounted on an out-of-plane arm. We describe the telescope positions by an angle in the reaction plane (θ_S) (0-360 deg) and an angle with respect to the reaction plane (φ). This out-of-plane angle should not be confused with the azimuthal angle in a spherical coordinate system. The telescopes were separated by $\Delta\varphi = 28$ deg and each had ≈ 10 msr solid angle acceptance. The c.m. angle with respect to the beam $\theta_{c.m.}$ and the c.m. energy ε are functions of both θ_S and φ as well as the measured lab-system energy. With the GT fixed at $\theta_G = 40°$ and 60° we swept

the light particle telescopes from $100° < \theta_S < 339°$. We used a Ni foil (51 mg/cm^2) to stop the scattered beam for θ_S = 320° and 339°; for more backward angles only a thin cover foil was used (0.2 mg/cm^2 Au). Energy thresholds for detection and identification of H and He were 2 and 8 MeV for the thin cover foil and 5 and 20 MeV for the thick one. Events were recorded simultaneously from each telescope in the singles mode and in the coincidence mode between the GT and each SST. In the computation of absolute cross sections we assumed a charge state of +18 for the ^{40}Ar beam collected in the Faraday cup.

III. RESULTS AND BRIEF DISCUSSION

The purpose of this section is to make a brief presentation of the body of experimental data that has been collected. In Section IV we will discuss the implications of the results in terms of the reaction mechanisms. Representative c.m. energy spectra for He and H in the singles mode are shown in Figs. 1 and 2 and parametrized for comparative purposes in Table I. Some technical problems could have flawed the energy measurements for particles that barely entered the third member of the solid state telescopes. Therefore we are doubtful of the reality of the minima shown in the spectra at forward angles. However, the more important features are unmarred: the evaporation-like spectra at back angles and the increasing quantity of high-energy H and He at forward angles. Angular distributions for He and H in the singles mode are shown in Figs. 3 and 4. Each particle distribution shows prominent forward peaking characteristic of direct mechanisms. For c.m. angles greater than 100 deg. the production of ^{1}H becomes isotropic and that for ^{4}He shows a modest backward peaking, both of which could characterize statistical nuclear evaporation from an equilibrated system. For ^{2}H and ^{3}H the forward peak comprises a greater fraction of the total emission probability

and direct mechanisms could contribute significantly even for $\theta_{c.m.} \sim 100$ deg. In Fig. 5 we compare typical back-angle spectra for ^{4}He and ^{1}H observed here with corresponding spectra from ^{194}Hg compound nuclei formed in several reactions.[12,19] The general shapes of the spectra are very similar and appear to be typical evaporation spectra from systems of comparable temperature (high energy slopes). For the $^{40}Ar + ^{197}Au$ reaction, both the ^{4}He and ^{1}H spectra in Fig. 5 are somewhat broader and shifted to higher energies, compared to the ^{194}Hg data. These significant differences will be discussed more fully in Section IV.

In Fig. 3 we have decomposed the angular distribution of ^{4}He particles into a "direct" component (labeled D) and an "evaporative" component (labeled C), making use of the theoretical requirement of symmetry about $\theta_{c.m.} = 90$ deg for emission from an equilibrated system. In the theory of nuclear evaporation,[18,20-22] the deviations from angular isotropy are related to angular momentum effects associated with the particle emission and depend on the spin of the emitter $(I_o+\frac{1}{2})$, the orbital angular momentum of the emitted particle $(\ell+\frac{1}{2})$, and the spin-cutoff factor σ^2 in the nuclear level density. We have collected in Table II a set of relevant parameters calculated for ^{4}He evaporation from equilibrated ^{237}Bk systems of various assumed spins $(I_o+\frac{1}{2})$. The details of the calculations and the inferences to be drawn from the results in Table II will be described in Section IV.

In this study we have made an initial survey of the correlations between H/He emission and one heavy fragment detected at 40° or 60° in the laboratory. As our objective was to get an overall view of the coincidence pattern, the angular coverage was rather extensive but the number of detected events was quite modest. A complete summary of the characteristics of the $^{1}H/^{4}He$ particles

detected in the coincidence mode is given in Tables III-VI and Figs. 6 and 7. Table III presents the basic coincidence data for each angular configuration. For each measurement we have computed the average c.m. energies $\langle \varepsilon_{c.m.} \rangle$ for ^{4}He and ^{1}H and the double differential cross sections $(d^2\sigma/d\Omega_S d\Omega_G)$, and these are listed in Table III. The coincidence angular distributions are displayed in Fig. 6 and the energy spectra, grouped by angular region, are shown in Fig. 7. These figures together with the numbers of individual coincidence events in Table III give a feeling for the statistical uncertainties in the measurements. Yet within the limitations imposed by the statistics, it is apparent that the angular and energy distributions of the coincidence events are consistent with the measurements of $^{4}He/^{1}H$ in the singles mode (Figs. 1,3 and 4). These observations suggest that the bulk of the light particles detected in the singles mode are also associated with the nuclear events detected in the coincidence mode.

For any coincidence study one must assess the kinds of reaction processes that are selected by the positions and thresholds of the detectors. For example, the study of Gamp et al. (373 MeV ^{32}S + Au) selected high energy ^{4}He (> 25 MeV) in coincidence with high energy projectile-like fragments of $Z \leq 23$.[15] Their integrated coincidence cross sections constituted a small but very interesting fraction of the 800 mb of ^{4}He observed in singles. In this work we have used a gas telescope which could record fragments with $Z \geq 15$ and energies as low as $\approx$ 20 MeV. The trigger angle $\theta_G = 60°$ was well aft of the grazing angle and therefore it emphasized fission-like fragments of $27 < Z < 70$. For the smaller trigger angle $\theta_G = 40°$ a large number of projectile-like fragments was observed in singles from both quasi-elastic and very inelastic processes. Studies of elastic scattering give an estimate of $\approx$ 2.5 b for the reaction cross section,[3,40] and our results show that $\approx$ 1.4 b or $\approx$ 56% give fission-like

fragments of $27 < Z < 70$. In Table IV we give the integrated cross sections for the forward and symmetric components of H/He detected in singles and the symmetric components detected in coincidence with a heavy fragment. Despite considerable uncertainties associated with the coincidence cross sections, it is clear that the symmetric components in singles and in coincidence are of comparable magnitudes. This result is strongly supportive of the suggestion that the coincidence experiments have been recording dominant processes for H/He production. Furthermore, the Z determinations from the gas telescope ($\theta_G = 40°$ and $60°$) indicate that $\approx 90\%$ of the fragments in coincidence with H/He have $27 < Z < 70$. Thus the major mechanisms for H/He emission involve fission-like reactions rather than quasi-elastic or deeply inelastic reactions that lead to projectile-like fragments.

Table V presents the coincidence data from Table III grouped to maximize the statistical significance and reveal differences between forward and backward emissions and between in-plane and out-of-plane coincidence events. Table VI gives the characteristics of the energy distributions for H/He, grouped by emission direction as in Table V. From these tables, it appears that the cross sections and energies for ^{4}He and ^{1}H emitted out of the reaction plane ($\varphi = 28$ and 42 deg) are significantly different from the in-plane emissions ($\varphi = 0$ and 14 deg). We will discuss these correlations and the inferences to be drawn from them later in this paper. It can also be seen, particularly from Fig. 6 but also from Table V, that the major parts of the forward peaking in the H/He singles angular distributions are also reflected in the coincidence cross sections. Hence we conclude that the predominant fraction of the H/He recorded in the singles mode is emitted in coincidence with a heavy fragment and that $\approx 90\%$ of these have $27 < Z < 70$. Only $\approx 10\%$ of the coincidence events

were found to be associated with a projectile-like fragment of $Z \leq 27$. Little if any cross section remains for H/He emission from residual nuclei that survive fission-like breakups.

The large probability for coincidence between H/He and fission-like products does not distinguish between H/He emitted from the ^{237}Bk composite system or from the separating products. The shapes of the energy spectra in singles give us one of several means for distinction. In Fig. 8 we show results of a Monte Carlo simulation[41] of H/He emission from fully accelerated fission fragments. In the calculation we have assumed a Gaussian mass distribution of standard deviation 30 mass units centered about A = 237/2. Evaporation of H/He was assumed to be equally probable from each fragment. The calculated curves for ^{4}He in Fig. 8 are much wider than the measured spectra at corresponding angles in Fig. 1; thus this mechanism is clearly not dominant. For ^{1}H the calculated curves are steeper at high energies than the experimental ones and their angular dependence (Fig. 8) is also not reflected in the observed data. Therefore we are led to the interesting conclusion that most H/He emission precedes full fragment acceleration. A more detailed discussion of this matter is given in the next section.

IV. MECHANISTIC IMPLICATIONS OF THE RESULTS

In the last section we considered the general features of the H/He emission and the nature of the reaction products with which it is associated. We showed that $\approx$ 90% of the coincident H/He emission is correlated with fission-like products of $27 < Z < 70$. In addition, the mean Z values for fragments detected in singles and in coincidence differ by less than three charge units. In the present work, we will focus on these prominent fission-like processes. The earlier work of Ref. 15 (373 MeV ^{32}S + Au) dealt with the small fraction

of high energy ^{4}He in coincidence with projectile-like fragments ($Z \leq 23$).

We would now like to discuss in more detail the question of whether the H/He emission precedes or follows scission and full acceleration of the fragments. There are four experimental observations that indicate that such emission precedes significant fragment acceleration: (1) the average energies of H/He in coincidence are not enhanced in the direction of either fragment (Table III). (2) The coincidence cross sections show no enhancement in the direction of either fragment (Table III and Fig. 6). (3) The shape of the singles energy spectra for $\theta_{c.m.} > 100°$ (Figs. 1 and 5) are quite different from those expected for isotropic emission from fully accelerated fragments (Fig. 8). (4) The shapes of the H/He energy spectra observed in the coincidence mode are similar to those observed in the singles mode (Figs. 1 and 7). Two more observations suggest that H/He emission occurs even before the act of scission: (5) The average energies are consistent with evaporation from a composite of total $Z \approx 97$ (Tables I, III, and VI and Figs. 5, 7).[19] In Fig. 5 the back-angle energy spectra are compared to those observed for the reactions ^{12}C + ^{182}W and ^{40}Ar + ^{154}Sm leading to ^{194}Hg excited to 98 and 142 MeV. The peak energies can be seen to be consistent with the Z ratio of 97/80. (For the ^{194}Hg system at 98 MeV less than 10% of H/He emission was found to be in coincidence with fission.)[12] (6) The ratio of He to H cross sections is ≈ 0.9 (for $\theta_{c.m.} > 100°$). This ratio would be expected to be ≈ 0.2 for a fragment of mass 78-117 with spin ≈ 20.[8.9,21,22] For such a fragment a spin of ≈ 60 would be implied by this He/H ratio of 0.9. Such large spins are well above estimates from the "sticking model". By contrast this ratio is consistent with that of a compound nucleus ^{194}Hg (and by implication ^{237}Bk) of mean spin ≈ 60.[12,21] We conclude that the predominant

fraction of H/He emission precedes scission of ^{237}Bk even for this highly excited composite system which must have a very short lifetime.[42] (The abundance of H/He with energies below their most probable value may signify emission from a very deformed composite system, but detailed calculations of the spectral shapes must be made to explore this point.[19])

To what extent has energy damping or relaxation occurred in the exit channels associated with H/He emission? In Ref. 15 (373 MeV ^{32}S + Au) it was shown that forward-peaked high energy ^{4}He emission occurs in coincidence with quasi-elastic reactions giving projectile-like residues. In the present work we have shown that $\approx$ 90% of the coincident H/He emission is with fission-like products ($27 < Z < 70$). The energies of these fission-like fragments are typical of the gross fission product distribution with average c.m. energies $\approx$ 90 MeV. In short, the exit channel heavy fragment energies are for the most part, completely damped. Hence we can infer that for these fragments the memory of the entrance channel was largely erased by complex processes of energy, charge and mass exchange.

What information do the H/He energy spectra give regarding the energy sharing among particles in the composite system? We have seen that the H/He emission precedes a fission-like breakup with complete energy damping in a composite system which must not live longer than several nanopico-seconds.[42] The energy spectra of H/He at forward angles have many high energy particles with velocities near those of the projectile (Figs. 1, 2 and 7). Presumably these emissions reflect a memory of the projectile's speed and relatively little energy mixing with other constituents of the intermediate complex. It is convenient to discuss the energy mixing more generally in terms of effective temperatures as a function of angle.[11] We have made fits of the

spectra in Figs. 1 and 2 to the functional form:

$$P(\varepsilon) = (\varepsilon - B) \exp(-\varepsilon/T) \quad (1)$$

where B and T are the effective barrier and temperature, respectively. These fits are not useful for the lower energies but can provide a parameter T to characterize the high energy tail of each spectrum. The values of T are given in Table I along with "peak" energy and width parameters to characterize the spectrum at each angle. We see that these spectral parameters become independent of angle for $\theta_{c.m.} > \sim 100°$ for ^{1}H and $\sim 127°$ for ^{4}He. The T values for ^{1}H and ^{4}He are both ≈ 2.5 MeV, a value very close to that observed for ^{194}Hg compound nuclei excited to 100-140 MeV.[12,19] (See Fig. 5.) Such low temperatures imply essentially complete energy mixing among the H and He particles in the intermediate complex. Similarly the "peak" energy is $\approx 15\%$ greater than that observed for the system ^{194}Hg. This is as expected from the relevant Coulomb barrier ratio for the two systems. In short, these H/He emissions at back angles have energy and angular distributions that are consistent with an equilibrated compound nucleus, a remarkable result for a system of such high charge, energy and spin (Figs. 3-8).

McMahan and Alexander have shown that for the ^{194}Hg system ($E^{*} = 98$ MeV) the barrier to evaporation is $\approx 10\%$ lower than the barrier to fusion.[19] The widths (FWHM) of the particle energy spectra from the ^{237}Bk composite are ≈ 12 MeV compared to about 8 MeV for ^{194}Hg (see Fig. 5). This additional width for ^{4}He and the low-energy shelf for ^{1}H (Fig. 1) could imply significant emission from a very deformed complex or from a neck between fragments. This could then offer a very interesting possibility for studying the composite system at an early stage in its evolution toward scission.

The spectra at forward angles are characterized by a high temperature component that seems to reflect a memory of the projectile's speed. In addition, however, there are many H/He particles with near-barrier energies at the forward angles. Their abundance is significantly larger than that obtained by reflection symmetry of the back-angle spectra about $\theta_{c.m.} = 90°$. This may be illustrated in the case of ^{4}He. If one imagines that these forward-peaked particles can be decomposed into low (L) and high (H) temperature components, then the curves in Fig. 3 labeled L and H give a feeling for their relative magnitudes. Alternatively, of course, the processes of H/He emission may result from a continuum of effective temperatures and lifetimes of the composite system that are almost completely thermalized for $\theta_{c.m.} > \sim 100°$, but only partially thermalized for $\theta_{c.m.} < \sim 100°$.[43]

As a large fraction of the H/He emission appears to be characteristic of evaporation from an essentially equilibrated system, it is of interest to consider the observed angular distributions and correlations as probes of the angular momenta. To do this we shall first make some estimates of the theoretical angular and energy correlations, using the relationships derived from the statistical model for nuclear evaporation.[18,20-22] Following the treatment given by Ericson and Strutinski[20] (but using semiclassical approximations for the magnitudes of the various angular momenta[21,22]), there is a correlation of emission probability $W(\varphi^*)$ with the angle φ^* between the emitted particle of energy ε and orbital angular momentum $(\ell+\frac{1}{2})\hbar$ and the angular momentum of the emitter $(I_o+\frac{1}{2})\hbar$:

$$W_{I_o,\ell,\mathcal{J}_T}(\varphi^*) \propto J_o\left\{\frac{i(I_o+\frac{1}{2})(\ell+\frac{1}{2})}{\bar{\sigma}^2}\sin\varphi^*\right\}. \qquad (2)$$

In this equation $J_o\{x\}$ is the zero-order Bessel function of argument x and σ^2 is the spin-cutoff factor in the nuclear level density given by

$$\sigma^2 = \mathcal{J}T/\hbar^2, \tag{3}$$

where $\mathcal{J}$ and T are the moment of inertia and the temperature of the residual nucleus. One must recognize that Eq. (2) applies when the angular momentum of the emitter has a unique orientation in space, as might be selected by the requirements of a coincidence experiment. Our experimental out-of-plane angle φ can be related to φ^* in Eq. (2) if we identify the spin of the emitter with the normal to the reaction plane. In this case, $(\pi/2 - \varphi)$ transformed to the c.m. system is φ^*. The specification of $\mathcal{J}T$ or σ^2 in Eq. (2) requires selection of particular emissions (e.g. E^*, ε, etc.) and a knowledge of the level density. For an ensemble of nuclei with angular momenta uniformly distributed perpendicular to the beam axis (as might be expected in observations with a single detector in a compound nucleus reaction), particles will be emitted at angles θ with respect to the beam:

$$W_{I_o,\ell,\mathcal{J}T}(\theta) \propto \sum_{k=0}^{\infty} (-)^k (4k+1) j_{2k} \left\{ \frac{i(I_o+\frac{1}{2})(\ell+\frac{1}{2})}{\sigma^2} \right\} [P_{2k}(0)]^2 P_{2k}(\cos\theta), \tag{4}$$

where j_{2k} and P_{2k} are, respectively, a spherical Bessel function and Legendre polynomial of order 2k. Equations (2) and (4) depend only on the parameter $\beta_1 = (I_o+\frac{1}{2})(\ell+\frac{1}{2})/2\sigma^2$. On expansion of Eqs. (2) and (4) the first term is of order β_1^2:

$$\beta_1^2 = \frac{(I_o+\frac{1}{2})^2(\ell+\frac{1}{2})^2}{(2\sigma^2)^2} \tag{5}$$

and therefore the root-mean-square values of $(I_o+\frac{1}{2})$ and $(\ell+\frac{1}{2})$ are of primary importance. For I_o values of any practical interest, one must consider the

distribution of ℓ values and we may use the relation given by Døssing:[21]

$$P_{I_o,\mathcal{J}_T}(\ell) \propto \left[\exp\left\{\frac{(I_o+\frac{1}{2})(\ell+\frac{1}{2})}{\sigma^2} - \frac{\hbar^2(\ell+\frac{1}{2})^2}{2T\mu R^2}\left(\frac{\mathcal{J}_\perp}{\mathcal{J}}\right)\right\}\right]$$

$$x\left[1 - \exp\left\{-\frac{2(I_o+\frac{1}{2})(\ell+\frac{1}{2})}{\sigma^2}\right\}\right], \qquad (6)$$

where μ is the reduced mass of the emitted particle and R and T are the radius and temperature of the residual nucleus. Also, $\mathcal{J}_\perp = \mathcal{J} + \mu R^2$, and one should note that μR^2 refers to the centrifugal barrier for evaporation. Because of Eq. (5), the most important average related to $P_{I_o,\mathcal{J}_T}(\ell)$ in Eq. (6) is the quantity $\langle(\ell+\frac{1}{2})^2\rangle$. Catchen, et al.[22] have derived an exact expression for this average:

$$\langle(\ell+\tfrac{1}{2})^2\rangle = \frac{[1+(\gamma^2/2)]\ \mathrm{erf}(\gamma/2) + (\gamma/\sqrt{\pi})\ \exp(-\gamma^2/4)}{2b\ \mathrm{erf}\ (\gamma/2)}, \qquad (7)$$

where
$$\gamma = (I_o+\tfrac{1}{2})/b^{1/2}\sigma^2 = \eta(I_o+\tfrac{1}{2}), \qquad (8)$$

$$b = \hbar^2\mathcal{J}_\perp/2\mu R^2\mathcal{J}T, \qquad (9)$$

and
$$\eta = (2\mu R^2\hbar^2/\mathcal{J}\mathcal{J}_\perp T)^{1/2}. \qquad (10)$$

From these equations, one can see that the quantity $\langle(\ell+\frac{1}{2})^2\rangle \cdot b$ is a function only of I_o for a given value of η.

Equations (2) and (4) are strictly applicable for one value of $\beta_1 = \hbar^2(I_o+\frac{1}{2})(\ell+\frac{1}{2})/2\mathcal{J}T$ and therefore for distributions of I_o, ℓ and/or $\mathcal{J}T$ one should take the most appropriate average or specifically perform the summations of interest. Our approach here is to estimate

$$\beta_1^2 = \frac{\langle (I_o+\frac{1}{2})^2 \rangle \langle (\ell+\frac{1}{2})^2 \rangle}{(2\sigma^2)^2} \qquad (5')$$

and use it in Eqs. (2) and (4). A second approach is to weight Eqs. (2) and (4) appropriately and sum over the spectrum of ℓ and ε for the evaporated particles. Using standard approximations Dø ssing has carried out such integrations.[21] Analogous to Eq. (2) he obtains

$$W_{I_o,\mathcal{J}_T}(\varphi^*) \propto \exp(\beta_2 \sin^2\varphi^*), \qquad (11)$$

and analogous to Eq. (4) he finds

$$W_{I_o,\mathcal{J}_T}(\theta) \propto [\exp(-\beta_2 \sin^2\theta/2)]J_o\{i\beta_2 \sin^2\theta/2\}, \qquad (12)$$

where

$$\beta_2 = \frac{(I_o+\frac{1}{2})^2}{2\sigma^2}\left(\frac{\mu R^2}{\mathcal{J}_\perp}\right). \qquad (13)$$

Either Eq. (2) or Eq. (11) can be used to interpret angular correlations of emitted particles with respect to a unique spin vector. Correspondingly, Eqs. (4) or (12) should apply to angular distributions measured with respect to the beam in compound-nucleus experiments, since here no unique reaction plane is defined and the spin vectors of the emitting nuclei are uniformly distributed in (or close to) a plane perpendicular to the beam direction. In either case, attention must be given to the appropriate choice of the parameters β_1 and β_2. These parameters may be computed theoretically as functions of $(I_o+\frac{1}{2})$ using the equations given above. Implicit in such a calculation is the assumption that the particle emission occurs at the first step of the evaporation chain. We also require absolute estimates of $\mathcal{J}$,T, and μR^2 which we have made in the following manner. For μR^2 we use $\mu(1.42\ A^{1/3}\ \text{fm} + R_p \text{ or } R_\alpha)^2$

as discussed in Ref. 19. The moment of inertia $\mathcal{I}$ we take as

$$\mathcal{I} = \frac{2}{5} Mr^2, \tag{14}$$

with M the mass of the nucleus and $r = 1.2\ A^{1/3}$ fm (for the matter radius). The temperature is related to the average energy available for thermal excitation:

$$U = aT^2, \tag{15}$$

with "a" = (A/10) MeV^{-1} and

$$U = E^* - \langle \varepsilon \rangle - S - E_{rot}. \tag{16}$$

The separation energy of the emitted particle is S and its average kinetic energy $\langle \varepsilon \rangle$ is taken to be (B+2T) where B is the exit channel barrier.[19] The rotational energy E_{rot} and moment of inertia $\mathcal{I}$ refer to the emitting nucleus and are related by

$$E_{rot} = \hbar^2 (I_o + \tfrac{1}{2})^2 / 2\mathcal{I}. \tag{17}$$

We present in Table II a calculated set of the relevant parameters for ^{4}He evaporation from the system of interest here, 340 MeV $^{40}Ar + {}^{197}Au \rightarrow {}^{237}Bk$. For selected values of the emitter spin $(I_o + \frac{1}{2})$ listed in the first column, we give values of the quantities E_{rot}, U, T, $2\sigma^2$, $\langle (\ell + \frac{1}{2})^2 \rangle^{1/2}$, β_1 and β_2 in columns 2-8 respectively. The last column in Table II represents the average total kinetic energy (above the barrier) of an evaporated particle, consisting of the average thermal energy 2T and a centrifugal part ξ from the rotating emitter

$$\xi = 4E_{rot}\ \mu R^2 / 3\mathcal{I}. \tag{18}$$

Several points should be noted from the results in Table II. For spins nearing the maximum entrance channel spin (ℓ_{max} = 190 $\hbar$), the rotational energy of a spherical nucleus would be very large and its temperature would be very small. An evaporated ^{4}He particle would have energy and angular correlations dominated by centrifugal spinoff. For spins $(I_o+\frac{1}{2}) \leq \sim 100$ $\hbar$ the rotational energies are more modest and the values of T, $2\sigma^2$, and $\langle(\ell+\frac{1}{2})^2\rangle^{1/2}$ are rather stable for various values of $(I_o+\frac{1}{2})$. In this region of spins the variation in the angular correlation parameters β_1 and β_2 is dominated by the spin of the emitter and hence may be used as its signature. Both $\langle(\ell+\frac{1}{2})^2\rangle^{1/2}$ and σ^2 are dependent on the size and shape of the residual nucleus, which are unknown. We make estimates with spherical shapes but a generalization of Eqs. (14)-(17) to other shapes may lead to partially compensating changes in the ratio $\langle(\ell+\frac{1}{2})^2\rangle/\sigma^4$. The average energy ($\xi$+2T) (over the barrier) in Table II is only slowly increasing with spin $(I_o+\frac{1}{2})$ and provides no strong signature unless E_{rot} approaches E^*. Perhaps the higher energy ^{4}He particles observed at $\theta_{c.m.} < 60$ deg could reflect such large spins.

Let us now consider the measured angular distributions. For the H isotopes the angular distributions in singles (at back angles) are essentially isotropic and no definitive information can be extracted (only a rather uninteresting upper limit). For the ^{4}He emission, however, we may use the experimental data to obtain estimates of β_1 and β_2. First we have fitted Eqs. (4) and (12) to the angular distribution in singles (Fig. 3, $\theta_{c.m.} > 100$ deg). This yields the values $\beta_1 = 1.0$ and $\beta_2 = 0.73$. Comparison with the theoretical estimates as given in Table II results in the spins $\langle(I+\frac{1}{2})^2\rangle^{1/2} = 65$ $\hbar$ from β_1 and $\langle(I+\frac{1}{2})^2\rangle^{1/2} = 68$ $\hbar$ from β_2. Each of these has a probable uncertainty of $\sim$ 10% arising from the experimental fits alone. Quite independently, we

could obtain additional estimates by fitting Eqs. (2) and (11) to the out-of-plane coincidence correlation data from Table V. Unfortunately, the quality of these data is relatively poor, and even though we have grouped the data in Table V to maximize the statistical significance, the uncertainty in derived parameters will be large. Using Eq. (11) we estimate $\beta_2 \approx 1.1 \pm 0.4$, which translates into spins $\langle (I+\frac{s}{2})^2 \rangle^{1/2} \approx 82 \pm 15\ \hbar$. This result, while imprecise, is not inconsistent with the analysis of the singles data. Thus we can conclude that a typical initial spin associated with equilibrium ^{4}He evaporation is $\langle (I+\frac{s}{2})^2 \rangle^{1/2} \approx 70\ \hbar$. It is rather clear that ^{4}He evaporation does not occur predominantly from initial spin states very near to zero or very near to $\ell_{max} = 190\ \hbar$.

This discussion is all based on the assumption of ^{4}He emission early in the deexcitation cascade. Our evidence is clear that most observed ^{4}He emission does precede full fragment acceleration, and even scission itself. In addition the total multiplicity of ^{4}He emission is less than unity. Thus one would expect that each deexcitation chain would usually give zero or one ^{4}He particle. An extension of this reasoning to include prescission neutron and H emission (next paragraphs) would indicate prescission cascades of one to five particles. For average initial spins of ≤ 100 for the ^{237}Bk, such cascades would not be expected to bring the system very near to the Yrast line. Thus we do not expect H/He emission from near-Yrast states to greatly alter the above analysis.

If we grant that the energy and angular distributions for H/He emission (at back angles) imply emission from an essentially equilibrated system, then it is natural to ask if an equilibrium model can account for the ratio of particle emission to fission ($\Gamma_f/\Gamma_\alpha/\Gamma_p \approx 3/1/1$). Quite simply the answer is

negative. The calculated fission barrier for ^{237}Bk is ≈ 2 MeV for I = 0 and is reduced to near zero for spins of several tens.[35] The sum of proton or alpha binding energy plus Coulomb barrier is ≈ 14 MeV (see Table VII). Thus for T ≈ 2.5 MeV we can expect Γ_α/Γ_f or $\Gamma_p/\Gamma_f \approx \exp(-14/2.5) \tilde{=} 0.004$. Clearly the composite nucleus is not choosing its decay probabilities by counting open channels as in the Boltzmann equation. We infer that the energy sharing among particles must be very fast and even after this extensive mixing the intrinsic particle decay rates must be fast enough for significant particle evaporation to occur prior to scission (about one proton and α per 3 fissions).[42,43] This effect may simply reflect non-participation of the fission channels in the equilibrium model rather than its complete demise.[12,43-45]

It is interesting to digress briefly from our major track to explore more fully the implications of the Boltzmann equation for emission of neutrons, protons and alphas. In Table VII we list the particle separation energies[46] and emission Coulomb barriers for the nucleus ^{237}Bk and for some typical fission products. If we assume that the most probable charge to mass ratio of the primary fragments is 97/237 then ^{86}Br, ^{118}Cd and ^{151}Sm would be typical primary fragments (T ≈ 2.5 MeV). ^{78}Br, ^{110}Cd and ^{141}Sm would then correspond to products near the end of the neutron evaporation cascade (T ≈ 1 MeV). For ^{237}Bk one would estimate $\Gamma_n/\Gamma_p/\Gamma_\alpha \approx 1/\exp[-(S_p+B_p-S_n)/T]/\exp[-(S_\alpha+B_\alpha-S_n)/T] = 1/e^{-2}/e^{-3}$ or ≈ 5 neutrons per (H+He). This estimate is not expected to be very precise but it does suggest significant emission of prescission neutrons in addition to prescission H/He.[44,45] For the primary fragments ^{86}Br, ^{118}Cd and ^{151}Sm one might estimate Γ_{H+He}/Γ_n to be respectively 0.036, 0.064, and 0.044. For the cooler fragments ^{78}Br, ^{110}Cd and ^{141}Sm these ratios may be respectively 0.048, 0.014, and 0.037. Thus for a post-fission evaporation

cascade of 8-10 emission steps, a significant amount of H/He emission should occur. We infer that these processes are masked by the apparently more abundant prescission emissions.

Let us turn now to the forward-peaked or direct component of the particle emission. For the system $^{40}Ar + {}^{77}Se \rightarrow {}^{117}Te$, Galin et al. observed no direct components for H or He.[9] This suggests that either the direct component for ^{117}Te was masked by the evaporation (and escaped detection) or that for our ^{237}Bk system the high charge, excitation and/or spin gives rise to more prominent direct emission. Further, for ^{237}Bk the Z distribution of the heavy products in coincidence with these direct emissions is indistinguishable from that for the evaporation component (90% of emissions have $27 < Z < 70$ and the values of $\langle Z \rangle$ are equivalent). Thus it appears that many of these direct reactions are accompanied by fusion of the projectile residue with the target and a subsequent fission-like breakup.[47] Such a process is very similar to that reported in Refs. 10, 11, 13, 14 and 48 and termed massive transfer or transfert trés inelastique.

The out-of-plane correlation for the forward-peaked ^{4}He ejections is even stronger than for the evaporation-like component (Fig. 6 and Table V). In Table V and VI we give a summary of the out-of-plane data, grouped in such a way as to separate forward and backward emissions and to show the statistical significance. The coincidence cross sections for ^{4}He decrease strongly as one moves away from the reaction plane which would seem to reflect very large entrance-channel spins. Surprisingly the coincidence cross sections for ^{1}H seem to increase as one moves out of the reaction plane. This increase is only about two standard deviations and could, of course, be only an illusion of the counting statistics. However the first and second moments of the

observed energies ($\langle\varepsilon\rangle$ and σ_ε) also indicate a trend reversal between ^{1}H and ^{4}He. In Table VI one can see that the values of $\langle\varepsilon\rangle$ and σ_ε ($\theta_{c.m.} < 60°$) are greater for ^{4}He in the reaction plane and for ^{1}H out of the plane. This is consistent with a larger presence of direct emission in the plane for ^{4}He and out of the plane for ^{1}H (see Fig. 6 as well). This pattern seems to us to be very interesting and surprising and should be investigated further with much better statistics.

In the Appendix we describe one possible mechanism for the strange behavior of the ^{1}H emissions. As the ^{4}He direct emission decreases with increasing φ we suspect that its major driving force is a large spin of the composite system perpendicular to the reaction plane. Eqs. (2) or (11) based on equilibrium considerations must fail in detail for the out-of-plane correlation. Nevertheless, one might consider this suggestive that the direct emissions arise from larger partial waves. If the projectile-like fragments are formed for $140 < \ell < 190$ then possibly the forward peaked ^{4}He is formed for ℓ waves approaching 140. Centrifugal effects could enhance their out-of-plane correlation and their average energies.

The energy spectra of the forward peaked component for ^{4}He can be examined in more detail by subtraction of an assumed symmetric component. Such a subtraction reveals two distinct aspects of these forward peaked emissions (Fig. 3): First the high-temperature component (H) with $T \approx 3$-7 MeV is obvious (Figs. 1,2,7 and Tables I and VI), but also there is significant forward peaking in the near-barrier part of the spectrum (L) with most probable $\varepsilon_\alpha \approx 23$ MeV and $\varepsilon_H \approx 12$ MeV. The high-energy component may well reflect memory of the projectile velocity as in Refs. 10, 11, 13, and 14. The low-energy component would seem to reflect considerable energy sharing among particles even for

these forward peaked emissions.

As shown by the separation and Coulomb energies in Table VII, any phase space calculation would be expected to favor fission over H/He emission by much more than the observed ratios. We have been driven to the conclusion that the intrinsic rate of H/He emission is faster than the time of several nanopicoseconds required to arrive at the scission point.[42] This is not surprising for the very high speed forward peaked emission of clearly pre-equilibrium character.[43] It is surprising for the backward emission that shows temperatures and angular distributions consistent with evaporation. If both direct and evaporative H/He emission are bleeding away spin, charge and energy from the higher spin composite nuclei, this could strongly influence the fission probability for lower Z systems.[12] For a high Z system, such as ^{237}Bk, fission would be expected to occur even after He emission. For ^{194}Hg and lighter systems studied earlier, the fission process might be aborted by this phenomenon,[29] and phase space interpretations may be led astray.[49,50]

The implications of this study are quite important for reaction phenomena between complex nuclei. Even prior to the very rapid fission and quasi-fission processes,[51] "quasi-fusion" and "quasi-evaporation" must be taking place. These processes as well as their forward peaked preequilibrium cousins[52] provide a means of studying the reaction process on a time scale comparable to that for energy damping in the entrance channel.

V. SUMMARY AND CONCLUSIONS

We now attempt to collect the various mechanistic suggestions that emerge from the literature and from this work. Of the $\approx$ 2500 mb reaction cross section for 340 MeV ^{40}Ar + Au, $\approx$ 1400 mb goes to totally relaxed fission-like products of $27 < Z < 70$. The remaining $\approx$ 1100 mb is presumed to lead to projectile-target-like breakups via quasi-elastic and very inelastic reactions. Of the

$\approx$ 190 reactive partial waves in the entrance channel, the latter reactions are expected to dominate the highest $\approx$ 50 partial waves and the former probably dominate from $0 < \ell < \sim 140$. The total cross section for H + He is $\approx$ 1500 mb with emission predominantly preceding scission into fission-like fragments of $27 < Z < 70$. Most of this H/He emission exhibits low temperatures ($\approx$ 2.5 MeV) and seems to derive from an energy equilibrated system. However, significant forward peaking is observed for both a high-temperature component ($T \approx 3$-7 MeV) and for ^{1}H/He with near barrier energies. A strict statistical equilibrium model could not account for such high cross sections for evaporated H/He in comparison to fission from ^{237}Bk of relatively high spin and low fission barrier. It would appear that energy mixing among the particles and even quasi-evaporation must occur in times comparable to that for the scission time of several nanopicoseconds. If the Boltzmann Equation is applicable for the ratio of neutron to alpha quasi-evaporation, one would infer that several neutrons would usually be emitted prior to scission. From the analysis of the angular distributions, it appears that low temperature ^{4}He emission occurs from composite nuclei of $\langle (I+\frac{1}{2})^2 \rangle^{1/2} \approx 70\ \hbar$ and higher temperature emission may come from even higher spin states. The backward ^{1}H emission seems to be nearly isotropic and, as the expected exit-channel ℓ values are small, no definite information on spins can be obtained from that source. The very fast H/He emissions seem to provide an interesting tool for investigating the energy mixing in reactions between complex nuclei and thus the very early history of the composite system.

APPENDIX

As mentioned above the anisotropy for H emission (singles mode, $\theta_{c.m.} > 100°$) is not visible in Fig. 4; presumably it is small although it could have been

masked by a gradual intrusion of forward peaked direct processes. The out-of-plane correlation for H seems to be significant as shown in Fig. 6 and Table V. There is a suggestion of a preference for out-of-plane emission. Although this suggestion is based on about two standard deviations from isotropy and should not be taken as a definitive observation it is consistent with a similar and somewhat stronger effect that has been noted[24] in the reaction ^{86}Kr + Au at 724 MeV.

These observations, tentative as they are, stimulate us to search for a possible cause. Imagine that the H emission takes place on a time scale slow enough for extensive energy sharing but considerably faster than that for the collective motions leading to scission and complete fragment acceleration. In addition, imagine that most H emission takes place from a neck region between the fragments, and their Coulomb fields focus the H into a plane perpendicular to the line between the fragment centers. Substantial rotation of this line of centers, prior to full acceleration of the fragments, would give a set of planes that share a common emission direction perpendicular to the reaction plane. In the limit of long rotation times, emission probability would follow $1/\sin(90° - \varphi)$ just analogous to the very familiar $1/\sin\theta$ limit for fission.

Note,that, for ^{4}He emission, the expected out-of-plane correlation was observed; this calls for composite-nucleus spin as a correlating force. For ^{40}Ar + Au there is apparently no preferential emission of He perpendicular to the final axis of fragment separation (see Fig. 6 and Table III). Therefore, if the emission is from the neck, it must occur over the time period required to rotate $\approx 180°$ or without much focusing by the nascent fragments. This could imply that H and He may be emitted at different ages of the evolving system.

ACKNOWLEDGEMENTS

The staff of the SuperHILAC accelerator at the Lawrence Berkeley Laboratory has been very cooperative. Special thanks are due to H. Delagrange, E. Duek, H. Grunder, C. Maples, and M. F. Rivet for helpful discussions and continued interest in our work. This project was supported by the Division of Nuclear Physics of the U. S. Department of Energy.

REFERENCES

1. W. J. Knox, A. R. Quinton and C. E. Anderson, Phys. Rev. 120, 2120 (1960).
2. C. E. Hunting, Phys. Rev. 123, 606 (1961).
3. H. C. Britt and A. R. Quinton, Phys. Rev. 124, 877 (1961).
4. D. V. Reames, Phys. Rev. 137, B332 (1965).
5. F. E. Durham and M. L. Halbert, Phys. Rev. 137, B850 (1965).
6. A. Kapuszik, V. P. Perelygin, S. P. Tret'yakova and L. V. Ukraintseva, Sov. J. Nucl. Phys. 6, 829 (1968).
7. C. Brun, B. Gatty, M. Lefort and X. Tarrago, Nucl. Phys. A116, 177 (1968).
8. R. C. Reedy, M. J. Fluss, G. F. Herzog, L. Kowalski and J. M. Miller, Phys. Rev. 188, 1771 (1969); J. M. D'Auria, M. J. Fluss, G. Herzog, L. Kowalski, J. M. Miller and R. C. Reedy, Phys. Rev. 174, 1409 (1968).
9. J. Galin, B. Gatty, D. Guerreau, C. Rousset, U. C. Schlotthauer-Voos and X. Tarrago, Phys. Rev. C9, 1113, 1126 (1974); ibid C10, 638 (1974).
10. T. Inamura, M. Ishihara, T. Fukuda and T. Shimoda, Phys. Letts. 68B, 51 (1977).
11. T. Nomura, H. Utsunomiya, T. Motobayashi, T. Inamura and M. Yanokura, Phys. Rev. Letts. 40, 694 (1978).
12. J. M. Miller, D. Logan, G. L. Catchen, M. Rajagopalan, J. M. Alexander, M. Kaplan, J. W. Ball, M. S. Zisman and L. Kowalski, Phys. Rev. Letts. 40, 1074 (1978), and unpublished data from the same group.
13. D. R. Zolnowski, H. Yamada, S. E. Cala, A. C. Kahler and T. T. Sugihara, Phys. Rev. Letts. 41, 92 (1978); H. Yamada, D. R. Zolnowski, S. E. Cala, A. C. Kahler, J. Pierce, and T. T. Sugihara, Phys. Rev. Letts. 43, 605 (1979).
14. D. G. Sarantities, L. Westerberg, M. L. Halbert, R. A. Dayras, D. C. Hensley and J. H. Barker, Phys. Rev. C18, 774 (1978).
15. A. Gamp, J. C. Jacmart, N. Poffé, H. Doubre, J. C. Roynette, and J. Wilczynski, Phys. Letts. 74B, 215 (1978); A. Gamp, H. L. Harney, J. C. Roynette, E. Plagnol, H. Fuchs, H. Doubre, J. C. Jacmart, and N. Poffé, Z. Physik A291, 347 (1979).

16. J. M. Blatt and V. F. Weisskopf, Theoretical Nuclear Physics (Wiley, New York, 1952).

17. H. A. Bethe, Revs. Mod. Phys. 9, 71 (1937).

18. T. Ericson, Adv. in Phys. 9, 423 (1960).

19. M. A. McMahan and J. M. Alexander, Phys. Rev. C (in press).

20. T. Ericson and V. Strutinski, Nucl. Phys. 8, 284 (1958); ibid 9, 689 (1959).

21. T. Døssing, Preprint, 1978.

22. G. L. Catchen, M. Kaplan, J. M. Alexander, and M. F. Rivet, submitted to Phys. Rev. C.

23. J. M. Miller, G. L. Catchen, D. Logan, M. Rajagopalan, J. M. Alexander, M. Kaplan and M. S. Zisman, Phys. Rev. Letts. 40, 100 (1978).

24. G. L. Catchen, D. Logan, J. M. Miller, D. Benson, N. H. Lu, T. W. Debiak, M. Rajagopalan, J. M. Alexander, M. Kaplan and M. S. Zisman, Preprint (1979).

25. J. W. Harris, T. M. Cormier, D. F. Geesaman, L. L. Lee, Jr., R. L. McGrath and J. P. Wurm, Phys. Rev. Letts. 38, 1460 (1977).

26. R. Albrecht, W. Dünnweber, G. Graw, H. Ho, S. G. Steadman, and J. P. Wurm, Phys. Rev. Letts. 34, 1400 (1975); H. Ho, R. Albrecht, W. Dünnweber, G. Graw, S. G. Steadman, J. P. Wurm, D. Disdier, V. Rauch, and F. Scheibling, Z. Physik A283, 235 (1977).

27. G. K. Gelbke, M. Bini, C. Olmer, D. L. Hendrie, J. L. Laville, J. Mahoney, M. K. Mermaz, D. K. Scott and H. H. Wieman, Phys. Letts. 71B, 83 (1977).

28. I. Halpern, Ann. Rev. Nucl. Sci. 21, 245 (1971).

29. N. Carjan, A. Sundulescu and V. V. Pashkevich, Phys. Rev. C11, 782 (1975); N. Carjan, J. Physique 37, 1279 (1976); N. Carjan, Dissertation, Technischen Hochschule Darmstadt (Jan. 1977).

30. M. Rajagopalan and T. D. Thomas, Phys. Rev. C5, 1402, 2064 (1972) and references therein.

31. L. G. Moretto, J. Galin, R. Babinet, Z. Fraenkel, R. Schmitt, R. Jared, and S. G. Thompson, Nucl. Phys. A259, 173 (1976).

32. C. Ngô, J. Peter, B. Tamain, M. Berlanger, and F. Hanappe, Z. Physik A283, 161 (1977).

33. J. Galin, B. Gatty, D. Guerreau, M. Lefort, X. Tarrago, S. Agarwal, R. Babinet, B. Cauvin, J. Girard and H. Nifenecker, Z. Physik A283, 173 (1977).

34. R. Lucas, J. Poitou, H. Nifenecker, J. Peter, and B. Tamain, Z. Physik A283, 257 (1977).

35. S. Cohen, F. Plasil and W. J. Swiatecki, Annals. of Physics (N.Y.) 82, 557 (1974).

36. B. Tamain, C. Ngô, J. Peter and F. Hanappe, Nucl. Phys. A252, 187 (1975) and references therein.

37. M. M. Fowler and R. C. Jared, Nucl. Instr. Meth., 124, 341 (1975).

38. S. B. Kaufman, E. P. Steinberg, B. D. Wilkins, J. Unik, A. J. Gorski and M. J. Fluss, Nucl. Instr. Meth. 115, 47 (1974).

39. L. C. Northcliffe and R. G. Schilling, Nucl. Data Tables A7, 223 (1970).

40. J. R. Birkelund, J. R. Huizenga, H. Freiesleben, K. L. Wolf, J. P. Unik, and V. E. Viola, Jr., Phys. Rev. C13, 133 (1976).

41. Kinematic calculations carried out by T. W. Debiak, A. Fleury, and M. F. Rivet using a Monte Carlo method shows that isotropic evaporation from fission fragments [$W(\theta) \propto (1/\sin\theta)$] leads to a broad, relatively flat energy distribution of width ≈ 32 MeV for ^{4}He. The results of these calculations at several laboratory angles for ^{4}He and ^{1}H emission are shown in Fig. 8.

42. J. R. Nix, Argonne Natl. Lab. Rep. ANL/PHY/76-2, Vol. I, (1976).

43. M. Blann, Nucl. Phys. A235, 211 (1974). M. Blann, A. Mignerey, and W. Scobel, Nukleonika 21, 335 (1976).

44. E. Cheifetz, Z. Fraenkel, J. Galin, M. Lefort, J. Peter and X. Tarrago, Phys. Rev. C2, 256 (1970).

45. G. N. Harding and F. J. M. Farley, Proc. Phys. Soc. (London) A69, 853 (1956).

46. A. H. Wapstra and N. B. Gove, Nucl. Data, A9, 265 (1971).

47. L. Kowalski, J. M. Alexander, D. Logan, M. Rajagopalan, M. Kaplan, M. S. Zisman, and T. W. Debiak, unpublished data on linear momentum transfer in this system.

48. M. F. Rivet, These d'Etat, Orsay (1977).

49. M. Beckerman and M. Blann, Phys. Rev. Letts. 38, 272 (1977); Phys. Letts. 68B, 31 (1977).

50. H. Delagrange, A. Fleury and J. M. Alexander, Phys. Rev. C16, 706 (1977).

51. U. Schröder and J. R. Huizenga, Ann. Rev. Nucl. Sci. 27, 465 (1977).

52. J. P. Bondorf, J. N. De, A. O. T. Karvinen, G. Fai, and B. Jakobsson, Phys. Letts. 84B, 162 (1979).

Table I. Parameters that characterize the singles spectra

^{4}He				^{1}H			
$\langle\theta_{c.m.}\rangle$ (deg)	ε_{mp}[a] (MeV)	FWHM[b] (MeV)	T[c] (MeV)	$\langle\theta_{c.m.}\rangle$ (deg)	ε_{mp}[a] (MeV)	FWHM[b] (MeV)	T[c] (MeV)
160	23.5	11	2.3 ± 0.2	150	12	12	2.5 ± 0.2
150	23	11	2.4 ± 0.2	127	-	-	2.6 ± 0.2
127	23	10	3.2 ± 0.2	109	12	-	2.6 ± 0.2
98	23.5	12	3.6 ± 0.5	95	12	14	3.0 ± 0.5
71	22	13	3.7 ± 0.5	73	12	16	3.3 ± 0.5
57	25	-	6.0 ± 0.5	56	11	-	4.1 ± 0.5
48	25	13	6.1 ± 0.5	41	12	16	3.9 ± 0.5
42	25	14	6.4 ± 0.5	25	13	14	4.4 ± 0.5
25	25	17	6.9 ± 0.5				
^{2}H				^{3}H			
151	-	-	2.6 ± 0.3	98	14	13	3.6 ± 0.3
111	12	13	2.9 ± 0.3	49	15	13	4.9 ± 0.5
97	12	12	3.2 ± 0.3	43	14	17	6.9 ± 0.5
56	13	15	4.6 ± 0.5	25	15	17	7.1 ± 0.5
41	15	17	4.6 ± 0.5				
25	16	18	5.9 ± 0.5				

(a) The midpoint of the full width at half maximum; estimated uncertainty ~ 1 MeV.

(b) FWHM ≡ full width at half maximum; estimated uncertainty ~ 1 MeV.

(c) These values of T (temperature) are from fits of the spectra to the function $(\varepsilon-B)\exp(-\varepsilon/T)$ with B = 23 MeV, 12 MeV, and 11 MeV for ^{4}He, ^{1,2}H, and ^{3}H, respectively. (If B is reduced by 25%, then T for ^{4}He at 160 deg and for ^{1}H at 150 deg are both increased to 2.9 MeV.)

Table II. Parameters related to the angular momenta for ^{4}He emission from an equilibrated ^{237}Bk composite system.

340 MeV $^{40}Ar + ^{197}Au \rightarrow ^{237}Bk$

$\ell_{max} = 190\ \hbar$; $E^{*} = 160$ MeV; $\hbar^2/2\mathcal{I} = 4.0$ keV

$(I_o+\frac{1}{2})$ ($\hbar$)	E_{rot} (a) (MeV)	U (b) (MeV)	T (c) (MeV)	$2\sigma^2$ (d)	$\langle(\ell+\frac{1}{2})^2\rangle^{1/2}$ (e) ($\hbar$)	β_1 (f)	β_2 (g)	$(\xi+2T)$ (h) (MeV)
0	0	144	2.5	605	7.4	0	0	5.0
50	10.0	134	2.4	584	8.1	0.70	0.38	6.0
70	19.6	125	2.3	563	8.9	1.11	0.78	7.0
90	32.4	112	2.2	533	9.9	1.67	1.36	8.3
100	40.0	104	2.1	515	10.5	2.03	1.74	9.0
115	52.9	92	2.0	482	11.4	2.73	2.47	10.3
190	144.3	0.1	0.1	15	17.0	222.	217.	17.3

(a) Computed from Eq. (17).

(b) Computed from Eq. (16).

(c) Computed from Eq. (15) with the level density parameter "a" = (A/10) MeV^{-1}.

(d) As defined in Eq. (3).

(e) Obtained from Eq. (7).

(f) Obtained from Eq. (5').

(g) Obtained from Eq. (13).

(h) The average total energy (above the barrier) due to thermal motions plus centrifugal spinoff as in Eq. (18).

Table III. Summary of Coincidence Results.

θ_S (deg)	φ (deg)	$\langle\theta_{c.m.}\rangle$ (deg)		$\langle\varepsilon_{c.m.}\rangle$ (MeV)		Number of events[a]		$d^2\sigma/d\Omega_S d\Omega_G$[b] (mb/sr^2)	
		^{4}He	^{1}H	^{4}He	^{1}H	^{4}He	^{1}H	^{4}He	^{1}H
				θ_G = 40 deg					
100	0	112	109	21.4	11.1	12	7	8.4	4.7
	14	112	108	21.8	11.4	24	11	13.6	6.0
	28	111	108	21.6	11.7	21	20	11.1	10.3
	42	110	107	23.6	12.6	13	20	5.3	7.9
150	0	156	154	24.4	10.0	7	1	11.8	1.5
	14	153	152	23.8	10.8	4	3	6.0	4.0
	28	148	146	20.2	13.0	12	4	15.5	4.7
	42	139	138	22.5	11.4	5	6	4.8	5.3
255	0	116	112	26.7	13.8	18	8	12.5	5.3
	14	115	114	26.6	9.3	12	4	9.0	2.9
	28	114	111	27.5	13.8	15	19	7.7	9.4
	42	113	113	22.7	14.2	8	12	4.3	6.1
300	0	71	69	22.7	7.0	16	5	10.1	3.3
	14	72	69	22.7	11.4	28	9	11.1	3.8
	28	74	72	26.2	12.3	15	22	7.0	10.7
	42	80	78	23.2	11.7	23	13	6.8	4.0
320	0	46	46	28.1	9.9	27	9	16.6	5.7
	28	53	54	25.9	15.8	17	13	7.9	6.7
339	0	25	24	29.0	10.3	66	7	19.9	2.2
	28	40	40	24.3	13.3	33	33	7.5	8.3
				θ_G = 60 deg					
120	0	131	127	23.2	12.1	19	16	4.2	3.0
	28	127	124	23.8	12.6	16	27	2.6	4.3
150	0	156	155	24.3	10.0	8	6	6.0	4.2
	28	147	144	24.3	14.7	11	9	5.8	4.3
205	0	160	158	23.1	15.3	11	6	6.9	3.2
	28	150	148	22.7	13.9	12	9	5.3	3.6
275	0	96	94	26.5	11.2	12	6	6.6	3.3
	28	98	95	23.7	12.1	10	10	4.1	4.1
300	0	71	68	22.8	10.0	11	5	5.8	2.8
	28	74	73	26.1	14.8	11	7	4.3	2.9
320	0	47	46	28.6	10.6	23	10	11.7	5.3
	28	54	54	25.3	16.2	14	18	5.5	7.6
339	0	25	24	25.1	11.3	31	8	13.6	3.8
	28	42	42	24.7	15.6	9	14	3.0	5.2

(a) Number of coincidence events recorded between light-particle telescopes (SST) at angle θ_S and heavy fragment telescope (GT) at angle θ_G. SST 1 subtended 9.1 msr and was used for the φ = 0 and φ = 14 deg measurements; SST 2 subtended 12.9 msr and was used at φ = 28 and φ = 42 deg.

(b) These cross sections have been transformed to the c.m. system only for the light particle (H/He); no transformation has been made for the heavy fragment.

Table IV. Integrated light-particle cross sections (mb).

	Singles measurement		Coincidence measurement
	Symmetric component[(a)]	Forward component[(b)]	Symmetric component[(c)]
^{4}He	519	260	384
^{1}H	553	155	273
^{2}H	64	45	-
^{3}H	(12.8)[(d)]	8.0	-

(a) For ^{4}He the c.m. angular distribution was fitted to the function $W(\theta) = A \exp(-\gamma\theta) + B + C \cos^2\theta$, and the symmetric part $(B + C \cos^2\theta)$ was integrated. For the H isotopes we assumed the symmetric component to be isotropic, and multiplied the back-angle cross sections (see Fig. 4) by 4π.

(b) These values were obtained by integration after subtraction of the symmetric component and linear extrapolation from $\theta_{c.m.} = 25$ deg to zero deg. (If we use an exponential extrapolation from 25 to zero deg, we get 290 mb for ^{4}He.)

(c) The cross sections $(d^2\sigma/d\Omega_S d\Omega_G)$ from Table III at $\theta_G = 60$ deg and $\varphi = 0$ were averaged for all $\theta_{c.m.} > 60$ deg. Noting that $\theta_G = 60$ deg (lab) corresponds to $\theta_G = 90$ deg (c.m.), we transformed the averaged cross sections to the c.m. for the heavy fragment using an average factor 0.667 and then multiplied by π^2 to include all fission events. These values were then multiplied by 4π for ^{1}H and by 9.89 for ^{4}He to account for the apparent isotropy in ^{1}H emission and strong out-of-plane correlation in ^{4}He emission as described in Ref. 22.

(d) Poor statistics limited the determination of an effective temperature for ^{3}H at back angles. Therefore this cross section is more subject to the possible inclusion of contributions from high temperature emissions.

Table V. Ratios of total coincidence events and relative cross sections for φ = 28 and 42 deg to those for φ = 0 and 14 deg.

Span of c.m. angles (deg)[a]	$(N_{28+42})/(N_{0+14})$[b]		$(\sigma_{28+42})/(\sigma_{0+14})$[c]	
	^{4}He	^{1}H	^{4}He	^{1}H
60 - 180	172/182	178/87	0.72 ± 0.10	1.52 ± 0.18
0 - 60	73/147	78/34	0.38 ± 0.06	1.82 ± 0.35

(a) Range of angles covered by the SST's.

(b) Ratios of numbers of coincidence events for θ_G of 40 deg and 60 deg combined.

(c) Ratios of summed numbers of events (corrected for deadtime effects) divided by the respective solid angles. These ratios are equivalent to average cross section ratios from Table III, with the averaging being weighted by the number of observed events at each angular configuration.

Table VI. First and second moments of the energy distributions for ^{1}H and ^{4}He detected in coincidence with heavy fragments.

$\langle\theta_{c.m.}\rangle$ (deg)	φ (deg)	^{1}H $N^{(a)}$	^{1}H $\langle\varepsilon\rangle^{(b)}$ (MeV)	^{1}H $\sigma_{\varepsilon}^{(b)}$ (MeV)	^{4}He $N^{(a)}$	^{4}He $\langle\varepsilon\rangle^{(b)}$ (MeV)	^{4}He $\sigma_{\varepsilon}^{(b)}$ (MeV)
				θ_G = 40 deg			
< 60	0-14	16	9.2	2.8	93	28.3	8.0
< 60	28-42	46	13.7	5.5	50	24.0	7.6
> 60	0-14	48	10.8	3.8	121	24.3	7.1
> 60	28-42	116	12.7	5.2	112	23.2	6.1
				θ_G = 60 deg			
< 60	0	18	10.6	3.7	54	26.0	7.6
< 60	28	32	15.1	6.7	23	23.7	4.7
> 60	0	39	11.9	3.6	61	23.7	4.7
> 60	28	62	13.1	4.7	60	23.6	4.3

(a) Number of events observed.

(b) $\langle\varepsilon\rangle$ and σ_{ε} are respectively the first and second moments of the observed energy distributions (c.m.). Note that the standard deviation of the mean $\langle\varepsilon\rangle$ is $\approx \sigma_{\varepsilon}/\sqrt{N}$.

Table VII. Separation energies[(a)] S_x and Coulomb barriers[(b)] B_x (all energies in MeV).

	$^{237}_{97}Bk$	$^{86}_{35}Br$	$^{78}_{35}Br$	$^{118}_{48}Cd$	$^{110}_{48}Cd$	$^{151}_{62}Sm$	$^{141}_{62}Sm$
E^*	160	73	5	110	20	127	25
S_n	8	5.4	8.3	8.4	9.9	5.6	8.5
S_p	2	9.6	6.7	11.1	8.9	8.3	5.0
B_p	11	4.7	4.7	6.0	6.0	7.3	7.3
$S_p + B_p$	13	14.3	11.4	17.1	14.9	15.6	12.3
S_α	- 8	8.4	5.0	4.9	2.8	1.2	- 0.8
B_α	23	9.0	9.0	12.0	12.0	13.5	13.5
$S_\alpha + B_\alpha$	15	17.4	14.0	16.9	14.8	14.7	12.7

(a) The subscripts "x" are n for neutron, p for ^1H, and α for ^4He. Separation energies were computed from Ref. 46.

(b) Coulomb barriers were estimated from Ref. 19.

FIGURE CAPTIONS

Figure 1: Singles energy spectra in the c.m. for ^{4}He and ^{1}H at various angles. The average c.m. angle is indicated. Parameters describing the spectra are given in Table I.

Figure 2. Energy spectra for ^{2}H and ^{3}H as in Fig. 1.

Figure 3. Angular distribution for ^{4}He in the singles mode. Data are shown as points; the symmetric component is indicated C; the forward-peaked component by D. The forward-peaked component is broken into a high-temperature part H and a low temperature part L.

Figure 4. Angular distributions for ^{1,2,3}H in the singles mode.

Figure 5: Energy distributions for ^{4}He and ^{1}H at $\langle\theta_{c.m.}\rangle$ = 160° and 150°, respectively. These are compared to spectra from reactions leading to ^{194}Hg as shown ($\langle\theta_{c.m.}\rangle \sim 150\text{-}165°$). The ^{194}Hg data are from Ref. 12.

Figure 6. Angular correlations for ^{4}He and ^{1}H with respect to heavy fragments detected in the gas telescope. The angle of the gas telescope is θ_G. The data for out-of-plane angles φ = 28° and 42° have been averaged and are designated by open points (○). The data for φ = 0° and 14° have likewise been averaged and are indicated by filled points (●). Data for θ_G = 40° have been normalized to that for θ_G = 60° by the relative fission cross sections (for comparative purposes). The smooth curves represent the shapes of the corresponding angular distributions in the singles mode. The data are from Table III with several points at similar c.m. angles combined.

continued →

FIGURE CAPTIONS CONTINUED

Figure 7. Energy distributions (c.m.) for ^{1}H and ^{4}He observed in the coincidence mode with θ_G = 40° and 60°. All events observed are included and grouped according to the value of $\theta_{c.m.}$ for ^{1}H or ^{4}He.

Figure 8. Energy spectra for ^{1}H and ^{4}He calculated by a Monte Carlo simulation of evaporation from fission fragments (smooth curves). Gaussian distributions were assumed for the mass and total energy distributions in fission with standard deviations of 30 mass units and 15 MeV, respectively. Angular distributions (c.m.) for each fission product were taken to be 1/sin θ and isotropic for H/He. The evaporation spectra were taken from Eq. (1) with barrier parameters B from Ref. 19 and T from Eqs. (15) and (16). Experimental spectra are shown as points.

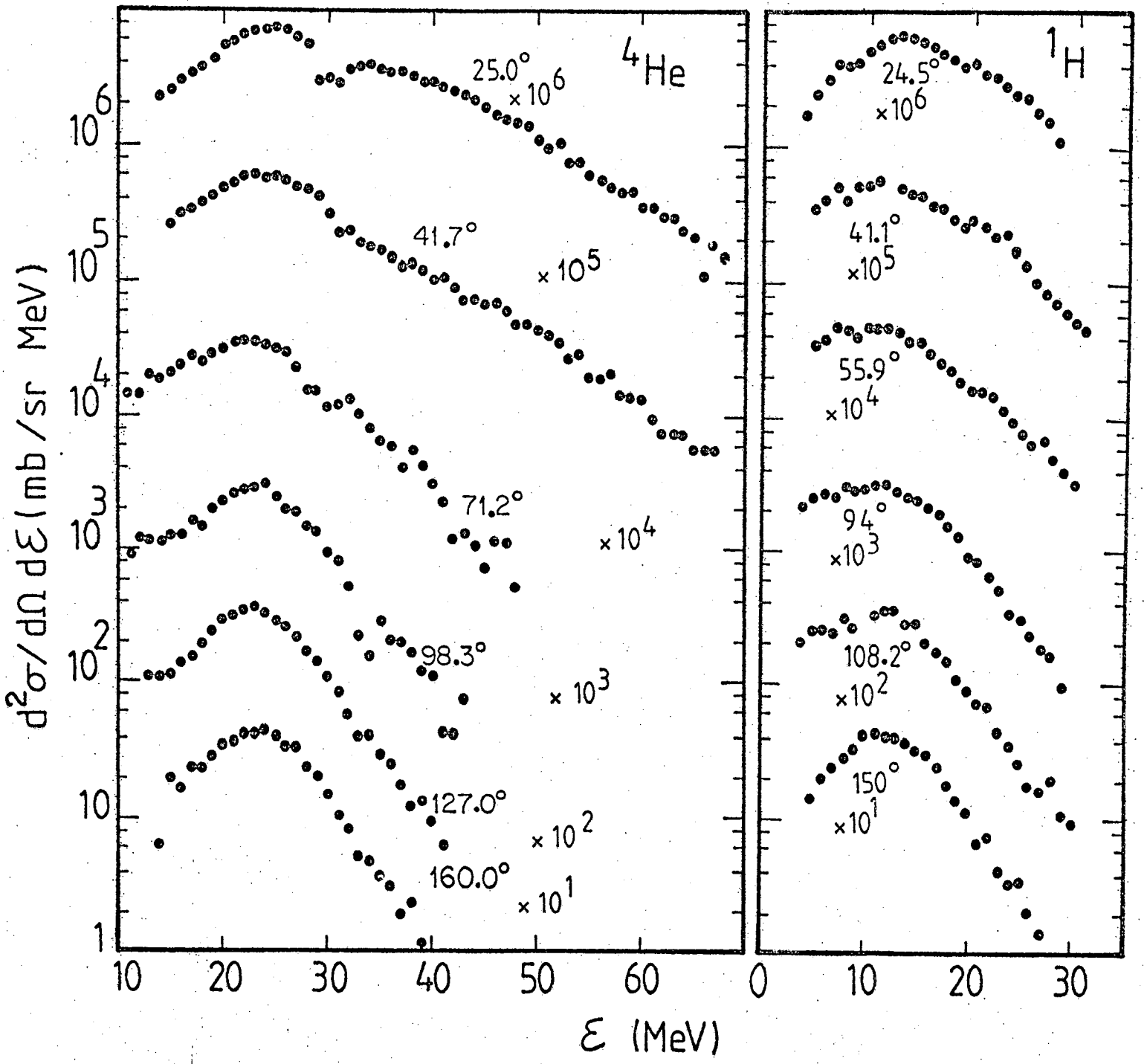
^{4}He
^{1}H
25.0° ×10^6
41.7° ×10^5
71.2° ×10^4
98.3° ×10^3
127.0° ×10^2
160.0° ×10^1
24.5° ×10^6
41.1° ×10^5
55.9° ×10^4
94° ×10^3
108.2° ×10^2
150° ×10^1
d$^2\sigma$/dΩ dε (mb/sr MeV)
ε (MeV)

Fig. 1

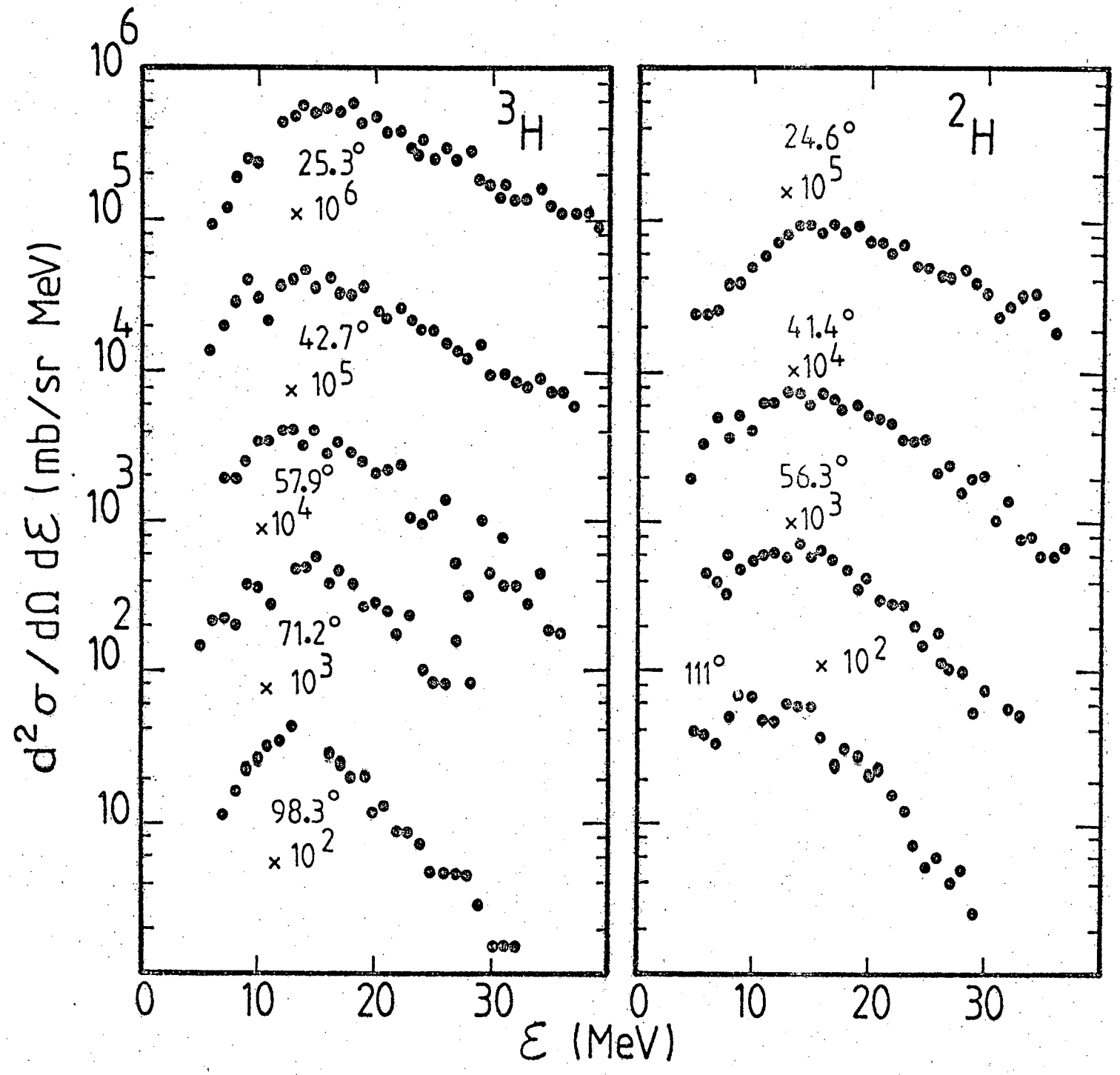
$d^2\sigma/d\Omega\, d\mathcal{E}$ (mb/sr MeV)
$\mathcal{E}$ (MeV)
^{3}H
^{2}H
25.3° × 10^6
42.7° × 10^5
57.9° ×10^4
71.2° × 10^3
98.3° × 10^2
24.6° ×10^5
41.4° ×10^4
56.3° ×10^3
111° × 10^2

Fig. 2

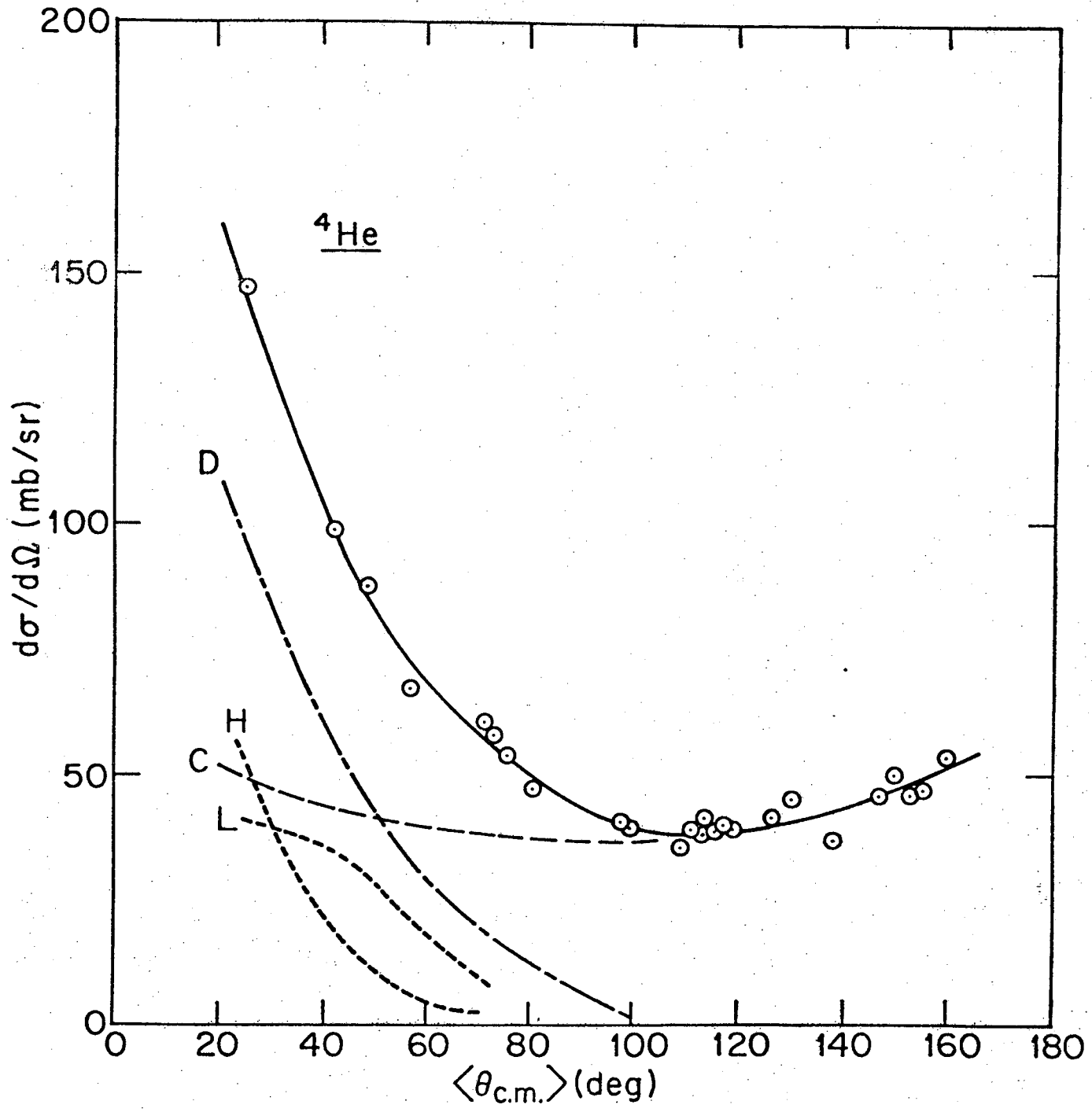
200
150
100
50
0
^{4}He
D
H
C
L
$d\sigma/d\Omega$ (mb/sr)
0
20
40
60
80
100
120
140
160
180
$\langle\theta_{c.m.}\rangle$ (deg)

Fig. 3

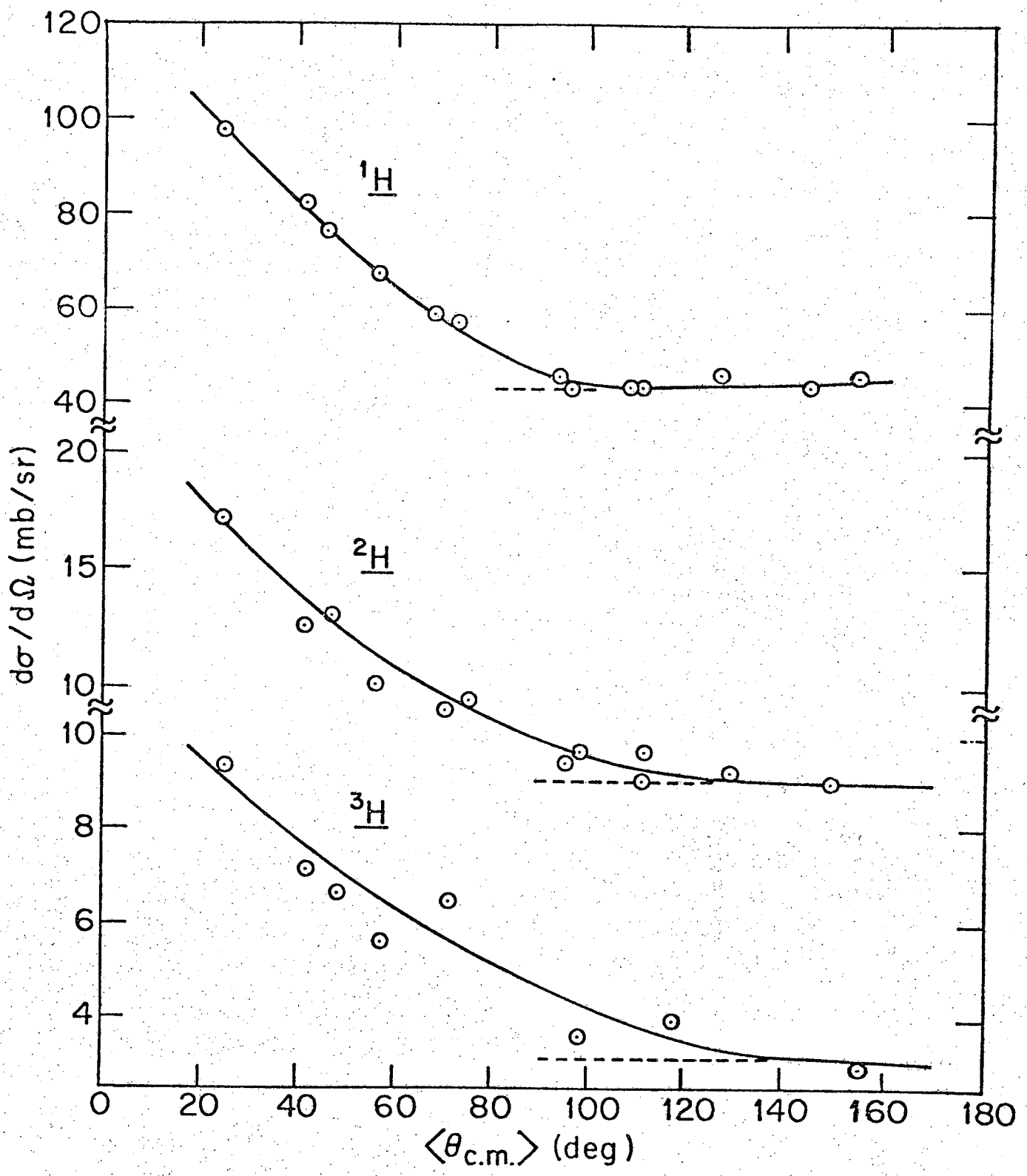
120
100
80
60
40
20
15
10
10
8
6
4
^{1}H
^{2}H
^{3}H
dσ/dΩ (mb/sr)
0
20
40
60
80
100
120
140
160
180
⟨θc.m.⟩ (deg)

Fig. 4

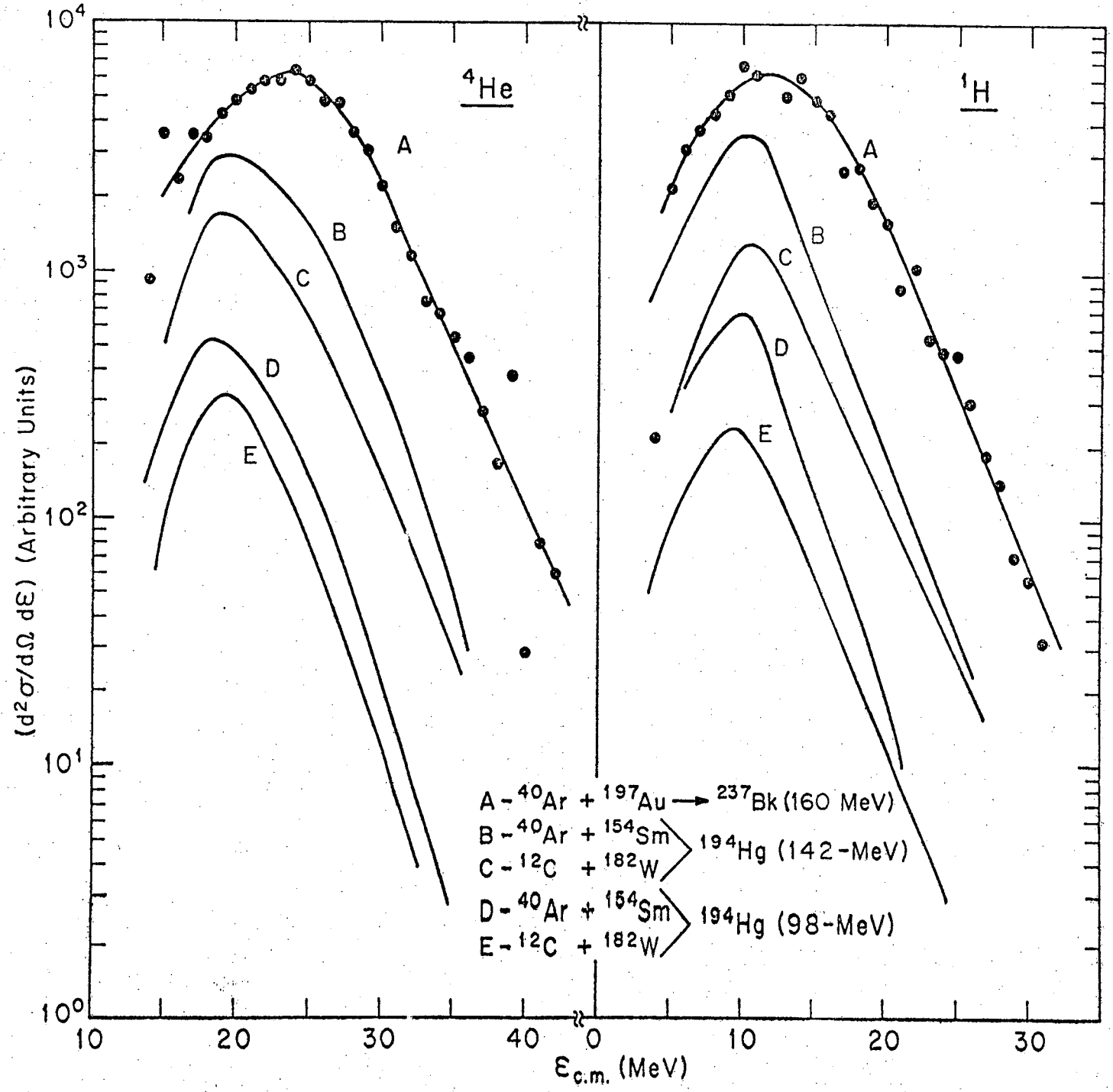
10^4
10^3
10^2
10^1
10^0
$(d^2\sigma/d\Omega\, dE)$ (Arbitrary Units)
^{4}He
^{1}H
A
B
C
D
E
10
20
30
40
0
10
20
30
$E_{c.m.}$ (MeV)
A - ^{40}Ar + ^{197}Au → ^{237}Bk (160 MeV)
B - ^{40}Ar + ^{154}Sm
C - ^{12}C + ^{182}W
^{194}Hg (142-MeV)
D - ^{40}Ar + ^{154}Sm
E - ^{12}C + ^{182}W
^{194}Hg (98-MeV)

FIG. 5

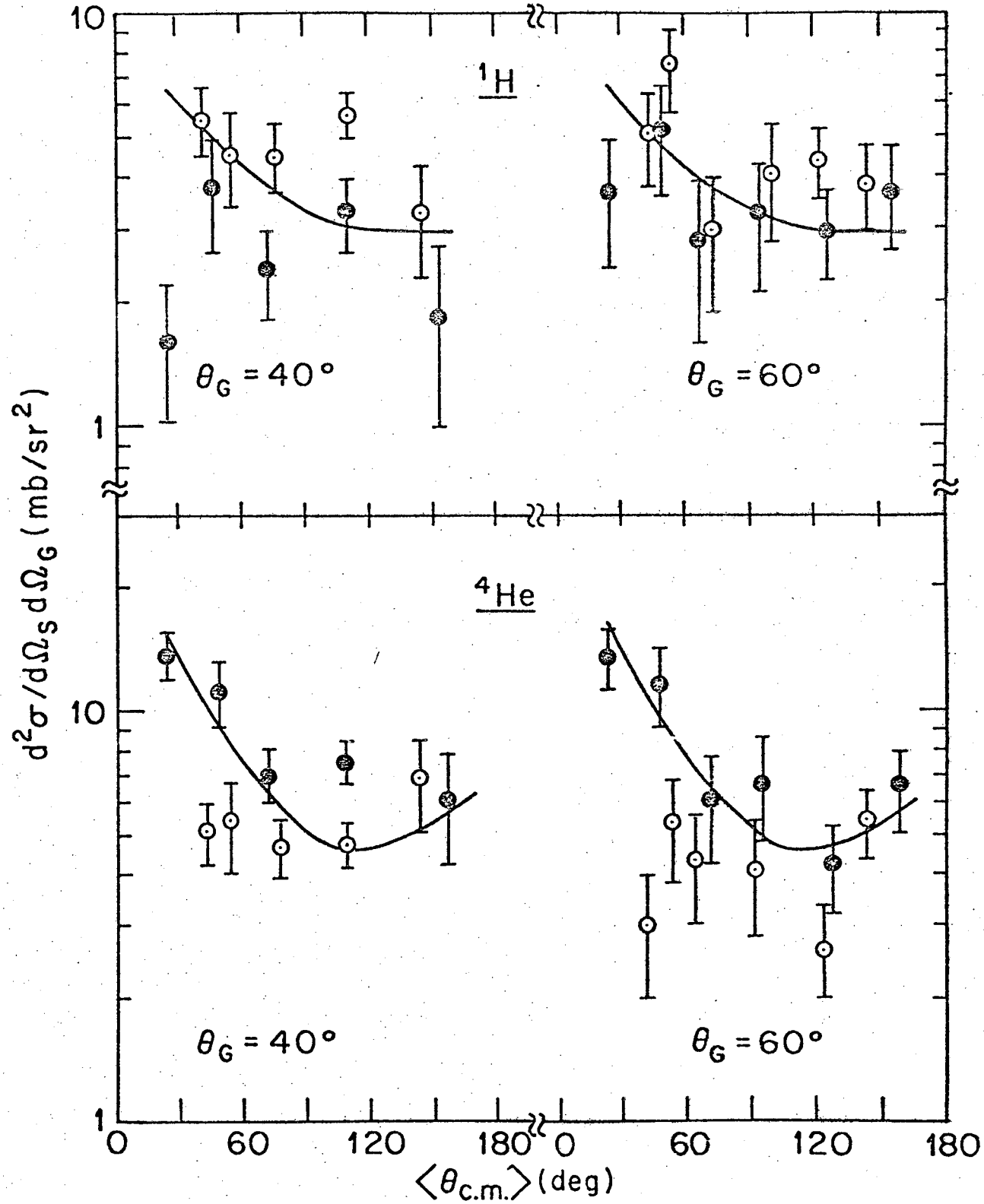
10
1
^{1}H
$\theta_G = 40°$
$\theta_G = 60°$
^{4}He
10
1
$\theta_G = 40°$
$\theta_G = 60°$
0
60
120
180
0
60
120
180
$\langle\theta_{c.m.}\rangle$ (deg)
$d^2\sigma/d\Omega_S\, d\Omega_G$ (mb/sr^2)

Fig. 6

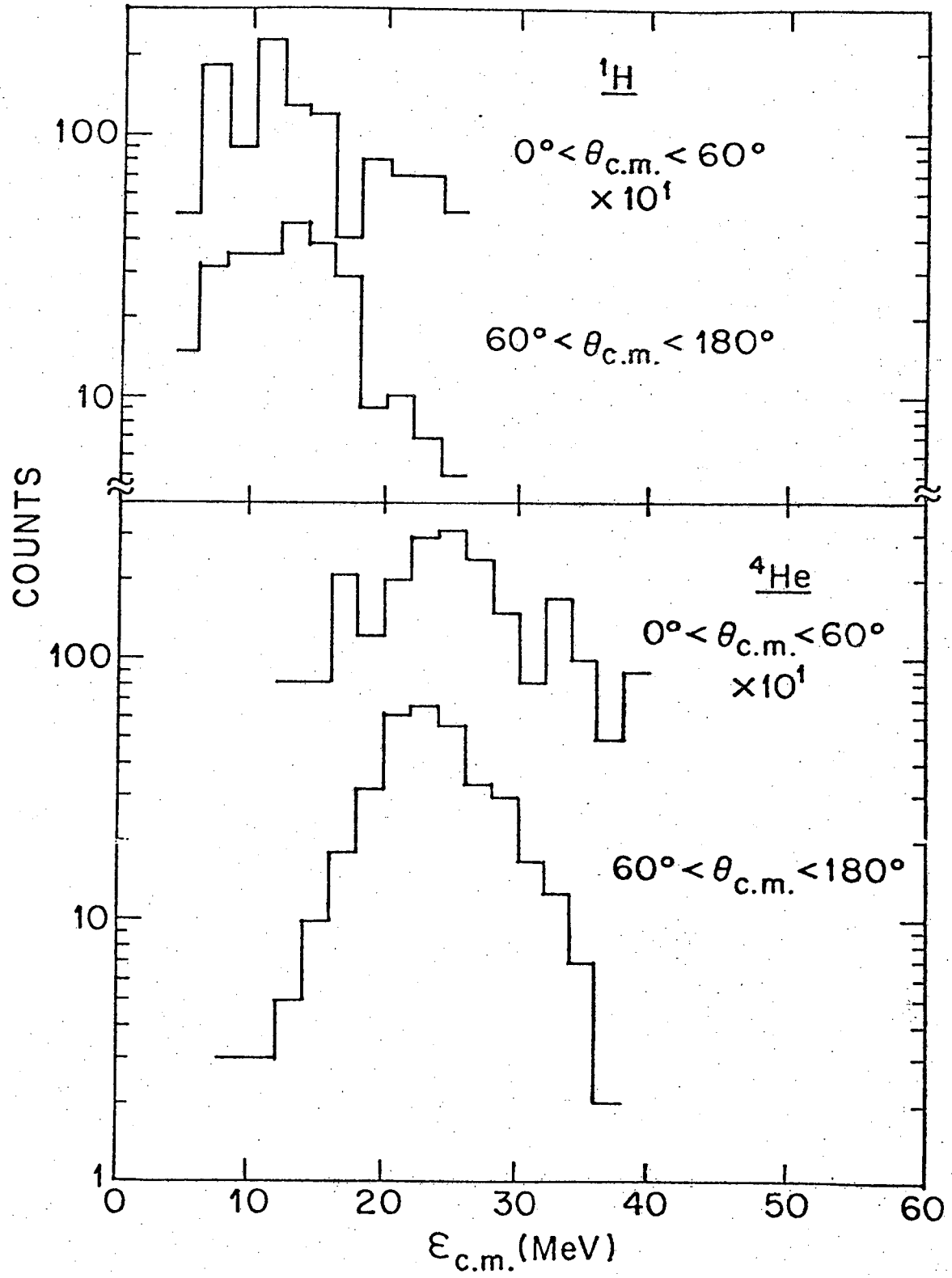
^{1}H
$0° < \theta_{c.m.} < 60°$
$\times 10^1$
$60° < \theta_{c.m.} < 180°$
^{4}He
$0° < \theta_{c.m.} < 60°$
$\times 10^1$
$60° < \theta_{c.m.} < 180°$
COUNTS
100
10
100
10
1
0
10
20
30
40
50
60
$\varepsilon_{c.m.}$(MeV)

Fig. 7

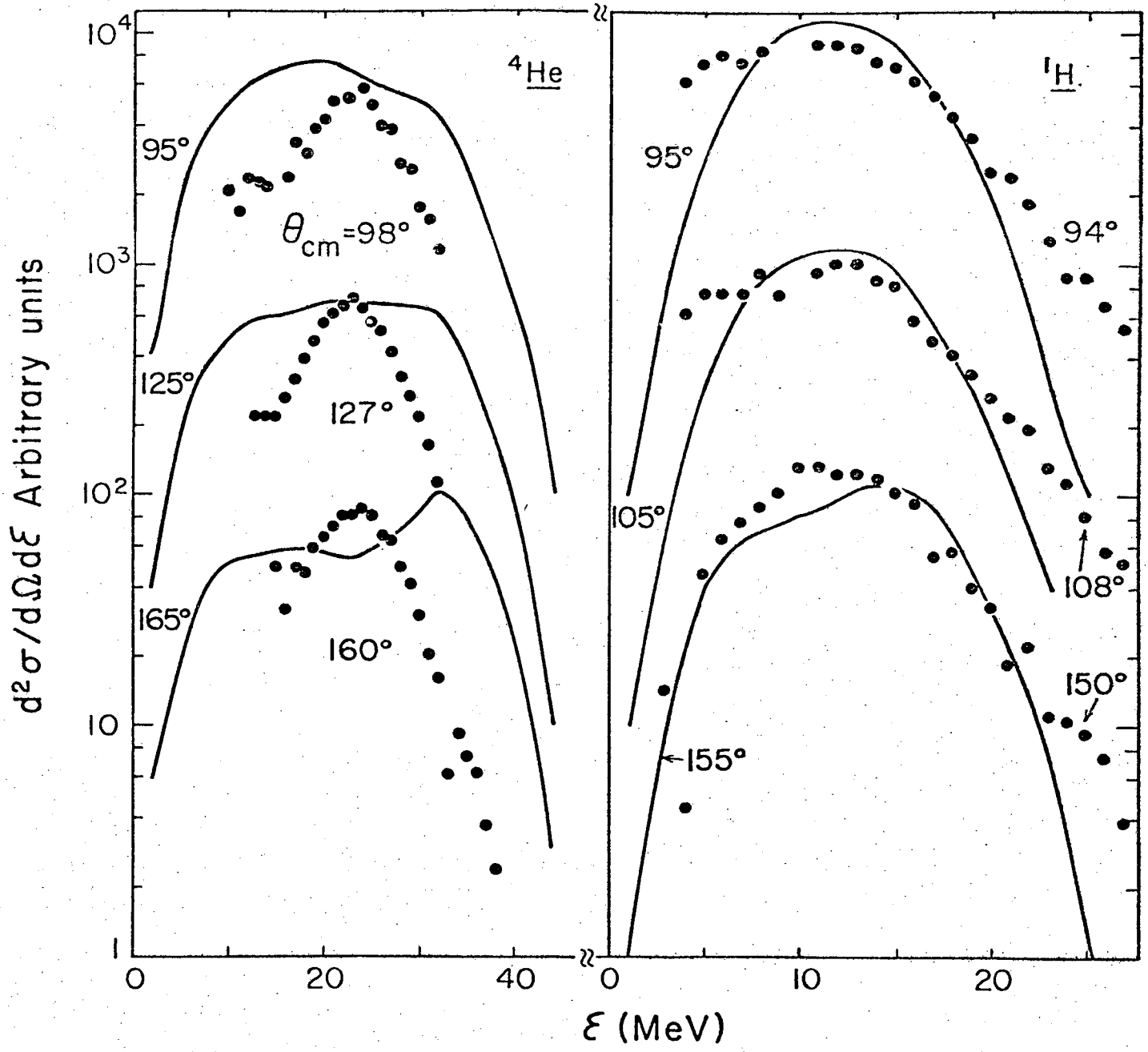
10^4
10^3
10^2
10
1
$d^2\sigma/d\Omega d\mathcal{E}$ Arbitrary units
^{4}He
95°
θ_{cm}=98°
125°
127°
165°
160°
0
20
40
^{1}H
95°
94°
105°
108°
150°
155°
0
10
20
$\mathcal{E}$ (MeV)

Fig. 8

PUBLICATIONS

1. Coincidence Studies of Heavy Fragments in Deeply Inelastic Collisions Between Heavy Ions: Sequential Fission Probability in Reactions of 730-MeV ^{86}Kr with Au. M. Rajagopalan, L. Kowalski, D. Logan, M. Kaplan, J. M. Alexander, M. S. Zisman, and J. M. Miller, Phys. Rev. C19, 54 (1979).

2. Perturbed Angular Correlation Studies of Hf Binding to Cyanocobalamin (Vitamin B_{12}). J. W . Ball and M. Kaplan, J. Chem. Phys. 70, 1337 (1979).

3. Fusion and Emission of ^{1}H and ^{4}He in Reactions Between Complex Nuclei at High Energies. H. Delagrange, D. Logan, M. F. Rivet, M. Rajagopalan, J. M. Alexander, M. S. Zisman, M. Kaplan, and J. W. Ball, Phys. Rev. Letters (in press).

4. Semiempirical Methods for Estimating Fragment Spins from Studies of ^{4}He and ^{1}H Emission. G. L. Catchen, M. Kaplan, J. M. Alexander, and M. F. Rivet, Phys. Rev. C (in press).

5. Rapid Energy Equilibration and Emission of H and He in the Reaction of 340 MeV ^{40}Ar with ^{197}Au. D. Logan, M. Rajagopalan, M. S. Zisman, J. M. Alexander, M. Kaplan, and L. Kowalski, submitted to Phys. Rev. C.

PAPERS IN PREPARATION

1. The Emission of H and He in Reactions of 724-MeV ^{86}Kr with Au. G. L. Catchen, D. Logan, J. M. Miller, D. Benson, N. H. Lu, T. W. Debiak, M. Rajagopalan, J. M. Alexander, M. Kaplan, and M. S. Zisman.

2. Coincidence Studies of Momentum Transfer in Reactions of 8.5 MeV/A ^{40}Ar and ^{20}Ne with ^{197}Au. L. Kowalski, J. M. Alexander, D. Logan, M. Rajagopalan, M. Kaplan, M. S. Zisman, and T. W. Debiak.

3. Quadrupole Interactions in DNA at Hf and Ag sites Studied by Perturbed Angular Correlations. J. W. Ball and M. Kaplan.

4. Search for Enhanced ^{12}B Formation from the Reaction $^{65}Cu(^{12}C, ^{12}B)^{65}Zn$. A. A. Caretto, Jr., M. Kaplan, R. J. Spector, M. V. Yester, and R. L. Ferguson.

5. Charged Particle Emission from ^{194}Hg Compound Nuclei: Energy and Spin Dependence of Fission-Evaporation Competition. M. Rajagopalan, D. Logan, J. W. Ball, M. Kaplan, H. Delagrange, M. F. Rivet, J. M. Alexander, and M. S. Zisman.

6. Fusion and Charged Particle Emission in ^{40}Ar Induced Reactions. D. Logan, H. Delagrange, M. F. Rivet, M. Rajagopalan, J. M. Alexander, M. Kaplan, M. S. Zisman, and E. Duek.